

Constructive Motives and Scattering

M. D. Sheppeard

Preface

This elementary text is intended for anyone interested in combinatorial methods in modern particle physics. Advanced concepts are only mentioned when there is some chance at a simple explanation. There is a development of ideas through the book, but hopefully each chapter is also reasonably well contained. All diagrams and tables are embedded in the text along with the equations.

At the heart of particle physics is the problem of emergence. As of 2013, nobody really understands what this is, but there is however general agreement that the answers involve the concept of *motive*. Throughout the book, our aim is to understand a little about motives, not from the standard mathematical point of view, but using a physicist's intuition. This can be done at an elementary level, because the underlying philosophy is a constructive one, meaning that theorems about motives should depend on their concrete construction. Motives are about both geometry and number theory, and hence about knots.

Unfortunately, there are many relevant topics that cannot be covered. The essential physical ideas do not appear before chapter 6, but are an integral part of the methods discussed. If the reader *really* wants to skip the abstract nonsense on a first reading, they may do so. The whole book is typeset in L^AT_EX, using mostly X_Y-pic for diagrams. It was written with no feedback, essentially no resources, and no doubt many errors remain.

Thanks to wikipedia for an endless supply of free information. It cannot all be acknowledged. During the blogging years there were many conversations with keen theorists, notably Carl Brannen, Michael Rios, Louise Riofrio, Alejandro Rivero and Tony Smith. This work was made possible by the kindness of Kerie and Allan. It also owes a great debt to Graham Dungworth, whose ceaseless online enthusiasm and clarification of the new cosmology has provided invaluable insights.

Contents

1	Introduction	3
2	Numbers and Sets	8
2.1	The Word Monoid	10
2.2	Continua and Quantum Numbers	12
2.3	Union, Disjoint Union and Cohomology	15
2.4	A Category of Relations	17
3	Duality and the Fourier Transform	19
3.1	The Quantum Fourier Transform	19
3.2	Unitary Bases and Decompositions	21
3.3	Honeycombs and Hermitian Matrices	24
4	The Ordinals and Discrete Duality	26
4.1	The d -Ordinals	26
4.2	Categorical Strings	28
4.3	Fourier Dualities and Topology	30
5	Trees, Polytopes and Braids	32
5.1	Permutations and Planar Trees	32
5.2	Solomon's Descent Algebra	36
5.3	Associahedra, Permutohedra and Polygons	38
5.4	Linear Orders and Forests	42
5.5	Three Dimensional Traces	46
5.6	Associated Braids and Knot Invariants	48
6	Twistor Scattering Theory	53
6.1	Scattering Amplitudes	55
6.2	N=8 Supergravity	60
6.3	Grassmannians and Associahedra	61
6.4	Symbology and Polylogarithms	64
6.5	Decorated Polygons for Symbols	66
7	The Ribbon Particle Spectrum	71
7.1	Braids and Ribbons	72
7.2	The Single Generation Spectrum	74
7.3	CPT and the Higgs Mechanism	78
7.4	Electroweak Quantum Numbers	82
7.5	The Burau Representation and Mirror Circulants	83
7.6	Neutrino and Quark Mixing	86
7.7	The Koide Rest Mass Phenomenology	90

8	Knots and Ribbon Graphs	95
8.1	The Temperley-Lieb Algebra	96
8.2	B_n and Khovanov Homology	99
8.3	Chorded Braids	101
8.4	Ribbons and Moduli Spaces	101
9	Bootstrapping Adjoint Actions	105
9.1	Duality with S_2	105
9.2	The Permutoassociahedron	107
9.3	The Klein Quartic and S_5	107
9.4	Nonassociative Braids	108
10	Entanglement and Entropy	110
10.1	Entanglement with Trees and Jordan Algebra	110
10.2	Categorical Entanglement	114
10.3	Secondary Polytopes and Hyperdeterminants	115
11	Non Local Cosmology	119
11.1	Modified Newtonian Dynamics	121
11.2	AdS, dS and FRW Cosmologies	123
11.3	Observational Notes	127
11.4	Mirror Neutrinos and the CMB	127
11.5	Discussion	129
A	Category Theory	131
A.1	Limits and Universality	133
A.2	Monoidal, Braided and Tortile Categories	135
A.3	Tricategories and Higher Dimensions	138
A.4	The Crans-Gray Tensor Product	140
B	Braid Groups	141
C	Elementary Algebra	144
C.1	Bialgebras and Hopf Algebras	145
C.2	Shuffles and Lattice Paths	147
C.3	Matrix Tensor Algebra and Distributivity	147
D	The Division Algebras	150
D.0.1	Particles from $\mathbb{R} \otimes \mathbb{C} \otimes \mathbb{H} \otimes \mathbb{O}$	151
D.0.2	Jordan Algebras	153

1 Introduction

The task of emergent geometry is to recover the rich mathematical structures underlying quantum field theory and general relativity. This means no less than unveiling classical geometry itself, in an axiomatic setting capable of transcending the limitations of set theory. Much progress has been made in recent decades, and the foundations of category theory are now essential to any serious endeavour in theoretical physics.

This basic text covers a range of combinatorial and categorical techniques lying behind the modern approach. These begin with the discrete permutation and braid groups, but the overall aim is to understand a constructive continuum, wherein the complex numbers and other division algebras appear in the motives of a universal cohomology. A *motive* is a gadget much beloved by mathematicians, although nobody really understands what it is. To a physicist, cohomology is an algorithm for cutting spaces down to their essential physical content. In a quantum universe, we would also like to do the reverse: start with measurement, and build the geometry defined by its logic. This means that concrete diagrams are interpreted not as classical spaces, but rather as symbols representing measurement questions. In field theory, Feynman diagrams are replaced by diagrams for twistor spaces.

We now know for certain that a motivic formulation of particle physics exists. Modern twistor methods for scattering amplitudes use motivic methods, as do studies of renormalisation algebras. Amplitudes for n particles are computed on a space whose dimension appears to increase with n , suggesting the increasing complexity of abstract information rather than an external reality of a fixed number of dimensions.

In order to explain clearly the choice of topics here, it is necessary to take a firm point of view on the physics. Our position on the Lagrangian is the following. The *local* theory is exactly the Standard Model, with Majorana neutrinos and no proper neutrino oscillations. The only observable local states come from this SM Lagrangian, and they are enumerated by a special set of ribbon diagrams. In the non local theory: the neutrinos, the Higgs boson, and in fact all neutral particles, may exhibit novel features. There is a natural spectrum of mirror fermions, but no additional bosons, suggesting that mirror fermions are merely a non local aspect of baryonic matter.

The algebraic structure of the local SM Lagrangian is outlined in [1] using adjoint actions for the division algebras. In this scheme, the unbroken $SU(2) \times U(1)$ symmetry comes essentially from the algebra $\mathbb{H} \otimes \mathbb{C}$. The octonions are responsible for color $SU(3)$ symmetry. Here we focus mostly on the complex numbers and the quaternions, but we insist these fields occur only in a way that respects the underlying structure of all the division algebras.

With emergence, we can start with the broken symmetries, which from a measurement perspective are more fundamental. Right handed states need

not be singlet states, since the states are not defined with respect to the classical gauge symmetry, itself an emergent structure.

Including right handed (mirror) neutrinos, we can speak about standard Dirac neutrinos. At first sight there is no see-saw mechanism, since the right handed neutrinos do not set a large mass scale. On the other hand, a dual mass scale may define an effective see-saw. The mirror neutrino scale in the non local theory is identical to that of the left handed triplet, fixing the temperature of the CMB at $T = 2.725$ K. These mirror neutrinos are only observed in their manifestation as CMB photons. They come from a land of supersymmetric information, which dissolves the distinction between fermions and bosons. Every electroweak boson may be viewed as a Fourier dual to a fundamental lepton state: W^\pm from e^\pm , γ from ν_L , and Z from a composite of three right handed lepton states.

Although we speak about the possibility of mirror dark matter, it is unclear whether a mirror Lagrangian serves any useful purpose. It is natural to consider the right handed mirror neutrino as the only additional particle, and to disallow localisation for all other mirror states. However, since the dark matter problem is thoroughly addressed by mirror matter proposals, we consider it in the final chapter. Motivated by the mirror neutrino CMB photon, one might view all physical electroweak bosons as transformed mirror states, since the Fourier supersymmetry transform may be applied to the mirror sector. More radically, perhaps the mirror fermions stand for known particles: the protons and neutrons. In these two cases, there is no dark matter, and general relativity must be abandoned on large scales. This is quite plausible, since the non local ribbon diagrams display a preon aspect to any particle, and one imagines zooming in and out of a complicated network of bunched, knotted strands.

The particle states are specified by the most basic ribbon diagrams in three dimensions. As quantum numbers, spin and rest mass must emerge algebraically in a natural way from such diagrams, along with the Poincare group symmetries. The diagrams *concretely* display the two values of spin and three of rest mass. As each ribbon strand twists, it represents two spin states coupling to create mass. The three ribbon strands represent the three mass states, interacting on the non local stage as they propagate.

This self representation of a propagator is a motivic process. In traditional quantum field theory, motives already play an important role [2][3], wherein renormalisation is studied using algebras of Feynman diagrams. Motives were originally described by Grothendieck [4], who pioneered the study of higher dimensional categories [5] with arithmetic structure. For us, motives are an instruction set for building geometries out of quantum information. Their homological character is apparent in the algebraic structure of this information.

As pointed out by Street [5], the axioms of homology may be interpreted in almost any category. Recall the basic idea of singular homology, with

coefficients in \mathbb{Z} [6][7]. A well behaved topological space M is triangulated to provide the combinatorial data for the computation of invariants. Usually M has a fixed classical dimension, so that all its pieces are triangular n -simplices. An m -chain is a linear combination, with coefficients in \mathbb{Z} , of the m dimensional simplices of M . The sign of an integer coefficient may be used to orient cells. In this way, an edge between two faces contributes positively to one face and negatively to the other, canceling out in a boundary sum.

If M is a category, rather than a set, a simplex is naturally oriented [5]. Oriented simplices are little categories in their own right. When the vertices are labeled $\{0, 1, \dots, n\}$ they denote an ordinal n in \mathbb{N} , with inclusion maps. Every edge is modeled by a fundamental $0 \rightarrow 1$ arrow. To a category theorist, this arrow is the very foundation of topology, because the simplest topological space consists of one point and the empty set [8]. In the category of topological spaces, there is a unique arrow from this space to any other space.

Categories are not algebraically trivial. Already by dimension three, it is an arduous task to enumerate their axioms [9], let alone work with them. And yet, the axioms are specified by simple polytopes. How do these all fit together? This is the subject of higher dimensional arithmetic, where trees replace counting numbers. Some things are simpler in higher dimensions. For instance, while it is difficult to count the partitions of an ordinal $n \in \mathbb{N}$, the noncommutative partitions of n , which distinguish $1 + 2$ and $2 + 1$, are easy to count: there are always 2^{n-1} of them. This equals the number of basic states for $n - 1$ qubits.

In a category, a binary tree node usually represents an arrow $A \otimes A \rightarrow A$, which is perhaps a multiplication for an algebra A . Dual to arrows in a 2-category we have line diagrams, and these are thickened into ribbon networks in categories with duality structures. If algebra is hiding in the ribbons, there is no need to look to an ad hoc category of algebras to find the numbers one needs. Everything is made of ribbons, and motivic functors are morally endofunctors.

The fundamental particle states are drawn as ribbon graphs in chapter (7). Our job is to understand ribbons well enough to see beyond dimension 3. Since a ribbon is itself a picture of the continuum, we need to know exactly what this abstract embedding space represents, else the continuum has snuck in by hand yet again.

One might restrict one's attention to a one dimensional continuum, since nice spaces may be filled with curves, as first noted by Peano [10]. A modern example is Thurston's fractal curve for filling the two dimensional sphere [11]. When two ribbon edges twist about each other, they define a surface without the surface really being there, since the ribbons form a braid diagram built only with line elements.

In category theory, the power of space filling first appears in dimension 3, with the dimension raising Crans-Gray tensor product [12]. But dimension

3 is special because it is the realm of knots. There is a topology with respect to which the integers \mathbb{Z} are three dimensional, and many mathematicians hope that knots will explain this mysterious fact. Knots are Wilson loops in a three dimensional quantum field theory known as Chern-Simons theory [13]. It does not bother us that spacetime appears to be four dimensional, because in twistor physics it is really a three dimensional complex space. Once we understand this complexification in terms of the spinors of the ribbon strands, we are back to the real dimension 3 again. Ribbons with full twists are doubled knots, specifying two copies of \mathbb{R}^3 for the complex structure.

Abstractly, the use of category theory for mass matrices goes back to the 1980s, when twistor theorists attempted to put mass into the Klein-Gordon field equation using higher dimensional sheaf cohomology [14]. Their partial success hinged on a coupling of two massless fermion objects, which is now seen in the pairing of edges along a ribbon strand. This tells us that the crucial leap from H^1 to the H^2 cohomology comes from a doubling of the number of strands in a braid diagram, from B_3 to B_6 .

Our first application of these ribbon graphs is to the rest mass phenomenology of Koide matrices. The diagrams shed some light on the phase parameters, leaving only a scale factor for each mass triplet. Even these scales display remarkable coincidences. For instance, the charged lepton triplet requires a scale factor that equals the dynamical quark mass. The data also hints at a quark lepton complementarity.

So how do we actually *measure* differences in inertia? Consider a mass spectrometer, with a magnetic field used to separate a fixed velocity beam of charged electrons, muons and tau particles. The masses are measured by the radius of curvature, as the beam is split into three streams, marking three points on the detector. This is analogous to the two way split of a spin measurement for an electron. Altogether, the six detection points for mass and spin represent some basic element of emergent geometry. These are the six points that we work with in ribbon diagrams for measurement processes. Dimension building in categories is supposed to take care of everything else.

Spin brings to mind Newton's spinning bucket, and Mach's principle for motion with respect to the distant cosmos [15]. Imagine first an ideal liquid in a perfect bucket, so that when the bucket is at rest relative to the human observer, the medium of fluid particles creates a flat surface inside the bucket. When the bucket spins, the surface appears to be curved. Our observer does not see the individual particles of the fluid, or the motion of the perfect bucket, but rather one of two static states: a flat surface or a curved surface. Only under the hypothesis of *particles* do these static observations correspond to rest and circular motion respectively.

Similarly, a static braid diagram is supposed to represent the motion of a collection of point particles along a braid strand. But this does not occur in any universal, macroscopic time. There can be no universal arrow of time,

as Boltzmann taught us [16]. Rather, it is the clocks of quantum processes, determined by *our* experimental apparatuses and questions, that tick along braid circuits. When we ask for a rest mass diagram, we include a set of three interacting objects, even though these do not propagate together in our own corner of spacetime.

In other words, the universe is *observer dependent*. One might call this an anthropic perspective, except that the aim is to make quantitative predictions. Every observer has access to multiple types of clock, be it laboratory ticks based on the motion of the sun, or the temperature of the cosmic microwave background radiation.

Thermodynamics appears in the observer's environment, and as a matter of principle temperature and mass will be closely related, in addition to their inverse relation according to the Bekenstein-Hawking law for black hole radiation. Recall that a direct correspondence between mass and temperature is the key to Planck's original derivation for the black body spectrum [17], where the hypothesis of *quanta* hinged on Wien's displacement law. This is the key to the CMB mirror neutrino correspondence. The mirror neutrino mass triplet specifies the present CMB scale, along with one future and one past temperature. In this way, the rest mass triality extends the scale matching of duality into a notion of *present* for the observer. It is the thermal environment itself that determines the emergence of cosmic time.

Today, black hole thermodynamics in M theory is investigated using quantum information theory [18][19] and twistor physics [20]. Quantum black hole entropies are given quantitatively in terms of generalised matrix invariants via the black hole qubit correspondence. These invariants are the same as those used to classify entanglement classes for n qudit systems, under the assumption of local operations and classical communication.

The entanglement of particle pairs is also crucial to the twistor methods of $N = 4$ Yang-Mills theory and $N = 8$ supergravity [21][22][23]. In these recent developments for gravity, one studies the breaking of conformal symmetry by the so called infinity twistor, which sets a mass scale. Associated to the compactification of complexified Minkowski spacetime, this object gives twistor space its elegant projective structure. To a category theorist, abstract conformal field theories are the study of ribbon graphs [24][25]. Compactification issues become concrete, combinatorial problems for polytopes, and these are precisely the polytopes that appear in modern twistor techniques.

These polytopes appear in chapter 5, after introductory comments on sets, matrices, quantum information and duality. Chapter 6 introduces twistor scattering theory, and we move onto particle ribbon graphs in chapter 7. This is followed by a little further development of the motivic ideas. In the last chapter, we summarise the critical situation in relativistic cosmology from the perspective of non local mirror matter.

2 Numbers and Sets

Number constructivism starts with the idea that a real number should be much more than an element of a set. In mathematics, number fields are often given a priori, without much regard for the underlying set theoretic axioms. Manifolds are modeled on number fields as if the notion of continuum is naturally specified. Physically, this is an unsatisfactory state of affairs. Numbers are, after all, the outcomes of measurement, and the relations between them are contingent upon our theoretical frameworks.

Category theory offers a natural way to add structure to numbers. A counting number $n \in \mathbb{N}$ is both the cardinality of an n element set and the dimension of a category. When n stands for a set with n elements, the permutations of the set become part of the structure of the number n .

We use cycle notation for permutations σ in the permutation group S_d on d objects. For example, $\sigma = (312)$ in S_3 is the cycle

$$\begin{pmatrix} 0 & 0 & 1 \\ 1 & 0 & 0 \\ 0 & 1 & 0 \end{pmatrix}. \quad (1)$$

As an operation that acts on a *set*, a permutation matrix selects one element of the set with each row. This has an interpretation in terms of binary logic, since one can either select an element X or not select it, and hence the choice between 1 or 0.

With two such valuations one often uses the terms *true* and *false*. A system of logic evaluates propositional statements, which are built from an alphabet of objects and operations on these objects, including the truth valuations. We would like to think of all numbers as symbols for some quantum logic. In Boolean logic, one permits the binary operations AND (denoted by the symbol \wedge) and OR (denoted \vee). Since these operations are binary, there are only four basic statements involving them. For \vee these are $1 \vee 1 = 1$, $1 \vee 0 = 1$, $0 \vee 1 = 1$ and $0 \vee 0 = 0$, which is summarised in the matrix table

$$\vee : \begin{pmatrix} 0 & 1 \\ 1 & 1 \end{pmatrix}, \quad (2)$$

where the matrix index always starts with 0. The operation \vee is commutative, since $X \vee Y = Y \vee X$, so an extension of the matrix tables to a larger index set of objects always results in a symmetric matrix. Negation \neg is a unary operation that interchanges 0 and 1. Combining \wedge and \neg we have the table

$$\wedge \neg : \begin{pmatrix} 0 & 0 \\ 1 & 0 \end{pmatrix}. \quad (3)$$

The allowed letters 0 and 1 define the *alphabet* of the logic [8]. Every such 2×2 matrix, and there are 16, is in principle a truth table for an operation.

Such operations may then be used to define a matrix multiplication, since this requires only an abstract $+$ and \times on the underlying symbols.

Example 2.1 The finite field \mathbb{F}_2 has addition and multiplication tables

$$+ : \begin{pmatrix} 0 & 1 \\ 1 & 0 \end{pmatrix} \quad \times : \begin{pmatrix} 0 & 0 \\ 0 & 1 \end{pmatrix} \quad (4)$$

which generate ordinary matrix multiplication over \mathbb{F}_2 .

Example 2.2 The Boolean logic tables

$$\vee : \begin{pmatrix} 0 & 1 \\ 1 & 1 \end{pmatrix} \quad \wedge : \begin{pmatrix} 0 & 0 \\ 0 & 1 \end{pmatrix} \quad (5)$$

specify a matrix product, for matrices with 0 and 1 entries, such that there are 11 projectors satisfying $P^2 = P$. These are

$$\begin{aligned} & \begin{pmatrix} 0 & 0 \\ 0 & 0 \end{pmatrix}, \quad \begin{pmatrix} 0 & 0 \\ 0 & 1 \end{pmatrix}, \quad \begin{pmatrix} 1 & 0 \\ 0 & 0 \end{pmatrix}, \quad \begin{pmatrix} 1 & 1 \\ 1 & 1 \end{pmatrix}, \\ & \begin{pmatrix} 1 & 0 \\ 1 & 1 \end{pmatrix}, \quad \begin{pmatrix} 1 & 1 \\ 0 & 1 \end{pmatrix}, \quad \begin{pmatrix} 1 & 0 \\ 1 & 0 \end{pmatrix}, \quad \begin{pmatrix} 0 & 1 \\ 0 & 1 \end{pmatrix}, \\ & \begin{pmatrix} 1 & 1 \\ 0 & 0 \end{pmatrix}, \quad \begin{pmatrix} 0 & 0 \\ 1 & 1 \end{pmatrix}, \quad \begin{pmatrix} 1 & 0 \\ 0 & 1 \end{pmatrix}. \end{aligned} \quad (6)$$

Projectors in an algebra are physically important. They appear in the planar diagram algebras that we study here [26], where the creation of a loop represents a scalar factor δ in the relation $P^2 = \delta P$. There are often only a finite number of them, because we are interested in restricted coefficient sets.

Although our finite alphabets are sometimes labeled by ordinals $\{0, 1, 2, \dots, n\}$, they are given generally by variable elements $\{X, Y, Z, \dots\}$. A binary operation for an n element alphabet gives an $n \times n$ matrix table of truth values, as in the example

$$\begin{pmatrix} XX & XY & XZ \\ YX & YY & YZ \\ ZX & ZY & ZZ \end{pmatrix}. \quad (7)$$

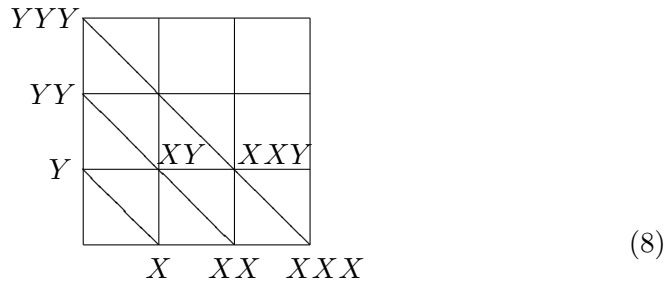
Similarly, a ternary operation would specify an $n \times n \times n$ array. Partial domains for operations allow a generalisation to $n_1 \times n_2 \times \dots \times n_k$ rectangular arrays. The dimension l of an array, if it is fixed, is the word length of the components. In what follows we focus mostly on square matrices, namely the truth tables for words of length 2.

2.1 The Word Monoid

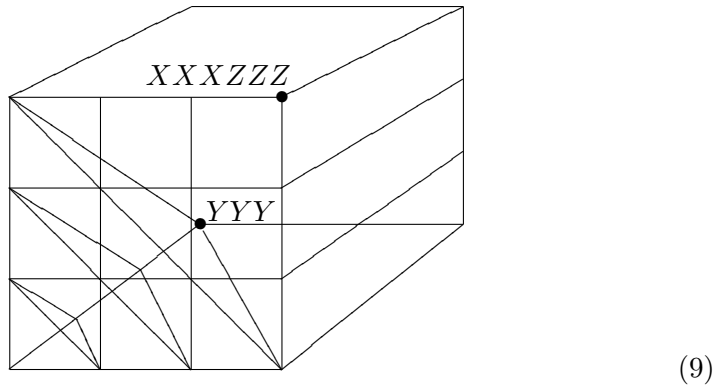
Polynomials are a lot like numbers. They can be added and multiplied, and usually inherit the distributivity of the coefficient field. The existence of noncommutative geometry suggests looking also at noncommutative polynomials. These are closely connected to quantum path spaces, since a monomial like XZX is interpreted as a sequence of noncommutative operations.

A noncommutative monomial is a single word in the letters of a given alphabet. The number of letters d determines the dimension d of a discrete cubic path space, defined by marking one letter steps along each axis. Here, d is usually the dimension of a quantum state space. When $d = 2$, we think of states of a *qubit* [27].

The *word monoid* is the collection of all finite noncommutative monomials, with concatenation of words as a noncommutative product. The qubit words are graded by the diagonals of the path square.

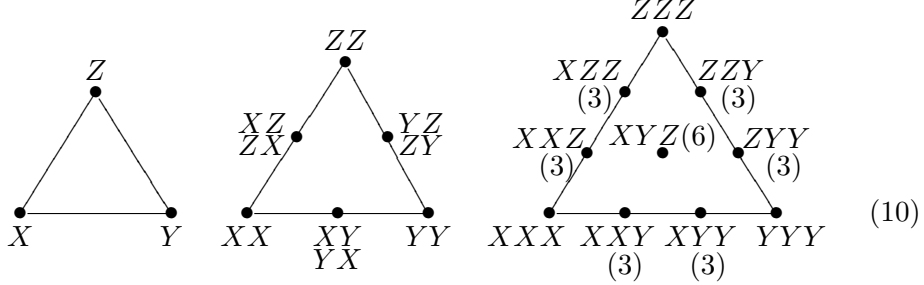


where both XY and YX end at the same point. Similarly, the qutrit words, in a three letter alphabet, sit on the triangular diagonal simplices of a path cube.



The edges of the triangle at word length l are divided into l pieces. In general, this creates triangular simplices with ruled edges. The first few simplices for qutrits are labeled so that the ten sets of unordered monomials on the tetractys contain a total of 27 paths. In general, the length 1 words

in a d letter alphabet form a standard triangular simplex in dimension $d - 1$.

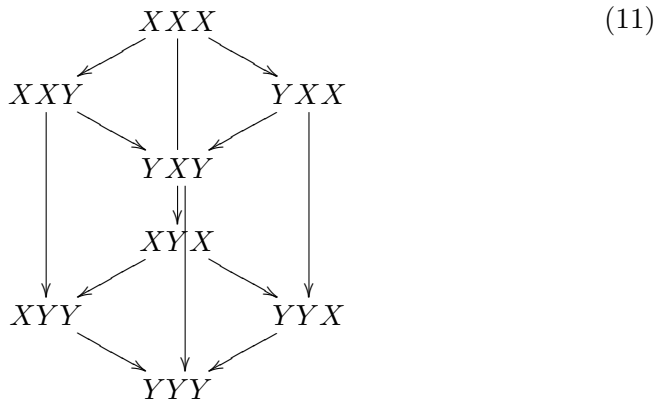


Measured simplices of longer word length will be used in the construction of interesting polytopes, starting in chapter 5.

The entire word monoid is graded in a table indexed by both l and d . There are no repeated words, because we assume that letters carry a knowledge of what alphabet they belong to. The first column of the monoid, for $l = 1$ letter, gives the standard simplex of dimension $d - 1$. The $l = 2$ column gives the halved simplices with d^2 paths. For the qutrit tetractys and beyond, we have the further option of bracketing words, distinguishing $(XY)Z$ and $X(YZ)$. We talk about $(d - 1, l)$ simplices, where $d - 1$ is the simplex dimension and l numbers the divisions along an edge.

A divided simplex is canonically coordinatised in the integer lattice \mathbb{Z}^d . Since the monomials in a diagram are of homogeneous degree, the sum of degrees over the letters in the word is always a constant. For the length two words in three letters, we then choose six vectors in \mathbb{Z}^3 that correspond to the degrees of X , Y and Z in each monomial. These are $(2, 0, 0)$, $(0, 2, 0)$, $(0, 0, 2)$, $(1, 1, 0)$, $(1, 0, 1)$ and $(0, 1, 1)$.

A $(d - 1, l)$ path simplex in path space is naturally expanded into the noncommutative cubic array. For example, the $(2, 3)$ tensor cube looks like



where we have shown how the cube can be oriented by $X \rightarrow Y$. See what has happened here. The path space gives both $(d - 1, l)$ divided simplices and $(l, d - 1)$ divided cubes. The two integers of the grading are swapped

between simplices and cubes. A tensor cube is a model for a matrix or array, like in (7). Arrays may be decomposed into symmetric and antisymmetric parts, as in

$$\begin{pmatrix} XX & XY \\ XY & YY \end{pmatrix} + \begin{pmatrix} 0 & 0 \\ YX - XY & 0 \end{pmatrix}. \quad (12)$$

The square arrays pick out two numbers, in this case 3 and 1, that partition d^2 into triangular simplices. One of these simplices accounts for the commutative path set. The second may be drawn inside the first using the midpoints of the divided simplex. For $d = 4$ this extends to an octahedron with vertices XY, YZ, ZW, XZ, XW and YW .

Remark 2.3 It turns out that any knot diagram can be represented as a word in four letters, on the surface of the universal ribbon graph of Ghrist [28]. Knots are embedded in this special branched surface as loops around four attractor holes, with crossing points at the branches. Such a branched surface is non orientable, in the sense that one can pass from one side of the ribbon to the other at the branch line without passing across a ribbon edge.

The noncommutative monomials on a divided simplex correspond one to one to a set of commutative monomials, as follows. Use the canonical coordinates to specify the powers of l variables p_1, p_2, \dots, p_l . For example, at $d \geq 2$ the words 000, 001, 011 and 111, along with permutations, give the monomials $1, \{p_1, p_2, p_3\}, \{p_1 p_2, p_1 p_3, p_2 p_3\}$ and $p_1 p_2 p_3$ respectively. This is the cube of set inclusions, or the list of divisors of $n = p_1 p_2 p_3$ in \mathbb{N} . The order of the letters in the noncommutative word specifies the variable choice, and the letter value denotes the power. In this way, divisors for any $n \in \mathbb{N}$ of the form $(p_1 \dots p_l)^{d-1}$ are listed on a qudit tensor cube, and arithmetic is then the subject of qudits.

Observe that a square matrix is typically a projector. For two complex conjugates p and \bar{p} , the 3×3 divisor matrix becomes

$$\begin{pmatrix} 1 & p & p^2 \\ \bar{p} & |p|^2 & |p|^2 p \\ \bar{p}^2 & |p|^2 \bar{p} & |p|^4 \end{pmatrix} = \begin{pmatrix} X\bar{X} & X\bar{Y} & X\bar{Z} \\ Y\bar{X} & Y\bar{Y} & Y\bar{Z} \\ Z\bar{X} & Z\bar{Y} & Z\bar{Z} \end{pmatrix}, \quad (13)$$

using the vectors $(1, p, p^2)^T$ and $(1, \bar{p}, \bar{p}^2)$. This contrasts with the real number case of vectors like (X, Y, Z) for the matrix index. The 2×2 complex case underlies the spinor decomposition for twistor physics, with (X, \bar{X}, Y, \bar{Y}) standing for four independent complex variables. In the word monoid, this 2×2 matrix is a submatrix of the 4×4 matrix for 4-dits.

2.2 Continua and Quantum Numbers

Since we don't like unnecessary set theoretic axioms, such as the axiom of choice, sets are always zero dimensional categories. If the geometry and

algebra of interest *looks* more than zero dimensional, then we know that sets won't do. The central problem of constructive arithmetic is to understand the extension from the countable rationals \mathbb{Q} to the complex numbers \mathbb{C} . Even \mathbb{Q} is a difficult beast, with many finite number field extensions for which there is no unique factorisation, until one goes to the theory of ideals.

Continuum fields like \mathbb{R} and \mathbb{C} require dissection into categorical structures of uncountable dimension. This is a very concrete idea, because we can begin with countable subsets. For instance, as everyone knows, the sixth complex root of unity $\omega_6 = \exp(2\pi i/3)$ is actually the infinite sequence

$$\omega_6 = 1 + 1 + 2 + 5 + 14 + 42 + \dots \quad (14)$$

of integer Catalan numbers [29][30]. As we will see, these Catalan numbers count rooted planar binary trees, and ω_6 is the *cardinality* of this infinite set of trees.

We can then do arithmetic using the first infinite cardinal, usually called ω . In the surreal number tree [31] construction for \mathbb{R} , ω appears after an infinite number of steps along one side of the surreal number tree. Despite appearances, there are no infinities around in the computations, which depend only on the correct rules for manipulating functions in ω and its infinitesimal inverse ω^{-1} . The surreal tree root marks the number 0, which branches to ± 1 . Then ω is the infinite sequence $(++++\dots)$, and ω^{-1} is the sequence $(-----\dots)$, where a sign marks the direction of the chosen branch. Immediately after 1 we obtain $3/2$ and $1/2$, and thereafter one uses the difference $\pm 2^{-n}$ at step $n + 1$. Only the dyadic numbers are obtained in a finite number of steps, but all the reals appear at step ω . In the surreals, this branching process continues beyond ω , to polynomials in ω and ω^ω and beyond.

Returning to matrices, we can start with the binary entries 0 and 1, gradually adding further numbers as information structures require them. The basic permutation

$$(21) = \begin{pmatrix} 0 & 1 \\ 1 & 0 \end{pmatrix}$$

can represent the number -1 , since $(21)^2 = I_2$. Thus $k \times k$ matrices with entries in $\{0, \pm 1\}$ can be written as $2k \times 2k$ matrices with entries in $\{0, 1\}$. For instance, the Pauli matrix σ_Z becomes the controlled NOT gate for two qubits [27]. The permutation (2341) similarly represents the complex number i , so that 2×2 matrices with entries in $\{0, \pm 1, \pm i\}$ could be expressed as 8×8 matrices with entries in $\{0, 1\}$. Pauli matrices would then be permutations in S_8 .

The entire set of complex numbers requires an uncountable matrix index! Fortunately, in practice we never work with all complex numbers at once. Rather than write out larger and larger binary matrices, we sensibly consider small sets of complex $d \times d$ matrices with special properties. We will often

restrict to those of circulant form for $d = 2$ and $d = 3$, since these are combinations of the permutation matrices.

The modular group $SL(2, \mathbb{Z})$ permits a deformation into the complex numbers such that the matrices are still interpreted as integers, known as *q-numbers* [32][33][34]. A complex parameter $q \neq 0$ defines the q-number

$$\lrcorner n \lrcorner q = \frac{q^{n/2} - q^{-n/2}}{q^{1/2} - q^{-1/2}} \quad (15)$$

for n usually in \mathbb{N} . As $q \rightarrow 1$, the classical number is recovered. The sum of such numbers is given by

$$\lrcorner m \lrcorner q + \lrcorner n \lrcorner q \equiv q^{-n/2} \lrcorner m \lrcorner q + q^{m/2} \lrcorner n \lrcorner q, \quad (16)$$

and for $n \in \mathbb{R}$, a copy of the ordered reals is obtained. For $n \in \mathbb{Z}$, the q-number $\lrcorner n \lrcorner q$ is a polynomial in $\lrcorner 2 \lrcorner q$ with integer coefficients [32][33]. So in some sense, every number is a polynomial!

In general, such numbers are used to deform commutative or cocommutative Hopf algebras. In particular, recall the Lie algebra $sl(2, \mathbb{F})$. Its irreducible representations R_k are given by the commutative, homogeneous polynomials of degree k in two variables X and Y [32][33], giving a plane. The natural deformation of the plane (X, Y) introduces a relation

$$YX = qXY. \quad (17)$$

The deformed matrices $M_q(2)$ acts on this plane as follows. These matrices

$$T = \begin{pmatrix} a & b \\ c & d \end{pmatrix} \quad (18)$$

satisfy the quantum relations

$$\begin{aligned} ab &= q^{-1/2}ba, & ac &= q^{-1/2}ca, & bd &= q^{-1/2}db, \\ cd &= q^{-1/2}dc, & bc &= cb, & ad - da &= -(q^{1/2} - q^{-1/2})bc. \end{aligned} \quad (19)$$

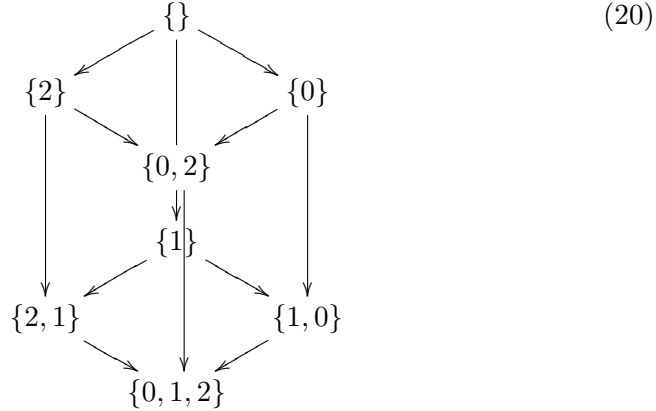
The quantum plane variables (X, Y) define a complex variable $z = YX^{-1}$. As with classical fractional linear transformations, one may construct an action of T on a polynomial $\phi(z)$. In particular, we can restrict to those matrices in $M_q(2)$ with quantum determinant $ad - q^{-1/2}bc = 1$.

The matrix entries may be thought of as functions on the group, making them elements of the deformed Hopf algebra. Dually, one deforms the universal enveloping algebra of a Lie algebra. Such algebras typically exist for any $q \in \mathbb{C} \setminus 0$, but for roots of unity the representation categories have nice properties. When \mathbb{C} is constructive, we care about each individual choice for q . For example, choosing the cubed root of unity $q = \omega_3$, the number $\lrcorner 2 \lrcorner q$ equals $\sqrt{3}i$. This introduces integers from the quadratic field $\mathbb{Q}(\sqrt{-3})$, and we begin to suspect that everything is an integer in disguise.

2.3 Union, Disjoint Union and Cohomology

For a mathematician, motives are supposed to provide a universal theory for cohomological invariants. To a physicist however, the invariants themselves are responsible for the emergence of classical spaces. It is surely a chicken and egg problem, trying to say that a torus has a hole without looking at the torus. Presumably one must look at a picture of a torus, but as a symbol rather than a complete classical space. Anyway, we need some idea of what cohomology is about.

Let $A_1 \cup A_2$ denote the union of two sets A_1 and A_2 , and $A_1 \cap A_2$ their intersection. We write $A_1 \coprod A_2$ for the disjoint union. For a three element set $\{0, 1, 2\}$, the subsets are illustrated on the cubic lattice of set inclusions



ending in $\{0, 1, 2\}$. Note that this cube is very similar to the commutative monomial cube from the word monoid, given variables p_0 , p_1 and p_2 , but instead of primes we multiply finite sets. To a category theorist, a finite set is simply a weaker representation of its own cardinality in \mathbb{N} .

The six elements at path length 2 actually give *two* copies of $\{0, 1, 2\}$ on taking the total disjoint union, so somehow one copy is taken away to recover the union $\{0, 1, 2\}$. This is like the omission of the factors n/p on division by the divisors p of n . Observe that the disjoint union here is definitely bigger than the resulting union. Now consider the principle of *inclusion exclusion*. Although often expressed in terms of cardinalities, we can write

$$A \cup B \cup C = A \coprod B \coprod C - A \cap B - B \cap C - C \cap A + A \cap B \cap C \quad (21)$$

for three sets, where it is understood that the cardinality of $A \coprod B$ equals $|A| + |B|$. In general

$$\bigcup_i A_i = \coprod A_i - \sum_{i,j} A_i \cap A_j + \sum_{i,j,k} A_i \cap A_j \cap A_k - \dots \quad (22)$$

These alternating sums of intersections are responsible for the alternating sums that appear in Čech cohomology [35][36], which uses open covers of

a classical manifold. A classical cover of open sets U_i for a space M is a *good cover* if all intersections $U_i \cap U_j$ are either empty or contractible. For example, the Riemann sphere $\mathbb{C}\mathbb{P}^1$ requires three open sets. Two is not sufficient, because an equatorial intersection is not contractible to a point. In this example, all possible intersections up to $U_1 \cap U_2 \cap U_3$ give the cube

$$\begin{array}{ccccc}
 & & U_1 \cap U_2 \cap U_3 & & \\
 & \swarrow & \downarrow & \searrow & \\
 U_2 \cap U_3 & & & & U_1 \cap U_2 \\
 & \swarrow & \downarrow & \searrow & \\
 & & U_2 & & \\
 & & \downarrow & & \\
 & & U_1 \cap U_3 & & \\
 & \swarrow & \downarrow & \searrow & \\
 U_3 & & & & U_1 \\
 & \swarrow & \downarrow & \searrow & \\
 & & M & &
 \end{array} \tag{23}$$

which is indexed by the original cube above. All arrows are again inclusions. For all good covers, the nested intersections define such a cube. Tracing a path backwards from M , one may encounter an empty intersection $U_i \cap \dots \cap U_k$. In that case, all objects above $U_i \cap \dots \cap U_k$ must be empty. Thus a cube is partitioned into two pieces: a top part marked with empty sets and the base with non empty ones. This binary partition is part of the topological data defining M . Since the basis directions on the cube represent the sets U_i in the cover, the objects at each node of the cube are fully specified once a basis is chosen. For example, the matrix

$$\begin{pmatrix} 0 & U_1 \\ U_2 & U_1 \cap U_2 \end{pmatrix}.$$

gives the incidence data for a general cover containing two open sets. The lattice of open sets for M is clearly a category, which we call $L(M)$. A reversal of the inclusion arrows, to set restrictions, defines the opposite category $L(M)^*$. A *presheaf* on M is a functor F from $L(M)^*$ into an algebraic category, such as the category of abelian groups.

For any such presheaf F , the 0-cochains of Čech cohomology [35] are the maps that send U_i to an element in $F(U_i)$. Then the 1-cochains come from $U_i \cap U_j$, and so on. The inclusion maps on the lattice induce a sequence of homomorphisms in the algebraic data, and the coboundary operator δ from d -cochains to $(d + 1)$ -cochains is defined as usual by an alternating sum. For $d = 0$, $\delta \equiv F(i_1) - F(i_2)$ on the two inclusion arrows i_1 and i_2 for $U_i \cap U_j \rightarrow U_i$. That is, for two open sets U and V there are inclusion maps

$$U \cap V \rightrightarrows U \amalg V \rightrightarrows U \cup V \tag{24}$$

where a map on the left chooses one of the two sets, ignoring the other. Classically, there is only one inclusion on the right, but we permit the possibility of distinct inclusions for noncommutative objects U and V .

The Mayer-Vietoris principle for the de Rham cohomology of manifolds uses the differential form functor, applied to the sequence (24). What is the useful intuition behind Mayer-Vietoris? When the differential form functor F is applied, it gives a reversed sequence of restriction maps

$$F(U \cup V) \rightarrow F(U) \oplus F(V) \rightarrow F(U \cap V) \quad (25)$$

where the double map is absorbed into the algebraic splitting $F(U) \oplus F(V)$. Clearly there should be more differential forms in $F(U \cup V)$ than in the disjoint $F(U) \oplus F(V)$, which has no joining information. This is really the point of considering $U \cup V$ as a larger object.

When F is a 1-functor there is no way to avoid the set like properties of unions, but we will not be restricting the categorical dimension. Consider, for instance, the sequence of inclusions

$$\coprod_{ijk} U_i \cap U_j \cap U_k \rightrightarrows \coprod_{ij} U_i \cap U_j \rightrightarrows \coprod_i U_i \rightarrow M \quad (26)$$

on a cube, which form a simplex, in this case a tetrahedron. In the word monoid, the vertices become the four qubit objects XXX , XXY , XYY and YYY and the inclusions end with the unique map $Y^0 \rightarrow Y^1$ from XXX . The qubit diagrams are permitted to live in a higher dimensional category, where the faces of the tetrahedron contain 2-arrows.

2.4 A Category of Relations

Please refer to Appendix A for the basic definitions of categories. This is our first categorical interlude. In the category **Set** of all sets, the inclusion of disjoint union in union is given in a coproduct diagram

$$\begin{array}{ccc} \{\} & \xrightarrow{!} & A \\ \downarrow ! & & \downarrow \\ B & \xrightarrow{\quad} & A \amalg B \\ & \searrow b & \downarrow i \\ & & A \cup B \end{array} \quad (27)$$

where $!$ is the unique inclusion of the empty set in any set. The coproduct property of \amalg states that for any maps a and b , there exists an inclusion i . When one does not adopt **Set** as a base category, this assumption may be weakened. Actually, we should start with an even better category of sets.

Let a finite index set be denoted J . It has cardinality $n = |J|$. An $n \times n$ matrix of zeroes and ones is a map $J \times J \rightarrow \Omega$. For example, when $n = 3$

the permutation (231) picks out the elements (X, Y) , (Y, Z) and (Z, X) in $J \times J$. That is, (231) sends the vector (X, Y, Z) to the vector (Y, Z, X) . This is a one to one function $J \rightarrow J$, but the use of a *relation* $J \times J \rightarrow \Omega$ is closer to the idea of a truth table.

Every square matrix may be viewed as a map $J \times J \rightarrow T$ for some set T of allowed truth values. The reason for choosing 0 and 1 as truth values is that these actually correspond to the cardinalities of the empty set and a one element set, respectively. More generally, for arbitrary relations, T can have any cardinality.

The choice of 0 or 1 as a means of selecting a subset J of K may be expressed using a diagram of functions between sets, where χ is the *characteristic function* that sends elements of J to 1 and the other elements to 0.

$$\begin{array}{ccc} J & \longrightarrow & K \\ \text{!} \downarrow & & \downarrow \chi \\ 1 & \xrightarrow{t} & \Omega \end{array} \quad (28)$$

In the diagram, the set 1 is any one element set, and the function t picks out *true*, namely the element 1 in Ω . The vertical arrow $!$ is unique, because there is only one function into a one element set. This diagram lives in the category **Set**, which is then a *topos* [37][8]. Similarly, the category **Rel** of sets and relations contains the square

$$\begin{array}{ccc} (J \times J) \times (J \times J) & \xrightarrow{r_1 \times r_2} & K \times K \\ \text{!} \downarrow & & \downarrow \chi \\ 1 \simeq 1 \times 1 & \xrightarrow{t} & \Omega \end{array} \quad (29)$$

where any one point set is isomorphic to the Cartesian product of two one point sets. When $J \times J$ is a subset of K , via both r_1 and r_2 , the square commutes, in the sense that both paths lead to the same relation $(J \times J)^2 \rightarrow \Omega$.

When $K = \Omega$, the relations r_i stand for matrices of zeroes and ones, and χ is a basic 2×2 table. We would like $r_1 \times r_2$ to be a tensor product of matrices, with respect to χ , because $|J \times J| = |J|^2$.

3 Duality and the Fourier Transform

Engineers and physicists learn that complex numbers are perfect for describing the properties of waves, but in emergent geometry waves do not give an ideal picture of what happens when quantum objects interact. In the word monoid, complex numbers were associated to the distinction between the letters X and \overline{X} , which appear when a projector is interpreted as a density matrix for a qudit state.

Consider the case of a qubit space. In a real plane, $(1, 1)$ and $(1, -1)$ are eigenvectors for the real Pauli matrix σ_X , which represents a spin measurement in the direction X . Together they give an orthogonal basis for the plane. These eigenvectors form the columns of the 2×2 Hadamard gate [27] of quantum computation,

$$F_2 = \frac{1}{\sqrt{2}} \begin{pmatrix} 1 & 1 \\ 1 & -1 \end{pmatrix}. \quad (30)$$

When it acts via conjugation $F_2 M F_2^\dagger$ on a matrix M , this is the quantum Fourier transform in dimension 2. Unlike in higher dimensions, where F_d^4 is the identity, F_2^2 is already the identity I_2 . This is another way of saying that we need a complex i in dimension 2, so that iF_2 shares the defining property of the higher dimensional transforms.

The quantum Fourier transform is the analogue, for a discrete set of non-commuting points, of the classical Fourier transform. Classical duality for the Fourier transform uses a rich notion of duality from harmonic analysis, and this may be formulated in the language of categories as *Stone duality* [38]. Such concepts are central to categorical attempts at unifying spaces and algebras in a motivic context.

The next section introduces the quantum Fourier transform, and the following section the important arithmetic concept of *mutually unbiased basis*.

3.1 The Quantum Fourier Transform

As usual, the indices of a finite matrix take values $i, j \in 0, 1, 2, \dots, d-1$. The primitive d th root of unity $\exp(2\pi i/d)$ will be denoted ω_d . The d dimensional Fourier transform F_d defines a matrix transform $F_d M F_d^\dagger$ on a $d \times d$ matrix M . It is usually given by [27]

$$(F_d)_{ij} = \frac{1}{\sqrt{d}} (\omega_d)^{ij}. \quad (31)$$

The choice of ω_d rather than $\overline{\omega_d}$ is arbitrary, as is the choice of row and column order. That is, there are a total of $2d^2$ matrices that we might have written down for F_d . All are elements of the unitary group $U(d)$, since $F_d F_d^\dagger$ equals the identity matrix I_d .

Let D_d be the democratic probability matrix with entries all equal to $1/\sqrt{d}$. For example,

$$D_3 = \frac{1}{\sqrt{3}} \begin{pmatrix} 1 & 1 & 1 \\ 1 & 1 & 1 \\ 1 & 1 & 1 \end{pmatrix}.$$

The elementary matrix E_{ij} , with only one non zero entry equal to 1 in the position ij , is given by $E_{ij} = F_d(D_d)$ for one of the d^2 choices for F_d , at a fixed ordering for the complex roots. This gives a decomposition of all square matrices in terms of multiples of the democratic matrix. The democratic matrix D_d is itself a unit for the Schur product of matrices, defined entrywise by $(AB)_{ij} = A_{ij}B_{ij}$.

A quantum *Fourier series* is a $d \times d$ 1-circulant matrix, which is specified by its first row, with each successive row a right cyclic shift, by one step, of the first row. For $d = 3$, it is given by $a_1I + a_2(231) + a_3(312)$. The Fourier transform of such a circulant is a diagonal matrix, as in

$$\frac{1}{2} \begin{pmatrix} 1 & 1 \\ 1 & -1 \end{pmatrix} \begin{pmatrix} a & b \\ b & a \end{pmatrix} \begin{pmatrix} 1 & 1 \\ 1 & -1 \end{pmatrix} = \begin{pmatrix} a+b & 0 \\ 0 & a-b \end{pmatrix} \quad (32)$$

for the simplest 2×2 case. Thus a Fourier series is a linear combination of cyclic permutation matrices from S_d . Inversely, the Fourier transform of a diagonal matrix is a 1-circulant matrix.

Observe that the entries of F_d only take values in the complex d th roots of unity. When $d+1$ is a prime power, these d roots represent the d non zero elements of the field \mathbb{F}_{d+1} with $d+1$ elements, along with their multiplication table. When $d = 3$, we choose

$$F_3 = \frac{1}{\sqrt{3}} \begin{pmatrix} 1 & 1 & 1 \\ 1 & \omega_3 & \bar{\omega}_3 \\ 1 & \bar{\omega}_3 & \omega_3 \end{pmatrix} \quad (33)$$

and its complex conjugate F_3^\dagger . For $d = 3$ there exist both 1-circulants, for the odd elements of S_3 , and 2-circulants, for the even permutations in the S_2 subgroups. Including the determinant zero 0-circulants, there are always d classes of circulant. For $d = 3$, let

$$x = \begin{pmatrix} 0 & 1 & 0 \\ 0 & 0 & 1 \\ 1 & 0 & 0 \end{pmatrix} \quad p = \begin{pmatrix} 1 & 0 & 0 \\ 0 & \omega_3 & 0 \\ 0 & 0 & \bar{\omega}_3 \end{pmatrix}. \quad (34)$$

Observe that $xp = \omega_3px$. This is a Weyl commutation relation [39], usually written with an \hbar . It also expresses the noncommutativity of a quantum plane (x, p) with q a root of unity. Cycles of x define three points for the space, and there are 3 forms for the momentum p , giving a six point phase space.

The matrix F_d is the character table for the finite abelian cyclic group with d elements. This group is generated by a 1-circulant in S_d , and the Fourier series is a sum over the cyclic group. Such a $d \times d$ circulant is then an element of the group algebra $\mathbb{C}S_d$ for the permutation group S_d . These Hopf algebras appear in appendix C. In much of what follows, we would like to restrict attention to circulant matrices.

3.2 Unitary Bases and Decompositions

The normalised Pauli spin matrices

$$\sigma_X = \frac{1}{\sqrt{2}} \begin{pmatrix} 0 & 1 \\ 1 & 0 \end{pmatrix} \quad \sigma_Y = \frac{1}{\sqrt{2}} \begin{pmatrix} 0 & i \\ -i & 0 \end{pmatrix} \quad \sigma_Z = \frac{1}{\sqrt{2}} \begin{pmatrix} 1 & 0 \\ 0 & -1 \end{pmatrix} \quad (35)$$

define three directions in laboratory space. These matrices, along with the identity I_2 , form a basis for the quaternions \mathbb{H} , in the form

$$Q = x^0 I_2 + x^1 \sigma_X + x^2 \sigma_Y + x^3 \sigma_Z = \frac{1}{\sqrt{2}} \begin{pmatrix} x^3 + x^0 & x^1 + ix^2 \\ x^1 - ix^2 & x^3 - x^0 \end{pmatrix}. \quad (36)$$

When the x^i are complex, (x^0, x^1, x^2, x^3) is a point in complexified Minkowski space \mathbb{C}^4 , with x^0 playing the role of time. This 2×2 form leads naturally to twistor geometry [40][41]. We will always take Minkowski space to be in matrix form. The Pauli matrices are used to create projectors that are normalised forms of $I_2 + \sigma_i$,

$$X = \frac{1}{2} \begin{pmatrix} 1 & 1 \\ 1 & 1 \end{pmatrix} \quad Y = \frac{1}{2} \begin{pmatrix} 1 & i \\ -i & 1 \end{pmatrix} \quad Z = \begin{pmatrix} 1 & 0 \\ 0 & 0 \end{pmatrix}. \quad (37)$$

A noncommutative path with the same end points, such as $XYZX$, is an analogue to a loop in a commutative space. The loop is directed because $YZ \neq ZY$. A point X is a kind of trivial loop. Observe that the product $XYZX$ equals $\exp(-\pi i/4)X$. In order to cancel the anomalous phase in a loop, and maintain a law $XYZX \simeq X$, each of X , Y and Z is multiplied by the basic phase $\omega_{24} = \exp(\pi i/12)$.

The classical fundamental group $\pi_1(M, x)$ of a space M is the group of all path loops based at a point x , with loop reversal as an inverse. The rule $XYZX \simeq X$ for noncommutative paths is then a statement of *contractibility*, saying that loops can be shrunk without hitting any obstacles. This rule is no longer strict, because there is a scale factor of $1/2\sqrt{2}$ on traversing the loop.

The Pauli matrices are themselves a noncommutative analogue of the cubed roots of unity, in the sense that

$$1 + \overline{\omega_3} = -\omega_3 \quad \omega_3 + 1 = -\overline{\omega_3} \quad \overline{\omega_3} + \omega_3 = -1 \quad (38)$$

may be turned into a product rule. The *Pauli group* [27] for one qubit is the group generated by $\{I_2, \sigma_X, \sigma_Y, \sigma_Z\}$ with coefficients in $\{\pm 1, \pm i\}$.

Each Pauli matrix has a pair of eigenvectors, one for each eigenvalue $\pm 1/2$. The eigenvector pair forms the columns of another 2×2 matrix. Since an eigenvector is unchanged under multiplication by a complex scalar, there are many equivalent forms for such operators.

The three eigenvector matrices form what is known as a set of *mutually unbiased bases* for dimension $d = 2$ [42][43][44]. Any two members M_1 and M_2 of the set have the property that the inner product $\langle v_1 | v_2 \rangle$, for an eigenvector v_1 in M_1 and eigenvector v_2 in M_2 , is always of norm square $1/d$. For example, take the eigenvectors $(1, -1)$ and $(1, 0)$, and remember the normalisation factor of $1/\sqrt{2}$ for $(1, -1)$. The Pauli matrices provide a maximal set of $d + 1 = 3$ such bases for dimension 2.

The $d + 1$ mutually unbiased bases [43][44] in prime power dimension $d = p^k$ are given by a $d \times d$ matrix set $\{F_d, R_d, R_d^2, \dots, R_d^d\}$, where R_d is a unitary circulant matrix. First,

$$R_2 = \frac{1}{\sqrt{2}} \begin{pmatrix} 1 & i \\ i & 1 \end{pmatrix}. \quad (39)$$

We can use $R_2^8 = I_2$ to specify the three mutually unbiased bases $\{F_2, R_2, I\}$ in dimension 2, since

$$R_2^2 = e^{i\pi/4} \sigma_X$$

has a zero diagonal, and so provides essentially the same eigenvectors as the identity I_2 . In dimension 3 a convenient choice is

$$R_3 = \frac{1}{\sqrt{3}} \begin{pmatrix} 1 & \omega_3 & 1 \\ 1 & 1 & \omega_3 \\ \omega_3 & 1 & 1 \end{pmatrix} \quad (40)$$

for ω_3 the cubed root of unity, so that $R_3^3 = I_3$ up to a phase i . The set of four mutually unbiased bases is $\{F_3, R_3, R_3^2, I\}$. The circulants $\{R_3, R_3^{-1}, I\}$ represent multiplication in the finite field \mathbb{F}_4 . The Fourier matrix F_3 represents the zero in the weak sense that $F_3 R_3$ is another form of F_3 . The general circulant R_d in odd dimension d is

$$(R_d)_{ij} = \frac{1}{\sqrt{d}} (\omega_d)^{(k-j)(j-k+1)/2} \quad (41)$$

for $i, j \in \{0, 1, \dots, d-1\}$ [45][46]. When $d = 1$ any phase defines a basis that is mutually unbiased with respect to another phase, since phases always multiply to a number of norm 1. In this way, \mathbb{C} is clearly of uncountable dimension. However, we imagine that two bases are sufficient to characterise the one dimensional space. These should be F_1 and $I_1 = 1$, where F_1 must be i in order to have the Fourier property.

Let us look closer at the Pauli bases in dimension 2. The diagonal element 1 of R_2 will be generalised to a rotation parameter. The R_2 matrix is defined by the phase $t = \pm\pi/2$, which is special as a fixed point under the map $t \mapsto -1/t$. With the normalisation factors taken as given, the general circulants in $\mathbb{C}S_2$ are written as

$$R_2(r) \equiv R(r) = \begin{pmatrix} r & i \\ i & r \end{pmatrix} \quad (42)$$

for $r \in \mathbb{R}^+$. This is the general Fourier transform of a diagonal

$$\begin{pmatrix} z & 0 \\ 0 & \bar{z} \end{pmatrix} \quad (43)$$

for z a complex number, under the scaling invariance $z \mapsto \lambda z$ with λ real. With the normalisation convention we are free to put the ratio of real to imaginary parts into the parameter r . Such an $R_2(r)$ is no longer unbiased with respect to F_2 and I_2 , but instead stands for a general 2×2 probability matrix.

When $r > 1$, $(R(r))^2$ has non zero diagonal elements $r_2 \equiv r^2 - 1$, as does the n th power $(R(r))^n$. However, as $n \rightarrow \infty$ the parameter r_n approaches zero, because it goes as r/n . The recursion is given by

$$r_{j+1} = \frac{rr_j - 1}{r_j + r} \quad (44)$$

where $r = r_1$. Thus $(R(r))^\infty$ looks like R_2^2 . Observe that the sequence is monotonic if and only if $r \geq \phi$, where $\phi \sim 1.618$ is the Golden ratio. Since an infinite number of time steps was never a problem for tortoises or hares, we can repeat the process and observe that

$$(R(r)^\infty)^4 R(r) = R(r). \quad (45)$$

Thus for any $r \geq 1$, $R(r)$ has an infinite cyclicity. Moreover,

$$(R(r))^{\infty+1} = \begin{pmatrix} r & i \\ i & r \end{pmatrix} \begin{pmatrix} 0 & i \\ i & 0 \end{pmatrix} = \begin{pmatrix} \frac{-1}{r} & i \\ i & \frac{-1}{r} \end{pmatrix} \quad (46)$$

so the parameters $r < 1$ appear naturally after the first infinite number of steps. When $r < 1$, there is no convergence in the $R(r_j)$, as is easily seen by looking at the first few terms of the sequence. However, the pseudoidentity

$$R(0) = \begin{pmatrix} 0 & i \\ i & 0 \end{pmatrix} = \begin{pmatrix} r & i \\ i & r \end{pmatrix} \begin{pmatrix} \frac{-1}{r} & i \\ i & \frac{-1}{r} \end{pmatrix} \quad (47)$$

relates the two parameter types. Note that $r \in \{0, \pm 1\}$ sets up a binary alternating sequence.

The Pauli matrices provide a basis for the Lie algebra $su(2)$ of traceless Hermitian matrices. The group $SU(2)$ is obtained by exponentiating elements of the Lie algebra. A 1-circulant

$$\begin{pmatrix} 0 & x \\ x & 0 \end{pmatrix} \quad (48)$$

in $su(2)$, where $x \in \mathbb{R}$, is exponentiated to a unitary circulant of the form

$$\begin{pmatrix} \cos(x^2) & i \sin(x^2) \\ i \sin(x^2) & \cos(x^2) \end{pmatrix}. \quad (49)$$

This corresponds to the parameter $r = \cot(x^2)$. The inverse parameter $-1/r$ arises from the tangent of $-x^2$, which comes from pure imaginary elements of the form

$$\begin{pmatrix} 0 & ix \\ ix & 0 \end{pmatrix}. \quad (50)$$

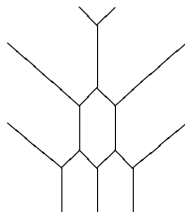
Unlike in the Lie algebra $su(2)$, the Pauli matrices are each playing different roles in information theory. Note that σ_X is the only 1-circulant. What is special about σ_X ? For any $d \geq 2$, the analogous 1-circulant $V_d = (234 \cdots d1)$ always has an eigenvector set giving the columns of F_d . The eigenvalues happen to be $\{\omega_d, \omega_d^2, \dots, 1\}$. So σ_X is dual to F_2 , the only *non circulant* in the canonical set of mutually unbiased bases. The mixed circulant set $\{\sigma_X, R_2, I_2\}$ then accounts for all Pauli matrices and their unbiased bases, in the sense that R_2 is dual to σ_Y and I_2 dual to σ_Z . Similarly for any prime power dimension.

3.3 Honeycombs and Hermitian Matrices

The eigenvalues of complex Hermitian $n \times n$ matrices M are given by the Fourier transform $F_n M F_n^\dagger$. Given two such matrices A and B , their eigenvalue sets are related to the eigenvalues of $C = A + B$ in an interesting way. Let λ_A be the set of n eigenvalues for A , and similarly for λ_B and λ_C . We say that these sets are in a relation $[\lambda_A, \lambda_B, \lambda_C]$ if

$$A + B + C = 0. \quad (51)$$

A theorem of Tao and Knutson [47] shows that $[\lambda_A, \lambda_B, \lambda_C]$ holds if and only if there exists a *honeycomb graph* for the eigenvalue sets. These are planar graphs built with line segments on each of six possible directions, as in the example



which is the dual graph to the tetractys. The semi-infinite lines always run off in the three directions shown, but the internal diagram need not be entirely trivalent, if some edges are contracted. Any valency from 2 to 6 is possible. The real eigenvalues λ_i specify the constant coordinates for the rays in one of the three special orientations, once the plane takes coordinates (x, y, z) such that $x + y + z = 0$. Thus the example shown is a honeycomb for 3×3 matrices. The vertices must satisfy the zero tension rule: the sum of coordinate vectors around the vertex must be zero, up to allowed multiplicities. For trivalent vertices, this means that all edges at a vertex have the same multiplicity x . For instance

$$x((0, 1, -1) + (1, -1, 0) + (-1, 0, 1)) = 0. \quad (52)$$

There is only one constant coordinate in each of the special directions, as the lines are specified by shifting the other two coordinates.

So the quantum Fourier transform maps the triplet of Hermitian matrices (A, B, C) to its honeycomb graph. In chapter (7), rest mass triplets are parameterised using 3×3 Hermitian matrices. We attempt to characterise their parameters using the tetractys honeycomb.

4 The Ordinals and Discrete Duality

The globule 2-arrows that make up a 2-category are pasted both horizontally and vertically, and this is also depicted with rooted trees with two levels. Such two level trees represent higher dimensional 2-ordinals, and similarly with globules in any dimension n . As ordinals, globule diagrams give any category an arithmetic structure.

The basic globule 2-arrow is a symbol for various dualities, such as the exchange of points and lines for a one dimensional geometry. The string and ribbon diagrams that form the subject of this text are dual to arrow diagrams in a two or three dimensional category. We are mostly interested in structures with three levels, where a string edge network passes through points and sits amongst labeled areas in the plane.

Beyond duality there is triality, which is already known to be significant to number theory. One aspect of categorical triality is an underlying triple of dualities, thought of as edges on a triangle. Geometrically, two of these are familiar: the interchange of points and lines in dimension 1, and the interchange of points and faces in dimension 2. But what of the interchange of edges and faces? Although ostensibly a piece of duality in dimension 4, we would really like a three dimensional representation of this duality.

The following sections introduce the basic diagram elements for dual structures, sticking only to what we need for later chapters. Mostly, it is about planar trees. In perturbative quantum field theory, trees are the lowest order Feynman diagrams, which now obtain their algebraic structure from categorical algebra.

4.1 The d -Ordinals

The ordinary ordinals $n \in \mathbb{N}$ are represented by single level planar, rooted trees

$$\begin{array}{ccccccc}
 | & \vee & \vee & \vee & \dots & & \\
 0 & 1 & 2 & 3 & & &
 \end{array} \tag{53}$$

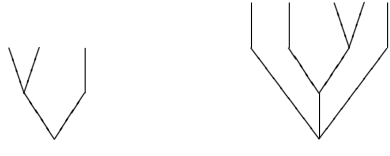
with $n + 1$ leaves. These are the 1-ordinals. A dual way to draw the 1-ordinals is as a string

$$\begin{array}{ccccccc}
 \rightarrow & \rightarrow\rightarrow & \rightarrow\rightarrow\rightarrow & \dots & & & \\
 0 & 1 & 2 & & & &
 \end{array} \tag{54}$$

of arrows, where the tree root provides the n horizontal compositions. This is the representation of ordinals on the tree of the surreal numbers, indicating that higher ordinals are required for ordinary real numbers. Why does the number 1 have two leaves? As a polytope, the two leaves will represent a geometric point, because there is only one way to draw a binary tree with two leaves. That is, this one tree set has cardinality 1. And there is only

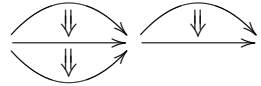
one area between the leaves, representing the trivial permutation group S_1 . The single leaf tree is like an empty set of binary trees, with cardinality 0.

A d -ordinal is specified by a planar tree with $d + 1$ node levels, including the root [48]. For example, the trees



(55)

represent a 2-ordinal and 3-ordinal respectively. As the number of levels increases so does the categorical dimension, as indicated by the equivalent globule diagram. The 2-ordinal on the left becomes the pasting diagram



(56)

with five edges on the tree giving the five 1-arrows, the tree root specifying the horizontal composition, and the vertical composition occurring at the higher node. Similarly, the right hand tree is a diagram with five 3-arrows and three directions of composition.

The 2-ordinals are specified by strings of 1-ordinals (n_1, n_2, \dots, n_k) , since a two level tree has k base edges at the root and each higher node has n_i leaves attached. The horizontal and vertical arrow compositions correspond to the trees



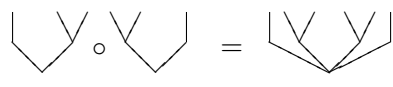
(57)

with a root node or a higher node respectively. All 1-ordinals can be extended to 2-ordinals with the addition of a root edge. Addition $m + n$ of 1-ordinals is then essentially recovered with vertical composition. Similarly, all 1-ordinals can be extended by adding another leaf to every leaf. Then horizontal composition recovers addition. The globule form of the two leaved trees



(58)

makes the composition rules clear. Note that horizontal composition



(59)

preserves the number of lowest level edges, while vertical composition does not. The globule representation turns the basic associator edge

$$\begin{array}{ccc}
 \vee & \text{---} & \vee \\
 & & \vee \\
 & & \vee
 \end{array} \tag{60}$$

into an arrow between two dimensional pictures $((ab)c)$ and $(a(bc))$. Higher dimensional representations of word association appear naturally, because words are often shorthand for tensor products, such as $a \otimes b \otimes c$, which tend not to be associative. Recall that in the axioms for a monoidal category, where \otimes is an arrow composition, the arrows between words are really 2-arrows.

A globule picture for association raises the dimension yet again, but it becomes too unwieldy to work with higher dimensions, unless the categorical structure requires it. The most common form of monoidal category is a symmetric monoidal one, where $a \otimes b$ is the same as $b \otimes a$, but this is secretly a four dimensional category, because the symmetry rule is an equation for 3-arrows in the underlying *braided* monoidal category. The braiding structure $\gamma_{ab} : a \otimes b \rightarrow b \otimes a$ is itself another kind of categorical product [49].

The interplay of the two binary composition types for the 2-ordinals appears in the special example of the Tamarkin tree [50][51], which is the 2-ordinal

$$\begin{array}{c}
 \vee \quad \vee \quad \vee \\
 \diagdown \quad \diagup \quad \diagdown \\
 \vee \quad \vee \quad \vee \\
 \diagdown \quad \diagup \quad \diagdown \\
 \vee \quad \vee \quad \vee
 \end{array} \tag{61}$$

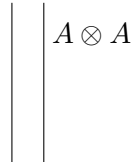
representing the composition of six 2-arrows. When these 2-arrows represent dual structure, the Tamarkin tree is an initial instance of a triple of duals. This 2-ordinal indexes a six dimensional polytope, and was instrumental in extending compactifications for classical configuration spaces beyond a surprising six point anomaly [52].

4.2 Categorical Strings

Dualities are ubiquitous in the mathematics and physics of M theory. For us, a basic duality interchanges a 0 and 1, whether that means geometric objects, qubit states, or elements in an abstract representation of S_2 . Classically, in dimension 2, Poincare duality swaps vertices for faces and edges for edges. It sends a triangle to a trivalent vertex. In a 2-category, this duality turns 2-arrows f and g into little box points

$$\begin{array}{ccc}
 \begin{array}{c}
 A \\
 \curvearrowright \\
 \downarrow f \\
 \downarrow g \\
 \curvearrowleft \\
 B
 \end{array} & & \begin{array}{c}
 |A \\
 \boxed{f} \\
 | \\
 \boxed{g} \\
 |B
 \end{array}
 \end{array}$$

where it is understood that edges are directed downwards, and these edges are 1-arrows. In the example drawn, the unique object is unmarked, but objects are permitted to label areas in string diagrams. Thus the two unmarked areas split by the string stand for source and target objects. Since a monoidal category is really a bicategory, such strings are used to represent its objects [53], with the concatenation

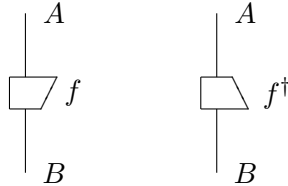


of strings standing for tensor product. In a string diagram, the multiplication $A \otimes A \rightarrow A$ for an algebra object A is given by a basic trivalent vertex. So trees can be interpreted as string diagrams after all.

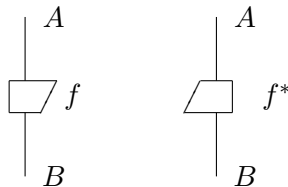
In a braided monoidal category the strings may pass over and under one another, but in the symmetric case an ambiguous crossing



is sufficient. In a higher dimensional category, arrows may be reversed at any level, defining many distinct notions of duality. An adjoint dual f^\dagger to a map f might be represented by a flipped box [54][55]



The \dagger structure for a symmetric monoidal category satisfies $f^{\dagger\dagger} = f$, coming from an identity natural transformation in the adjunction. When we want both dual objects and dual arrows, we need extra structure. Object duals A^* and B^* induce another dual arrow $f^* : B^* \rightarrow A^*$ given by *both* a left right and an up down box flip.



We can similarly define an f_* , so that the left right flip is covered. By fixing a direction for processes in the plane, we are permitted two underlying discrete

symmetries. These are rich enough to define interesting algebraic structures. A \dagger Frobenius structure [56][55] is a cocommutative comonoid object A with $\Delta_A : A \rightarrow A \otimes A$ and $\epsilon : A \rightarrow I$, such that $\Delta_A \dagger \Delta_A = 1_A$ and

$$\Delta_A \Delta_A \dagger = (\Delta_A \dagger \otimes 1_A) \circ (1_A \otimes \Delta_A).$$

The arrows $\Delta_A : A \rightarrow A \otimes A$ and $\Delta_A \dagger : A \otimes A \rightarrow A$ define dual trivalent vertices

$$\begin{array}{ccc} \begin{array}{c} \downarrow \\ \bullet \\ \swarrow \quad \searrow \end{array} & \begin{array}{c} \swarrow \quad \searrow \\ \bullet \\ \downarrow \end{array} & (62) \end{array}$$

in a category, subject to the Frobenius axioms. Using the category of finite dimensional Hilbert spaces as a guide, the \dagger Frobenius structures are in one to one correspondence with orthonormal bases for the Hilbert spaces. Thus quantum mechanical measurement bases may be used to build string network diagrams. Mixing a \dagger Frobenius structure with duals $\theta_A : A \rightarrow A^*$ allows a proper axiomatisation of bases, where we have $\theta_{A^*} = \theta_A \dagger$. This structure allows a symbol

$$\begin{array}{c} A \\ \downarrow \\ \bullet \\ \uparrow \\ A \end{array} \quad \theta_A$$

with a reversed pair of object arrows, and these are both reversed for the adjoint. These arrows are in some sense time directions for quantum processes. They permit the apparently acausal processes of standard protocols [57] to be replaced with objects for which the process time flows in a given direction.

In all such diagrams, the inputs and outputs fit on a one dimensional line, creating a rigid concept of *before* and *after* for unitary processes. In contrast, the diagrams of chapter 6 aim to capture the cyclicity of color structure in Yang-Mills theories. The usual diagrammatic representation for permutations, from n points to n points, will be replaced by a cyclic picture. In this scheme, trivalent vertices would no longer belong to an ordinary category, because the cyclicity must be taken seriously at the axiomatic level. The search for cyclic structure begins with the duality of S_2 , for which the twistor diagrams are the pieces of the Kauffman bracket (120). In chapter (9) these objects are considered within a hierarchy of S_d and B_d diagrams.

4.3 Fourier Dualities and Topology

The classical Fourier transform is associated to Pontrjagin duality [58], and a more abstract duality between a category of locally compact abelian groups

and a category of Hausdorff spaces [38]. Given a group G , its dual G^\wedge is the set of *characters* $G \rightarrow S^1$ into the unit circle. The circle S^1 is very special, representing both an abelian group and a space. It extends the special role of the two point set $\{0, 1\}$ in the category **Set**. The object $\{0, 1\}$ is also the elementary one point topological space, including its empty set [8].

The Pontrjagin duality is a natural transformation $\eta : (G^\wedge)^\wedge \simeq G$ between the double dual of G and G . That is, for every arrow $f : G_1 \rightarrow G_2$ in the group category, there is a commutative square

$$\begin{array}{ccc} G_1^{\wedge\wedge} & \xrightarrow{f^{\wedge\wedge}} & G_2^{\wedge\wedge} \\ \eta_{G_1} \downarrow & & \downarrow \eta_{G_2} \\ G_1 & \xrightarrow{f} & G_2 \end{array} \quad (63)$$

in the category of abelian groups. When the categorical dimension is not restricted, all such dualities are weakened by higher dimensional arrows. Our central example is the Fourier duality between \mathbb{Z} and S^1 . For us, \mathbb{Z} is usually the braid group B_2 on two strands, and it defines the fundamental group $\pi_1(S^1)$ for the circle.

Unlike this duality between distinct categories, a motivic duality functor should ideally be an endofunctor $\mathbf{C} \rightarrow \mathbf{C}$ for some category \mathbf{C} that has objects that are both spatial and algebraic. That is, emergent geometry expects *all* objects in nice categories to have topological properties analogous to $\{0, 1\}$ and S^1 .

Let us step back to the discrete Fourier transform, which was associated to the quantum arithmetic of mutually unbiased bases. In dimension d , there is an underlying *space* with d points, and the mutually unbiased bases in dimensions $d = p^n$ are associated to the ring $\mathbb{Z}/\mathbb{Z}_{p^n}$. This suggests that $\mathbb{Z} \simeq B_2$ secretly lives in dimension ω , and we have already assumed that continua such as S^1 are emergent. The Fourier duality of \mathbb{Z} and S^1 is approached with the inverse limits \mathbb{Z}_p

$$\mathbb{Z}/\mathbb{Z}_p \rightarrow \mathbb{Z}/\mathbb{Z}_{p^2} \rightarrow \cdots \rightarrow \mathbb{Z}/\mathbb{Z}_{p^3} \cdots \rightarrow \mathbb{Z}_p \quad (64)$$

of the p -dit rings. The set \mathbb{Z}_p is the p -adic integers, and it defines the division field \mathbb{Q}_p of p -adic numbers [59]. A p -adic integer is a sequence of elements $x_n \in \mathbb{Z}/\mathbb{Z}_{p^n}$ such that for $n \leq m$, $x_n = x_m \bmod p^n$. Amazingly, \mathbb{Z}_p is an uncountable set with the cardinality of the continuum.

The Fourier dual of \mathbb{Z}_p is the group of all p^n -th roots of unity on S^1 [60]. There are many interesting ways to embed the p -adic numbers into the complex plane [61]. Quantum arithmetic is somehow carrying \mathbb{Z} into \mathbb{C} , building S^1 up by the rules of an underlying categorical Stone duality [38]. Note also that for a nice classical space X , p -adic cohomology $H^i(X, \mathbb{Z}_p)$ is also defined as an inverse limit of the groups $H^i(X, (p^n))$ as $n \rightarrow \infty$.

5 Trees, Polytopes and Braids

A rooted tree is an example of a one dimensional contractible space, if embedded in some well behaved classical geometry. That trees have singularities does not concern us. On the contrary, everything is built from trees. Before we look at the contraction of an edge as an axiomatic process, we need to understand the combinatorics of trees. As good mathematicians sometimes say, combinatorics is an honest subject, because everyone agrees on what it means to count a finite set.

In this chapter we consider rooted, planar trees, mostly with binary branchings. The choice of a root turns cyclic trees into d -ordinals. Reading a tree downwards from the leaves, a binary node represents an operation $a \cdot b$. Many types of binary operation can occur. A bracketing (ab) of two letters is the main example.

Permutations can be tree diagrams, when the permutation labels the spaces between leaves. For example, a permutation in S_3 acts on the \otimes operations in the word $a \otimes b \otimes c \otimes d$. Such a four letter word may be bracketed in 5 ways, giving the vertices of the Mac Lane pentagon for weak associativity, as a set of 5 trees with four leaves. The edges of the pentagon correspond to a tree with one internal edge contracted, and the single face to the unique tree with all internal edges contracted. Similarly, the polytopes A_{n-1} for trees on n leaves are the *associahedra*, which occur as categorical axioms in dimension $n - 2$.

5.1 Permutations and Planar Trees

First consider the binary, rooted planar trees, where every node is distinguished by a unique vertical height. The empty permutation on the empty set is represented by a single leaf. A two leaf tree

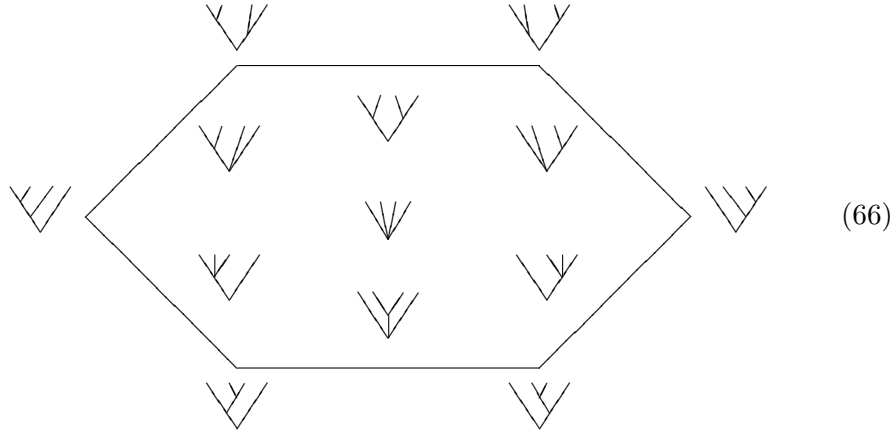


represents the trivial permutation (1) on one object, because there is only one node beneath the leaves. In general, a binary tree with $n + 1$ leaves gives a permutation in S_n , as in the example



where each entry in (132) is given by the appearance of a new area between leaves, moving down the page. The permutation really acts on the nodes of

the tree. Each permutation group S_d corresponds to a set of $d!$ such trees. The hexagon of S_3 is the diagram



indexed by the unique single level tree with 4 leaves, as was the pentagon above. The other geometric elements of the hexagon, namely vertices and edges, correspond to expansions of the root node into edges. Only two expansions are required to turn a 4 leaf node into a full binary tree, and this forces the dimension of the hexagon. An S_d diagram in dimension $d - 1$ is known as a *permutohedron* polytope [62].

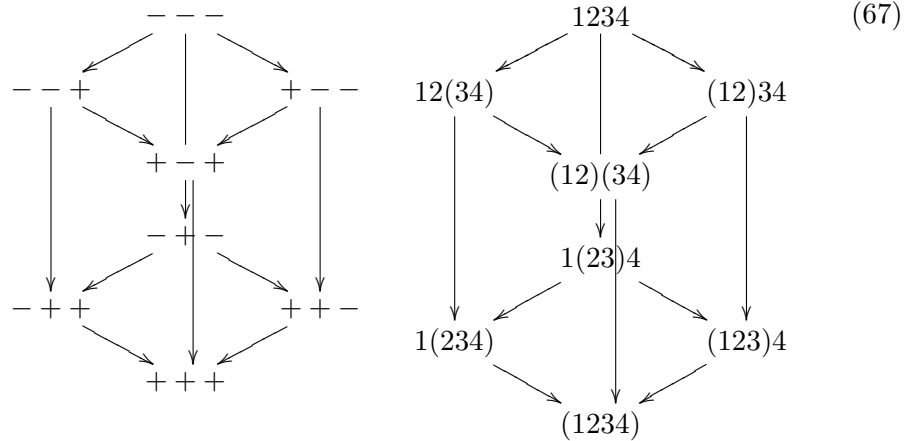
The *associahedra* polytopes A_d , also indexed by $d \in \mathbb{N}$, are given by the trees which do not distinguish node levels. For example, (132) and (312) in S_3 denote equivalent trees in A_3 , so that the six vertices of the hexagon are reduced to the five vertices on the pentagon, by shrinking the one edge that cannot be labeled with a trivalent node. For the categorical pentagon axiom, see appendix A. The set of associahedra were originally introduced by Tamari [63] and then by Stasheff [64], in the study of homotopy for classical spaces.

If the permutohedron S_d is embedded in a Euclidean space, it defines the convex hull of the vertices $\sigma \in S_d$. This parameterises the set of real, doubly stochastic $d \times d$ matrices, or *magic* matrices, with constant row and column sums. A physical probability matrix is of this kind, and we will always view them as sums of permutations from S_d , so that they belong to the group algebra.

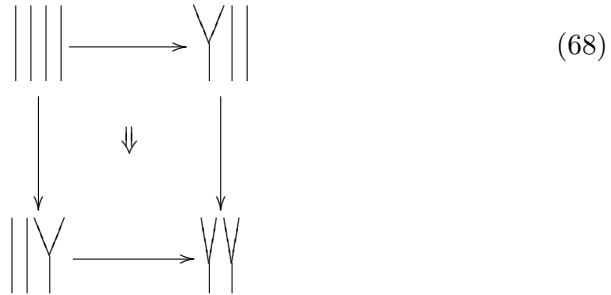
A permutation is reducible to its signature class, which lists the signs of the differences between consecutive entries. For example, (231) has signature $+-$, which is shared by (132). The signatures label the vertices of a parity cube. For S_4 , in dimension 3, the eight vertices are the components of a three qubit state (and might label the electric and magnetic charges of a black hole state in M theory [18]). To see the categorical importance of parity cubes, consider the following *categorification* of the bracketing process.

An associahedron binary tree with $d+1$ leaves represents a full bracketing of $d + 1$ objects, such as in $((a(bc)d)e)$. Using edges oriented by the basic

(21) flip, four objects are bracketed in the steps shown in the cube on the right.



The signs are an alternative representation of the bracket choices, giving here a parity cube P_4 . Observe that each face of the cube stands for one edge on the hexagon (66). The cube is then a categorification of the hexagon, in the sense that each geometric element is raised by one dimension. Categorically, a face is now a pseudonatural transformation in a 2-category. The cube is associated with three dimensional categories [9][65]. Every face except the top face represents an associator edge $(xy)z \Rightarrow x(yz)$ on the pentagon. The double arrow that labels the face indicates its dimensionality, and this arrow is the homotopy between the two paths that bound the square. Now the top square



breaks the Mac Lane axiom for monoidal categories [66], if it is not an identity. This happens already on the S_4 hexagon. Since permutations are fundamental to us, and categorical dimensions are not arbitrarily restricted, this square permits the deviation in tree node levels. When the vertical direction on a diagram denotes a time variable, as it usually does in physical applications, this S_d level splitting breaks the forward backward symmetry of time.

In the next section, the three dimensional associahedron A_4 is indexed by rooted hexagons, geometrically dual to the trees with 5 leaves. Two

vertices on this polytope are geometrically distinguished, namely the ones that include a copy of the ambiguous level 4-leaved tree above. The 24 vertices of the S_4 permutohedron are reduced to only 14 vertices on the associahedron. There is also a sequence of polytopes that combines the features of A_d and S_d . These are the *permutoassociahedra* [67], appearing in chapter (9). In fact, any d -ordinal tree defines a categorical polytope.

Now every permutation matrix is associated to a rooted, binary tree. The S_2 edge associahedron

$$\begin{array}{ccc} \vee & \text{---} & \vee \\ & & \vee \end{array} \quad (69)$$

may be thought of as the sum

$$\begin{pmatrix} 1 & 0 \\ 0 & 1 \end{pmatrix} + \begin{pmatrix} 0 & 1 \\ 1 & 0 \end{pmatrix} = \begin{pmatrix} 1 & 1 \\ 1 & 1 \end{pmatrix} = 2. \quad (70)$$

In [68], Loday explains how the arithmetic of $1 + 1 = 2$ works with trees.

For a contracted tree, where at least one node is not binary, the dimension of a permutation matrix may be reduced. This is a substitution process, which eventually reduces any tree to the one level index tree $d \in \mathbb{N}$, and the trivial permutation (1). Letting a matrix entry 1 be generalised to $k \in \mathbb{N}$, the hexagon edges of (66) should become matrices with row and column sums of 3. One solution is the unambiguous choice

$$\begin{array}{ccc} \begin{array}{c} \vee \\ \begin{pmatrix} 2 & 0 \\ 0 & 1 \end{pmatrix} \end{array} & \begin{array}{c} \vee \\ \begin{pmatrix} 1 & 0 & 1 \\ 1 & 0 & 1 \\ 0 & 2 & 0 \end{pmatrix} \end{array} & \begin{array}{c} \vee \\ \begin{pmatrix} 0 & 2 \\ 1 & 0 \end{pmatrix} \end{array} \\ \begin{array}{c} \vee \\ \begin{pmatrix} 1 & 0 \\ 0 & 2 \end{pmatrix} \end{array} & \begin{array}{c} \vee \\ \begin{pmatrix} 0 & 2 & 0 \\ 1 & 0 & 1 \\ 1 & 0 & 1 \end{pmatrix} \end{array} & \begin{array}{c} \vee \\ \begin{pmatrix} 0 & 1 \\ 2 & 0 \end{pmatrix} \end{array} \end{array} \quad (71)$$

where normalisation factors have been freely used. The 2×2 matrices are reductions of the obvious 3×3 ones, reflecting the ordinal substitution from S_3 down to S_2 . Two trees do not reduce to 2×2 operators, and these are the ones corresponding to full left right reflections. Then there should be a reduction from the hexagon to the pentagon, and finally to a square of 2×2 trees, which is the parity square of signatures for S_3 . The sum of matrix hexagon edges gives the democratic matrix

$$3 = \frac{1}{3} \begin{pmatrix} 1 & 1 & 1 \\ 1 & 1 & 1 \\ 1 & 1 & 1 \end{pmatrix}, \quad (72)$$

which now represents the ordinal hexagon face. For any d , the vertices of S_d clearly sum to the democratic matrix.

Since the two trees of type (65) are combined in the pentagon vertex (132) + (312), the pentagon face sums to the asymmetric probability matrix

$$\frac{1}{10} \begin{pmatrix} 3 & 4 & 3 \\ 3 & 4 & 3 \\ 4 & 2 & 4 \end{pmatrix}, \quad (73)$$

where a canonical normalisation is now included. This embeds in a 4×4 matrix as a pentagon face of A_4 . Similarly, a square face on S_4 is given by

$$(1234) + (2134) + (1243) + (2143) = \frac{1}{2} \begin{pmatrix} 1 & 1 & 0 & 0 \\ 1 & 1 & 0 & 0 \\ 0 & 0 & 1 & 1 \\ 0 & 0 & 1 & 1 \end{pmatrix} \quad (74)$$

but on A_4 we also include (4123) and (4213) to obtain the magic square

$$\frac{1}{16} \begin{pmatrix} 7 & 7 & 0 & 2 \\ 8 & 8 & 0 & 0 \\ 1 & 1 & 8 & 6 \\ 0 & 0 & 8 & 8 \end{pmatrix}. \quad (75)$$

Finally, one can easily verify the parity square and cube matrices

$$\frac{1}{8} \begin{pmatrix} 3 & 2 & 3 \\ 2 & 4 & 2 \\ 3 & 2 & 3 \end{pmatrix} \quad \frac{1}{10} \begin{pmatrix} 3 & 2 & 2 & 3 \\ 2 & 3 & 3 & 2 \\ 2 & 3 & 3 & 2 \\ 3 & 2 & 2 & 3 \end{pmatrix}. \quad (76)$$

The up down reflection of a parity cube matrix corresponds to a left right reversal of the sign string, with all signs flipped. Flipping all signs corresponds to the left right matrix symmetry.

And so ends our first attempt at uniquely specifying trees with matrix objects. In the search for motives, we always want algebraic objects that explicitly manifest the properties of their diagrams. These S_d objects do not quite achieve this, since trees do not share the symmetries of matrices, which represent maps from d to d objects.

5.2 Solomon's Descent Algebra

The signature class for a permutation $\sigma \in S_d$ is the string of $d - 1$ signs given by consecutive differences in the ordinal string of σ . A collection of signature classes determines a parity cube in dimension $d - 1$. For example, the signature of (32145) is $(- - ++)$.

Example 5.1 The eight signature classes of S_4 , and their orders, are

(---)	(4321)	1
(--+)	(4312), (4213), (3214)	3
(-+-)	(4231), (4132), (2143), (3142), (3241)	5
(+--)	(3421), (2431), (1432)	3
(++-)	(1243), (1342), (2341)	3
(+ - +)	(3412), (1423), (1324), (2413), (2314)	5
(- + +)	(4123), (3124), (2134)	3
(+++)	(1234)	1

There is an obvious source and target with which to orient the cube edges and faces. Let ρ denote a signature class for S_d . H_ρ is defined to be the sum of all permutations in the class, which is an element in the group Hopf algebra KS_d , for any suitable K that contains zero and one. Solomon's theorem [69] is the statement that $H_{\rho_1}H_{\rho_2}$ is a linear combination of the H_ρ for S_d .

Example 5.2 For the S_4 group algebra over \mathbb{N} ,

$$\begin{aligned} (-+++)(--+) &= [(4123) + (3124) + (2134)][(4312) + (4213) + (3214)] \\ &= (+--)\ +\ (+-+)\ +\ (---) \end{aligned}$$

Signature classes may also be labeled by *ordered partitions* as follows. The element $(+\dots+)$ is the single component partition d , as in the ordinal index. The descending $(-\dots-)$ element is the longest partition $1+1+\dots+1$ of all ones. For S_3 there are two remaining classes, $(-+)$ and $(+-)$, each containing two permutations. These are the partitions $1+2$ and $2+1$ respectively. The minus signs are used to indicate a tendency for ones. The more plus signs, the further one moves away from partitions built from ones. We see then that noncommutative partitions are far simpler than partitions in commutative arithmetic, which are difficult to count.

Atkinson [70] defines a matrix $M_{\rho_1\rho_2}$ using any pair of ordered partitions ρ_1 and ρ_2 . The row sums are given by the ordinals in ρ_1 and the column sums by the ordinals in ρ_2 . For example, let $\rho_1 = 1+2$ and $\rho_2 = 1+1+1$. Then there are three possibilities for the matrix $M_{\rho_1\rho_2}$, namely

$$\begin{pmatrix} 0 & 1 & 0 \\ 1 & 0 & 1 \end{pmatrix} \begin{pmatrix} 1 & 0 & 0 \\ 0 & 1 & 1 \end{pmatrix} \begin{pmatrix} 0 & 0 & 1 \\ 1 & 1 & 0 \end{pmatrix} \quad (77)$$

These matrices specify coefficients in the products $H_{\rho_1}H_{\rho_2}$. For example, $H_{1+2}H_{1+1+1} = 3H_{1+1+1}$, where the three given matrices each donate a copy of H_{1+1+1} . The general rule, for an $n \times m$ matrix, is

$$H_{\rho_1}H_{\rho_2} = \sum_M H_{M_{11}, M_{22}, \dots, M_{1m}, M_{21}, \dots, M_{2m}, \dots, M_{n1}, \dots, M_{nm}} \quad (78)$$

where it is understood that zeroes are omitted. These matrices may be helpful for computations in KS_d and the algebra KP_d .

Let KP_∞ be the disjoint union of all descent Hopf algebras KP_d , for $d \geq 0$, and let KS_∞ be $\oplus KS_d$. For most purposes, the ground field K is taken to be \mathbb{Q} . It is shown in [71] that Solomon's descent algebra KP_∞ is a sub Hopf algebra of KS_∞ , for any ground field K . Moreover, KP_∞ , as a Hopf algebra, is the image under a map $(\phi\psi)^*$, where

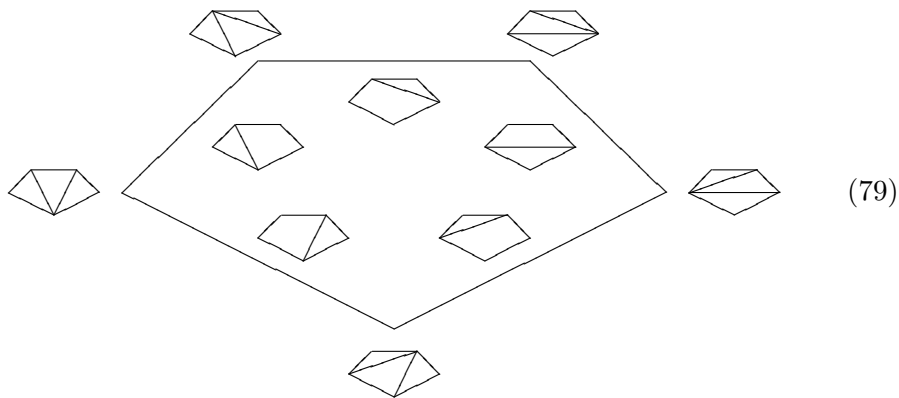
- using left right signed leaves on binary trees, ϕ_d maps the associahedron A_d to the parity cube, by noting the signs of interior leaves. The dual ϕ^* is the linear dual in the Hopf algebra.
- ψ_d is the reduction of S_d to A_d obtained by leveling the tree nodes.

In other words, there is an intimate link between S_d , its parity cube and the intermediary associahedron. For a tree T in A_d , the inclusion $\psi^*(T)$ in the Hopf algebra KS_∞ is the sum $\sum \sigma$ of permutations corresponding to T . This is like the matrix sums that appeared in the last section.

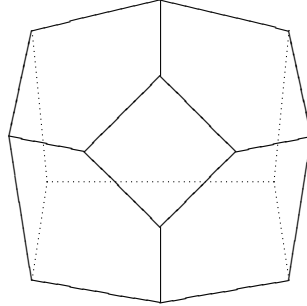
The descent algebra is an important property of probability matrices. Note that such matrices are not elements of a linear matrix group GL_n , because they tend to have determinant zero. They are thus somewhat neglected in the swamp of manifold mathematics.

5.3 Associahedra, Permutohedra and Polygons

A genus zero polytope in Euclidean dimension $d - 1$ will define a categorical axiom if it arises as an expansion set for a d -ordinal tree [48]. Instead of trees, we could use the rooted polygons that are dual to the trees. For example, the A_3 polytope is the pentagon of chorded pentagons



The number of chords on an index polygon clearly indicates the codimension of the face. The nine face A_4 polytope, without labels, looks like



(80)

The square faces come from a chorded hexagon where the chord cuts the hexagon in two. The 6 pentagonal faces are labeled by the other single chorded hexagons, the 21 edges by hexagons with two chords, and the 14 vertices by hexagons with three chords.

The *source* of A_4 is the tree (1234) and the *target* the tree (4321). This choice orients all edges on A_4 , and fills every face with a 2-arrow that potentially breaks the Mac Lane pentagon axiom. The set of all associahedra for $d \in \mathbb{N}$ give an example of an *operad* (see appendix A).

Let us enumerate the codimension k faces of A_d . The number of vertices on A_d is given by the Catalan number

$$C_d = \frac{1}{d+1} \binom{2d}{d}. \quad (81)$$

This is seen by dualising rooted trees with d leaves and one root edge to rooted polygons with $d+1$ sides. The Catalan number counts the triangulated polygons. It is further divided into Narayana numbers

$$N_{d,k} = \frac{1}{d} \binom{d}{k} \binom{d}{k-1} \quad \sum_{k=1}^d N_{d,k} = C_d \quad (82)$$

This partition of C_d groups trees according to the number of internal right directed leaves, as in the signature class maps. For example, on A_4 we have $N_{4,k} \in (1, 6, 6, 1)$. The decomposition of A_3 into Narayana sets is

$$\begin{array}{cccccc}
 - & + & - & + & - & + & - & + & - & + \\
 \begin{array}{c} \diagdown \quad \diagup \\ \diagdown \quad \diagup \\ | \end{array} & \begin{array}{c} \diagdown \quad \diagup \\ \diagdown \quad \diagup \\ | \end{array} & \begin{array}{c} \diagdown \quad \diagup \\ \diagdown \quad \diagup \\ | \end{array} & \begin{array}{c} \diagdown \quad \diagup \\ \diagdown \quad \diagup \\ | \end{array} & \begin{array}{c} \diagdown \quad \diagup \\ \diagdown \quad \diagup \\ | \end{array} & \begin{array}{c} \diagdown \quad \diagup \\ \diagdown \quad \diagup \\ | \end{array} & \begin{array}{c} \diagdown \quad \diagup \\ \diagdown \quad \diagup \\ | \end{array} & \begin{array}{c} \diagdown \quad \diagup \\ \diagdown \quad \diagup \\ | \end{array} & \begin{array}{c} \diagdown \quad \diagup \\ \diagdown \quad \diagup \\ | \end{array} & \begin{array}{c} \diagdown \quad \diagup \\ \diagdown \quad \diagup \\ | \end{array} \\
 + - & + - & + - & + - & + - & + - & + - & + - & + - & + - \\
 1 & 3 & 2 & 2 & 2 & & & & &
 \end{array} \quad (83)$$

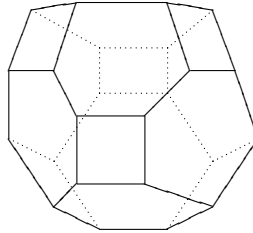
giving $N_{3,k} \in (1, 3, 1)$. This takes care of the maximal codimension. For codimension k , the cardinality of the A_d face set is

$$F_{d,k} = \frac{1}{d+1} \binom{d+k+1}{k+1} \binom{d-1}{k}. \quad (84)$$

This result was first proved by Cayley in 1891 [72][73].

There is much more to the A_4 associahedron. The 21 edges are symmetrically divided into seven sets of the objects $\{a, b, c\}$, with each pentagon carrying a label set of the form $ababc$, and each vertex carrying an $\{a, b, c\}$ triplet. A full triangulation of the 9 faces results in 24 triangles, defining 24 tetrahedra when a central vertex is added. Since this triangulation creates 36 edges, the Poincare dual polytope is the permutohedron S_4 .

For the permutohedron S_d there are $d!$ vertices and $d!(d-1)/2$ edges. The permutohedron always tiles \mathbb{R}^{d-1} , as do cubes and their decompositions. The polytope S_4



(85)

is coordinatised neatly as follows. Think of the 24 permutations as integral coordinates in \mathbb{R}^4 , so that (2341) sits at (2, 3, 4, 1). These points clearly lie on the \mathbb{R}^3 plane $x_1 + x_2 + x_3 + x_4 = 10$. This can be turned into the simplex plane $y_1 + y_2 + y_3 + y_4 = 0$ by sending each digit n to $(2n - 5)/2$, giving a vertex like $(-1/2, 1/2, 3/2, -3/2)$.

The *permutoassociahedron* in dimension three has $120 = 5!$ vertices, blending associator and braiding arrows by turning each vertex of S_4 into a pentagon. Other related polytopes include the *cyclohedra* [74], which bracket objects on a loop rather than on a line. This is a natural polytope sequence for theories that use cyclic tree diagrams, such as $N = 4$ Yang-Mills theory, and it is also associated to knot invariants. It is denoted by polygons with chord sets that are symmetric about a central axis.

Postnikov [62] defines the *mixed Eulerian* numbers, which come from volumes for simplices within polytopes. For the permutohedron at the integral vertices in \mathbb{Z}^{d+1} , the volume V_d equals $(d+1)^{d-1}$. This is a cardinality for *parking functions*, which are defined below. One studies volume formulas for general coordinates (x_1, \dots, x_{d+1}) . A *generalised permutohedron* is defined to be a sum

$$\sum_I \alpha_I \Delta_I$$

over subsets I of the standard d -simplex in \mathbb{R}^{d+1} , where Δ_I is the subset of faces of the simplex given by $i \in I$. These polytopes include the associahedra and cyclohedra. A *hypersimplex* $\Delta_{k,d}$ is the generalised permutohedron at coordinates $(1, 1, \dots, 0, 0, \dots, 0)$, that is with k ones and $d - k + 1$ zeroes. Using hypersimplices, define a polytope Q_d as a sum

$$Q_d \equiv z_1 \Delta_{1d} + z_2 \Delta_{2d} + \dots + z_d \Delta_{dd} \quad (86)$$

where we write $z_1 = x_1 - x_2$ and so on. Consider then the vectors $c = (c_1, \dots, c_d)$ for $c_i \geq 0$ such that $\sum c_i = d$. Let V_c be an integral volume for the collection $(\Delta_{1d}^{c_1}, \dots, \Delta_{dd}^{c_d})$ of hypersimplices. These V_c are the mixed Eulerian numbers of interest. Their properties include a decomposition

$$\sum_c \frac{V_c}{c_1! \cdots c_d!} = (d+1)^{d-1} \quad (87)$$

of the parking functions. The volume of Q_d may now be expressed as

$$V(Q_d) = \sum_c V_c \frac{z_1^{c_1} \cdots z_n^{c_n}}{c_1! \cdots c_d!}. \quad (88)$$

The mixed Eulerian numbers include the classical Eulerian numbers E_{kd} , defined for $c = (0, 0, \dots, 0, d, 0, \dots, 0)$, with the d in the k th position. Thus the volume of Δ_{kd} is $E_{kd}/d!$. In the special case that c satisfies

$$c_1 + \cdots + c_i \geq i \quad (89)$$

for all i , then

$$V_c = 1^{c_1} 2^{c_2} \cdots d^{c_d} \quad (90)$$

and there are C_d such vectors c . In other words, the vertices of the associahedron A_d naturally embed into a divided simplex from the word monoid. The Eulerian numbers appear in recent matrix structures for $N = 8$ supergravity [21].

Example 5.3 When $d = 4$, the 14 c vectors that satisfy $c_1 + \cdots + c_i \geq i$ give volumes V_c that are graded by the Narayana numbers.

1	$V_{4000} = 1$
6	$V_{1300} = 8, V_{3100} = 2, V_{3010} = 3, V_{3001} = 4, V_{2020} = 9, V_{2200} = 4$
6	$V_{1120} = 18, V_{1210} = 12, V_{1201} = 16, V_{2110} = 6, V_{2101} = 8, V_{2011} = 12$
1	$V_{1111} = 24$

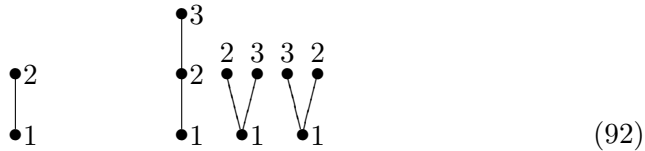
The c vectors show up in the factorisation of ordinary ordinals, recalling the replacement of noncommutative monomials in the word monoid by divisors. Consider homogeneous coordinates in \mathbb{Z}^4 for the parity cube. It is necessary to add a coordinate when using strings of zeroes and ones, since these vertices have distinct totals. We choose to put the extra variable at the start of the vector, where it will only pick up a volume factor (90) equal to 1. The resulting cube, labeled by integral volumes,

$$\quad (91)$$

clearly shows the factors of 24. Opposite corner pairs give multiplication to the target 24. This process works perfectly on all parity cubes up to dimension 4, where the target volume is $120 = 5!$, since all ordinals up to 5 are prime powers. Actually, a parity cube can be used to list the divisors of any square free $n \in \mathbb{N}$, with the target representing n . For example, 10 fits onto the homogenised parity square, with paths through 2 and 5. For numbers n that are cube free, it suffices to employ qutrit simplices.

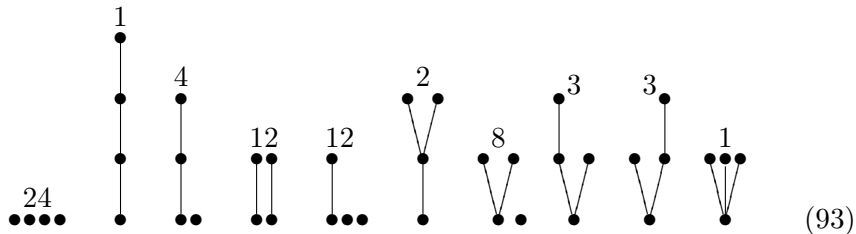
5.4 Linear Orders and Forests

Any rooted planar tree defines a set of *linear orders*. Each node of a linear order is a node on the tree, and the nodes are connected only by internal edges from the tree. The leaves are all deleted. The n nodes are then labeled by the numbers $1, 2, \dots, n$, with each number used only once. This is how tree nodes get labeled for S_n . The order restriction on the labels is that they must *decrease* as one travels on a downward path. The linear orders at $n = 2$ and $n = 3$ are then the diagrams



Consider the five vertex trees of the pentagon A_3 . Linear orders allow us to distinguish the special tree $(312) + (132)$ from the other four trees, and so to recover the hexagon S_3 . There is a unique order 321 associated to each of the four normal trees, but $(312) + (132)$ has two distinct orders, each with two leaves. Each order selects one of the permutations.

Given a *forest*, namely a finite union of disjoint rooted trees, one associates unions of linear orders, one order for each tree in the forest. Forests are graded according to the total number of nodes. To begin with, we consider forests with no ordering on element trees. For $n = 4$, the forest orders and their cardinalities are given by



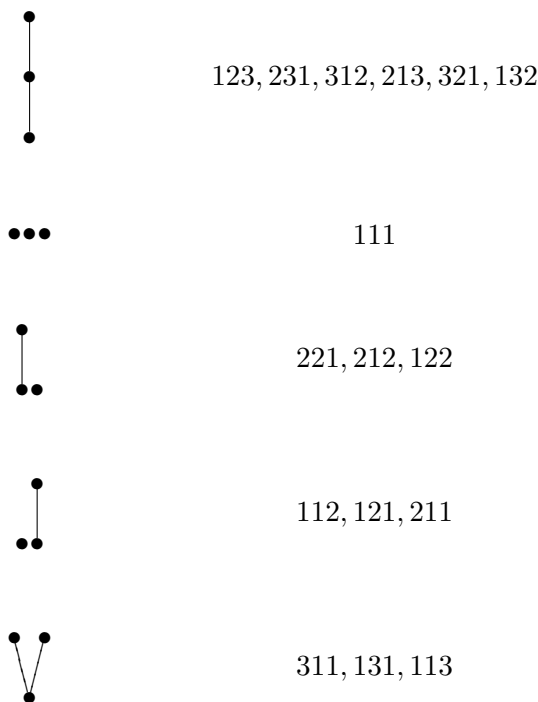
The set contains 70 objects. Without labels, such forests appear in the Connes-Kreimer renormalisation algebra of rooted trees, as given in appendix C. The *forest coefficient* [75] on unlabeled forests is the integer de-

fined by the product of cardinalities

$$f = \prod_v |\{w : w \geq v\}| \tag{94}$$

where v is the node set and $w \geq v$ if it lies above it on a path. For example, the vertical tree at $n = 3$ has $f = 6$, because the bottom node contributes three nodes, the middle contributes two, and the top node only itself. At $n = 3$, the sum of f values equals 12. The labeled orders also give a count of 12 for $n = 3$ forests. Verify that these two counts are *dual* in the sense that they swap pairs of forests.

A noncommutative analogue orders the tree set within the forest [76]. There are then five distinct forests at $n = 3$, rather than four, and 14 at $n = 4$. These are again the Catalan numbers. Now choose an order from *left to right* on nodes at a level within a forest. Verify that there are then 3 forests at $n = 2$, and 16 at $n = 3$.



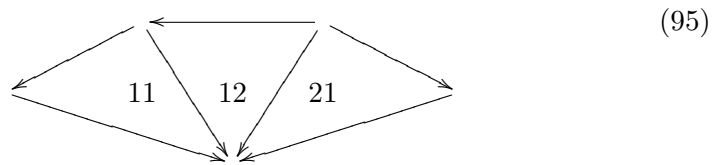
Ignore left right tree flips for asymmetric trees. The horizontal point set now has only one labeling, since it must be ordered 123. These diagrams are known as *parking functions* [77][78]. Their count for general n is

$$p_n = (n + 1)^{n-1}$$

The correspondence between the order types and the standard parking functions [79] at $n = 3$ is indicated below. The parking functions are permutations of sequences $i_1 i_2 \cdots i_n$ such that $i_k \leq k$. On the vertical tree, the

parking function entries just label the nodes freely. The 111 forest starts at 1 again for each root. The 212 forest chooses 13 for the root labels, as does 121.

The number $p_3 = 16$ is associated to the A_4 associahedron in a nice way: it counts the 3-simplices in a natural triangulation of A_4 . One could divide A_4 into 24 simplices, by triangulating each face and placing a new node in the centre of the polytope, but a more efficient 16 simplex picture uses parking functions. Consider first the pentagon A_3 . The 3 noncommutative forests at $n = 2$ label three triangles on an oriented chorded pentagon [79]. One selects chords that aim for the target vertex.



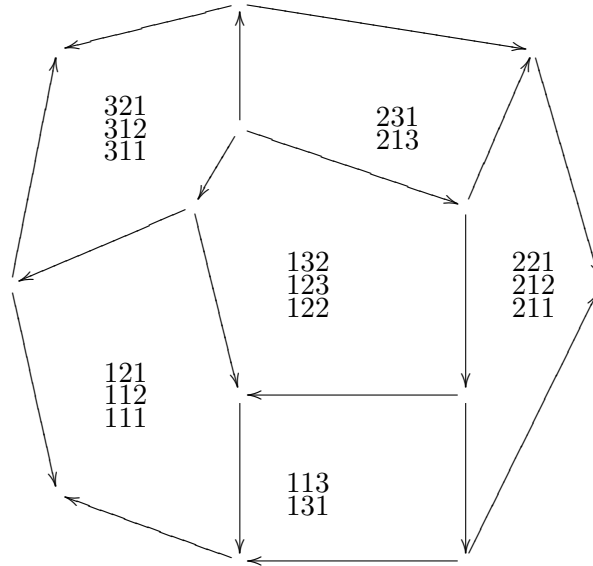
This also demonstrates the chording for a square. When all faces on the oriented A_4 are chorded in this manner there are 24 triangles, but only 16 of them can be parking functions. These 16 triangles sit on the four pentagons and two squares, as shown below.

The source vertex defines an S_3 hexagon, because the six S_3 triangles meet at the source. Although the parking functions divide A_4 into simplices, one could consider the remaining 8 triangles in the 24 surface triangles, and label them with the words

$$223, 232, 222 \quad 331, 313, 333 \quad 233, 323 \quad (96)$$

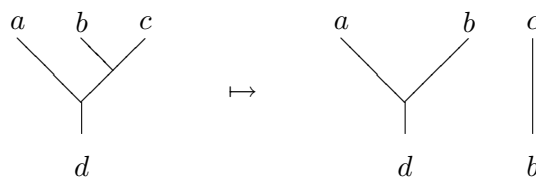
bringing us to 24 out of 27 three qutrit words, now labeling simplices created with the additional central point inside A_4 .

(97)

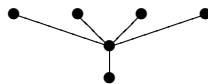


A *decorated* rooted planar tree has labels on all external leaves, including the root. Decorations take values in a fixed set S . Decorated forests are disjoint collections of decorated trees. We define a tree *splitting contraction* [80], which sends a decorated tree with n edges to one with $n - 1$ edges. On an internal edge, it simply contracts the edge. On an outside edge it (i) contracts the edge (ii) moves the label to the second vertex and (iii) splits the tree at this vertex, giving all subtrees the same label from that vertex. The contraction of a tree T at an edge e is denoted T/e .

Example 5.4 The (21) tree splits into two at T/b ,



Example 5.5 The tree



splits into four unary edges on the contraction of the root.

All tree contractions within an A_d polytope are internal edge contractions, which do not create disjoint forests, so the dimensional increases within A_d are simple examples of splitting contractions.

Let \mathbf{T}_e denote the set of all decorated forests, graded by the total number of edges e . A differential $d : \mathbf{T}_e \rightarrow \mathbf{T}_{e-1}$ is defined using the splitting contraction [80]. It also requires an *orientation* for a tree T , defined on the set of edges E . An orientation is written $w = e_1 \wedge e_2 \wedge \cdots \wedge e_m$, where m is the cardinality of E . This defines an orientation class in $\{+, -\}$. Given any permutation $\sigma \in S_m$, the orientation $e_{\sigma(1)} \wedge \cdots \wedge e_{\sigma(m)}$ differs from w by the sign of σ . Let iw be the contraction $e_2 \wedge \cdots \wedge e_m$. The differential is given by

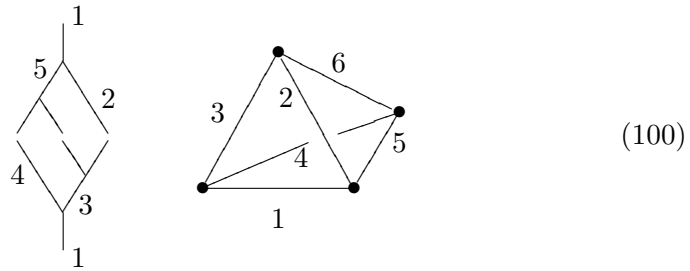
$$d(T, w) \equiv \sum_{e \in E} (T/e, iw). \quad (98)$$

It satisfies $d^2 = 0$. Under the disjoint union product and \otimes on orientation, it also satisfies the Leibniz rule [80]

$$d((T_1, w_1)(T_2, w_2)) = d(T_1, w_1) \cdot (T_2, w_2) + (-1)^{e(T_1)} (T_1, w_1) \cdot d(T_2, w_2). \quad (99)$$

5.5 Three Dimensional Traces

A tracing operation belongs to the realm of categories with duals, since dual objects permit arcs in a planar diagram. However, trees also allow traces. When two trees are glued together as a composition $1 \rightarrow m \rightarrow 1$, there is only one input and one output to be traced. These are joined by a loop segment, drawn in the plane. Because planar binary trees have trivalent nodes, they always glue to form surface graphs in three dimensions. For example, the gluing of an upside down (12) and a (21) from S_2 gives the tetrahedron graph

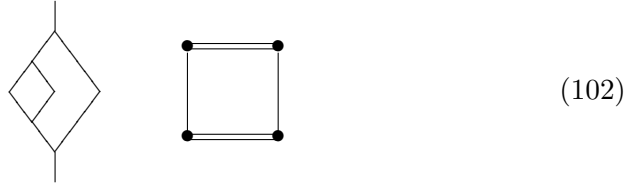


in a planar form. Let us denote an upside down tree in S_d by σ^* , where σ is the underlying permutation. A *trace* of two objects in S_d takes the tree σ^* and glues it to a tree τ . In another example, the trace of (23415) with

(15432) gives a pentagonal prism



A similar trace diagram in S_d gives a d -gon prism. Even for S_2 there is the *squashed can* prism



For S_3 the trace $\text{tr}((312)^*, (231))$ of 1-circulants is the triangular prism, which is a product of two basic simplices from the word monoid: one qubit edge and one qutrit triangle. Triangulations of this prism define the permutohedron S_4 .

For rooted trees, one can also construct the reverse gluing, as in the creation of a density matrix. This requires more than one joining string. For example, an associator $(21) \rightarrow (12)$



is glued using three strings, to give another form of the tetrahedron.

A general ribbon or multitree diagram has n inputs and n outputs, permitting several types of trace. The standard trace always matches the upper and lower points *in order*, a process that requires n joining strings. When arcs are freely available in the category, we consider other traces [81]. A *plat* trace can be defined when there are $2n$ strands, which is the case for ribbon diagrams. Instead of tracing from the top of the diagram to the bottom, strings are used to join top points and also to join bottom points. Most simply, one connects according to $(12)(34)(56) \cdots ((n-1)n)$, using the same connections at the top and the bottom of the diagram. We will also use a *cyclic plat* trace, which joins the points according to $(23)(45)(67) \cdots (n1)$.

Example 5.6



Three twists $\tau_1^2\tau_3^2\tau_5^2$ in B_6 are given the cyclic plat trace, to form a three component link.

5.6 Associated Braids and Knot Invariants

Permutations in S_d are usually represented by crossing strings, running from d points to d points in the plane. A braid diagram



permits crossing information in the third dimension. The braid group B_n on n strings composes two diagrams by joining one vertically to the other to create a new braid. As in appendix B, let τ_i represent the diagram with a crossing between the i -th and $(i + 1)$ -th strings, so that the left string passes over the right string, as in the top half of the diagram above. Then τ_i^{-1} is the diagram with the opposite crossing. Each group B_n has d generators $\{\tau_1, \tau_2, \dots, \tau_{n-1}\}$. Along with $\tau_i\tau_j = \tau_j\tau_i$ for $|i - j| > 1$, the group laws state that

$$\tau_i\tau_{i+1}\tau_i = \tau_{i+1}\tau_i\tau_{i+1} \tag{106}$$

for all i . The braid group B_n can be represented by either $n \times n$ or $(n - 1) \times (n - 1)$ matrices. The latter choice respects the role of B_3 as the cover of the 2×2 modular group $PSL_2(\mathbb{Z})$ of integer matrices up to ± 1 [82]. The modular group has the generators

$$t_1 = \begin{pmatrix} 1 & 1 \\ 0 & 1 \end{pmatrix} \quad t_2 = \begin{pmatrix} 1 & 0 \\ -1 & 1 \end{pmatrix}. \tag{107}$$

These satisfy the braid rule $t_1t_2t_1 = t_2t_1t_2$, but this rule collapses under the additional relation $(t_1t_2)^3 = I_2$.

The two natural representations of B_n are known as the *Burau representations* [83][84]. The Burau representation of dimension n has a generator τ_i , sent to a 2×2 block in the $n \times n$ matrix,

$$I_{i-1} \oplus \begin{pmatrix} 1-t & t \\ 1 & 0 \end{pmatrix} \oplus I_{n-i-1} \tag{108}$$

with entries in the polynomial ring $\mathbb{Z}[t, t^{-1}]$, assuming $t \neq 0$. At $t = 1$ the permutations in S_n are recovered. The $(n - 1)$ dimensional representation is obtained [84] by observing that the matrices above act on n -vectors to leave invariant the vectors whose entries sum to zero. Two B_3 generators are then given by

$$\tau_1 = \begin{pmatrix} -t & 0 \\ -1 & 1 \end{pmatrix} \quad \tau_2 = \begin{pmatrix} 1 & -t \\ 0 & -t \end{pmatrix}. \quad (109)$$

The pattern for higher n is indicated by the central B_5 generator

$$\tau_2 = \begin{pmatrix} 1 & -t & 0 & 0 \\ 0 & -t & 0 & 0 \\ 0 & -1 & 1 & 0 \\ 0 & 0 & 0 & 1 \end{pmatrix}. \quad (110)$$

In this representation, $(\tau_1 \tau_2)^3 = t^3 I_2$, so it does not collapse to the modular group if $t \neq 1$ or $t \neq \omega_3$. It is faithful for B_2 and B_3 but not for higher dimensional n [83]. However, in analogy to the construction of all permutations from S_2 flips, we hope to understand braids by looking particularly at B_2 and B_3 . The full set of B_3 generators is

$$\begin{aligned} \tau_1 &= \begin{pmatrix} -t & 0 \\ -1 & 1 \end{pmatrix} & \tau_1^{-1} &= \begin{pmatrix} -1/t & 0 \\ -1/t & 1 \end{pmatrix} \\ \tau_2 &= \begin{pmatrix} 1 & -t \\ 0 & -t \end{pmatrix} & \tau_2^{-1} &= \begin{pmatrix} 1 & -1 \\ 0 & -1/t \end{pmatrix}. \end{aligned} \quad (111)$$

Braid diagrams are traced with one connecting loop for each braid strand, attaching a top node to the bottom. This creates a closed knot or link diagram.

Modern link invariants [85][86] specialise to the older Alexander polynomial $\Delta_L(t)$, and this may be recovered from the $(n - 1)$ dimensional Burau representation as follows. Let the unnormalised Alexander polynomial be defined by

$$\Delta_L(t) = (1 + t + \dots + t^{n-1})^{-1} \det(1 - L) \quad (112)$$

where L is the matrix for the link L , formed from the τ_i generators. We will see that the polynomial coefficient comes from a determinant for unknot braids. Using B_3 , verify that the unknot invariant $\Delta_L = 1$ is obtained from $\tau_1 \tau_2$. The unknot invariant should also be obtained from a diagram of the form (105), such as $\tau_1^{-1} \tau_2$, but this gives

$$\Delta_L = (1 + t + t^2)^{-1} \cdot \left(\left(1 + \frac{1}{t}\right)t + \frac{1}{t} \right) = \frac{1}{t}. \quad (113)$$

In order to find the correct normalisation factor, we consider now the newer knot invariant, the Jones polynomial.

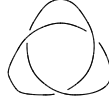
The Jones invariant $V_L(t)$ is defined by a *skein relation*. If three distinct links differ by only one crossing, there is a relation between their invariants. Let V_τ stand for the invariant when τ sits at the distinctive crossing. Then $V_L(t)$ is given by [85][84]

$$t^{-1}V_{\tau_1} - tV_{\tau_1^{-1}} = (t^{1/2} + t^{-1/2})V_{I_2} \quad (114)$$

where the identity I_2 stands for two vertical strands. We assume that the unknot is normalised to $V(t) = 1$. This is recursive, because we can always switch crossings in a messy knot to obtain a simpler knot, and evaluate invariants using the simpler diagrams.

Example 5.7 The three B_3 unknot diagrams, $\tau_1^{-1}\tau_2$, $\tau_1\tau_2$ and τ_2 , differ in only one crossing. The generator τ_2 is a two loop link, but the other one loop diagrams must satisfy $V_L = 1$. Thus V_L for two loops is $(t^{1/2} - t^{-1/2})$.

Example 5.8 The trefoil knot τ_1^3 in B_2



is computed using a few steps. Focus on changing the top right crossing. The two skein alternatives turn the trefoil into either a Hopf link or an unknot. We have computed the Hopf link $V_H = t^{1/2} + t^{5/2}$. The skein relation then states that V_T for the trefoil satisfies

$$(t^{1/2} + t^{-1/2})V_T = t^{-1}(t^{1/2} + t^{5/2}) - t$$

implying that $V_T = 1 + 1/t + t - t^{1/2} - t^{3/2} + t^2$. One often chooses a variable $q = t^{1/2}$, and a form of the skein relation that pulls out the determinant $1 + 1/t + t$. In that case, the trefoil polynomial takes the standard form $V_T = q^4 - q^3 - q$.

Fixing a value of V_L for the unknot is in fact sufficient to prove that V_L is a link invariant. But what has happened to the matrix invariant? We would really like an invariant that makes direct use of matrix representations. Recall that the unknot $\tau_1^{-1}\tau_2$ gave $\Delta_L = 1/t$. Let us list all such two crossing braids in B_3 .

$$\begin{aligned} \tau_1\tau_2 &= \begin{pmatrix} -t & t^2 \\ -1 & 0 \end{pmatrix} & \tau_1^{-1}\tau_2^{-1} &= \begin{pmatrix} -1/t & 1/t \\ -1/t & 0 \end{pmatrix} & (115) \\ \tau_2\tau_1 &= \begin{pmatrix} 0 & -t \\ t & -t \end{pmatrix} & \tau_2^{-1}\tau_1^{-1} &= \begin{pmatrix} 0 & -1 \\ 1/t^2 & -1/t \end{pmatrix} \\ \tau_1\tau_2^{-1} &= \begin{pmatrix} -t & t \\ -1 & 1 - 1/t \end{pmatrix} & \tau_1^{-1}\tau_2 &= \begin{pmatrix} -1/t & 1 \\ -1/t & 1 - t \end{pmatrix} \\ \tau_2\tau_1^{-1} &= \begin{pmatrix} 1 - 1/t & -t \\ 1 & -t \end{pmatrix} & \tau_2^{-1}\tau_1 &= \begin{pmatrix} 1 - t & -1 \\ 1/t & -1/t \end{pmatrix} \end{aligned}$$

Observe that in order to obtain $\Delta_L = 1$ for all these unknots, it seems we require a correction factor of t^k , where k is the number of *under* crossings in the braid diagram. Recall that the writhe w of a link is the difference $j - k$ between the number j of over crossings and the number k of under crossings. An inverse braid b^{-1} has j and k swapped, so that $w(b^{-1}) = -w(b)$. This suggests considering a corrected Alexander polynomial $\tilde{\Delta}_L(t) = t^x \Delta_L(t)$ for some x depending on w and n , so that all one loop unknot diagrams have $\tilde{\Delta}_L(t) = 1$. Since I_2 and powers of the B_3 generators all have $\tilde{\Delta}_L(t) = 0$, a factor such as t^{j+k} would not appear in $b \cdot b^{-1}$. But what about longer braids in B_3 ? The unknot $\tau_1 \tau_2^{-1} \tau_1^{-1} \tau_2$ needs a factor of t , but it has $k = 2$. This suggests instead the definition

$$\tilde{\Delta}_L(t) = t^{-w/2+1} \Delta_L(t) \quad (116)$$

which yields $\tilde{\Delta}_L(t) = 1$ for all the above braids. This is the correct normalisation for B_3 . For general n [84], we have the matrix invariant

$$\tilde{\Delta}_L(t) = (-1)^{w-n+1} t^{-w/2+(n-1)/2} \Delta_L(t). \quad (117)$$

The Jones polynomial agrees with $\tilde{\Delta}_L$ for B_3 braids. For $L \in B_3$ a knot, it is given by

$$V_L(t) = t^{w/2-1} (1 + t + t^2 + t^{w+1} - t \cdot \det(I - L)). \quad (118)$$

At $w = 0$ this reduces to

$$V_L^0(t) = 1 + \frac{1}{t} + t - \det(I - L) + 1. \quad (119)$$

That is, the special determinant for unknots is canceled out and the normalisation set at 1. Writhe zero knots have a simple skein relation for evaluating $V_L^0(t)$ known as the *Kauffman bracket* [87] K_L . This does not give a true knot invariant in general, because it does not account for the non planar writhe. Instead of two crossings, it uses both the I_2 diagram and its rotation by $\pi/2$, a two arc diagram. This mixture of two arc pictures is fundamental to all the combinatorics in this book, because it will represent S_2 . The initial normalisation is 1, and additional loops carry a factor of $-(t^{1/2} + t^{-1/2})$. Using diagram pieces to denote the invariant itself, the bracket says

$$\begin{array}{c} \diagup \quad \diagdown \\ \diagdown \quad \diagup \end{array} = t^{1/4} \begin{array}{c} | \\ | \end{array} + t^{-1/4} \begin{array}{c} \text{---} \\ \text{---} \end{array} \quad (120)$$

When suitably normalised, the Kauffman bracket becomes the standard Jones invariant V_L on multiplication by a writhe factor $(-1)^w (t)^{3w/4}$. One

can see the three dimensional invariance problem by considering a braid $b\tau_d^{\pm 1}$ in B_{d+1} , for any braid b . The addition of the extra crossing $\tau_d^{\pm 1}$ clearly does not change the actual knot, although it shifts w by ± 1 . Yet such a move would alter the Kauffman bracket. Chapter 8 looks more closely at the relation between the Kauffman bracket and the Jones invariant.

Soon after the discovery of the Jones polynomial, a two variable skein relation was found. It is known as the homflypt polynomial $P_L(x, y)$ [88], and generalises the previous invariants. Like V_L , it uses two crossings and an identity diagram, but one is free to change the coefficient of the identity so that the skein rule becomes

$$xP_\tau + x^{-1}P_{\tau^{-1}} + yP_I = 0. \quad (121)$$

The homflypt invariant distinguishes the mirror image of a knot, since it is defined by $P_{L^*}(x, y) = P_L(x^{-1}, y)$. It is also functorial, in the sense that P for the connected sum of two knots K_1 and K_2 is the same as $P_{K_1}P_{K_2}$. This invariant is related to the natural ribbon graph invariant, the Bollobas-Riordan polynomial [89].

Braids appear in the renormalisation Hopf algebras of the Standard Model [90][91][92], when tree vertices are transformed into nonassociative braid crossings. The braids contain extra information coming from loops in a Feynman diagram, and this may be encoded in chords joining two strands in a braid diagram. The Standard Model particle spectrum [93] is given as a set of ribbon diagrams in chapter 7, using the writhe 0 unknots from B_3 .

6 Twistor Scattering Theory

Instead of working with Feynman diagrams, twistor quantum field theory begins with polytopes in an abstract space whose dimension appears to increase with the number of particles entering into a scattering diagram. Although based on a continuum theory, the new diagram techniques work towards an emergent, combinatorial construction for the Standard Model.

In this chapter we look at these techniques for $N = 4$ planar Yang-Mills theory and $N = 8$ supergravity. While these are not Standard Model theories, there can be no doubt of their relevance to the true non local formulation for the Standard Model. However, whereas the stringy supersymmetry usually provides additional variables for the background geometry, for us it is merely indicative of arithmetic structure, and we focus here solely on the crucial combinatorial ideas.

Twistor space is a transform of complexified Minkowski space \mathbb{M} to the complex projective space $\mathbb{C}\mathbb{P}^3$ [40][41]. We start with the matrix form for a point in Minkowski space, namely a qudit path matrix

$$P = \begin{pmatrix} X\bar{X} & X\bar{Y} \\ Y\bar{X} & Y\bar{Y} \end{pmatrix} = \begin{pmatrix} x_3 + x_0 & x_1 + ix_2 \\ x_1 - ix_2 & x_3 - x_0 \end{pmatrix}, \quad (122)$$

where (x_0, x_1, x_2, x_3) are the usual coordinates for Minkowski space. The variables X and Y are *spinors*. For commutative variables $X, Y \dots$, the determinant of P is clearly zero. This determinant is a lightlike interval for the Lorentzian metric. Looking back at the word monoid, we see that P comes from a 4-dit matrix, and noncommutativity is directly associated to the metric.

For the twistor correspondence to work, the points of \mathbb{M} need to be complexified, so that we may consider complex spinors. And \mathbb{M} is compactified with a lightcone at infinity. A so called *infinity twistor* is crucial to the introduction of a mass scale in the $N = 8$ theory, and is the reason that mass is associated to higher dimensional sheaf cohomology in classical twistor geometry.

First, the group $G = SL_2(\mathbb{C})$ of unit determinant matrices acts by conjugation on P ,

$$g^\dagger \begin{pmatrix} X\bar{X} & X\bar{Y} \\ Y\bar{X} & Y\bar{Y} \end{pmatrix} g. \quad (123)$$

Here $SL_2(\mathbb{C})$ is locally the Lorentz group, because it clearly preserves the determinant

$$X\bar{X}Y\bar{Y} - X\bar{Y}Y\bar{X} = -x_0^2 + x_1^2 + x_2^2 + x_3^2. \quad (124)$$

As the double cover of the Lorentz group, G permits the introduction of the spinors. Twistor space \mathbb{T} is defined by pairs of spinors λ and μ , so that

a twistor $Z = (\lambda, \mu)$ can be a vector in \mathbb{C}^4 . The transformation between projective twistor space \mathbb{PT} and Minkowski space is a span 1-arrow

$$\begin{array}{ccc} & \mathbf{F}_{12}(\mathbb{T}) & \\ & \swarrow \quad \searrow & \\ \mathbb{M} = \mathbf{F}_2(\mathbb{T}) & & \mathbb{PT} = \mathbf{F}_1(\mathbb{T}) \end{array} \quad (125)$$

in a category of *flag manifolds* [41], which are sequences $V_1 \subset \dots \subset V_n$ of subspaces of a vector space. To begin with, \mathbb{PT} is \mathbb{CP}^3 , the one dimensional subspaces of \mathbb{C}^4 . Complexified Minkowski space \mathbb{M} is a flag manifold when viewed as a Grassmannian, namely the set of all 2-planes in \mathbb{C}^4 . This is what \mathbf{F}_2 means here.

Local coordinates for P may be expressed in Grassmannian form as a 4×2 matrix, $[P, I_2]$. The projective space \mathbb{CP}^3 similarly has homogeneous 4-vector coordinates $[iPv, v]$, where $v = [v_0, v_1]$ are homogeneous coordinates for \mathbb{CP}^1 , the Riemann sphere. A point in \mathbb{M} is mapped under the span to such a sphere in \mathbb{PT} , which we think of as a celestial sphere. The coordinates for \mathbf{F}_{12} are $[P, v]$, making it a five dimensional space.

The standard coordinates for \mathbb{T} start with the spinor μ , which is usually written with an index, as in $\mu_{A'} = (\mu_{0'}, \mu_{1'})$. A twistor is then a spinor pair $Z = (\lambda^A, \mu_{A'})$ with distinct indices. One usually works with a dual pair of twistor spaces, with a twistor $W \equiv (\bar{\mu}, \bar{\lambda})$ dual to Z . When the spinors are real, the conformal group acts simply as $SL_4(\mathbb{R})$ on \mathbb{R}^4 , and this covers the Lorentz group.

As 4-vectors, an independent Z and W define a two dimensional plane in \mathbb{T} . These planes form a fibre bundle over the Grassmannian manifold $Gr(2, 4)$. Recall that a fibre bundle over a manifold M is an arrow $\pi : E \rightarrow M$ with fibre F such that M is covered with sets U_i and there are homeomorphisms $\phi_i : E \simeq U_i \times F$ on E restricted to U_i [35]. The transition functions $g_{ij} = \phi_i \phi_j^{-1}$ on F take values in a structure group G .

A useful characterisation of the Grassmannian $G(2, 4)$ lives in $\mathbb{P}(\wedge^2 \mathbb{C}^4)$, for the exterior algebra $\wedge^2 \mathbb{C}^4$. The exterior algebra has basis 2-forms $\{v_1 \wedge v_2, v_1 \wedge v_3, v_1 \wedge v_4, v_2 \wedge v_3, v_2 \wedge v_4, v_3 \wedge v_4\}$ in terms of the basis v_i for \mathbb{C}^4 . A Minkowski Grassmannian point $[U, V]$, with coordinates viewed as vectors in \mathbb{C}^4 , maps to the 2-form $U \wedge V$ [41]. This gives a set of complex v_{ij} satisfying the Plücker relation

$$v_{12}v_{34} - v_{13}v_{24} + v_{23}v_{14} = 0, \quad (126)$$

where v_{ij} is shorthand for homogeneous coordinates in $\mathbb{P}(\wedge^2 \mathbb{C}^4)$. Later on we will see that Plücker coordinates are closely connected to the entanglement classification for three qubits, where \mathbb{C}^6 is viewed naturally as a three qubit state space.

In general, the path matrix (122) is noncommutative, and perhaps a projection in a 2×2 Jordan algebra. The matrix requires an alphabet of four letters, so it is a submatrix of the length 2, $d = 4$ word monoid matrix

$$\begin{pmatrix} XX & XY & X\bar{X} & X\bar{Y} \\ YX & YY & Y\bar{X} & Y\bar{Y} \\ \bar{X}X & \bar{X}Y & \bar{X}\bar{X} & \bar{X}\bar{Y} \\ \bar{Y}X & \bar{Y}Y & \bar{Y}\bar{X} & \bar{Y}\bar{Y} \end{pmatrix}. \quad (127)$$

Geometrically, the 2×2 block P determines a square, fitting into the divided tetrahedron simplex for $\{\bar{X}, X, Y, \bar{Y}\}$. Then the first two terms of the Plücker relation (126) give the determinant of P , while the whole relation comes from the tetrahedron.

The full twistor transform maps the solutions of simple massless field equations on Minkowski space to cohomology classes on twistor space [94][41]. The long term difficulty in extending this functorial cohomology to massive fields was a major motivation for studying universal motivic cohomology. Classically, massive solutions to the Klein-Gordon equation are possible [14] using a pair of massless spin 1/2 fields, which couple to form a non trivial H^2 sheaf cohomology. Such fermion pairs are drawn concretely in the ribbon diagrams of the next chapter.

6.1 Scattering Amplitudes

In category land, traditional supersymmetry does not introduce further physical states. It is rather a statement about the underlying number fields of the theory [95]. In particular, saying that a theory has $N = 4$ supersymmetry just means that it is expressed in quaternionic geometry. Twistor theory currently focuses on the planar $N = 4$ supersymmetric Yang-Mills theory, wherein we consider an S matrix for massless particle scattering, such that each particle is characterised by a momentum p and helicity \pm . We can think of these particles as gluons.

The color stripped scattering amplitude components are $M(\lambda_i, \bar{\lambda}_i, h_i)$, where h_i is the \pm helicity and spinors are used to specify the momentum [96][97][98][99]. These components fit into the full tree amplitude

$$A_n = g^{n-2} \sum \text{Tr}[T^{i_1} T^{i_2} \dots T^{i_n}] M(\lambda_i, \bar{\lambda}_i, h_i) \quad (128)$$

which includes the T^i matrices of the fundamental representation for color $SU(3)$. The helicity sign will be given by a left or right leaning tree leaf, since helicity is secretly the handedness of a particle braid and the tree orientation is a way of lining up the particles in color space.

Recall the Mandelstam variables for the s , t and u channels [100]

$$\begin{array}{ccc} \begin{array}{c} 1 \quad 2 \\ \diagdown \quad / \\ \text{---} \\ / \quad \diagdown \\ 4 \quad 3 \\ s \end{array} & \begin{array}{c} 1 \quad 2 \\ \diagdown \quad / \\ \text{---} \\ / \quad \diagdown \\ 4 \quad 3 \\ t \end{array} & \begin{array}{c} 1 \quad 2 \\ \diagdown \quad / \\ \text{---} \\ / \quad \diagdown \\ 4 \quad 3 \\ u \end{array} \end{array} \quad (129)$$

with $s + t + u = \sum_i m_i^2$. That is, $s = (p_1 + p_4)^2$, $t = (p_1 - p_2)^2$ and $u = (p_1 - p_3)^2$. In the zero mass limit $s \simeq 2p_1 \cdot p_4$, and so on. The particle momentum is now expressed in twistor variables as $p_i = \lambda_i \bar{\lambda}_i$, where in general the two variables are independent. Momentum conservation $\sum_i p_i = 0$ is used to define closed polygons of momenta in a dual twistor space, given by n coordinates such that $x_{i+1} - x_i \equiv p_i$. These polygons are dual to the tree diagrams that usually label the A_d polytopes, or a cyclic variant such as the cyclohedra.

In what follows we restrict to real spinors [96]. Under an $SL_2(\mathbb{C})$ Lorentzian transformation

$$\lambda_i \mapsto \phi_i \lambda_i \quad \bar{\lambda}_i \mapsto \phi_i^{-1} \bar{\lambda}_i \quad (130)$$

the amplitudes for a spin s particle should transform as

$$M(\phi Z, -) = \phi^{2(s-1)} M(Z, -) \quad M(\phi Z, +) = \phi^{-2(s+1)} M(Z, +). \quad (131)$$

The degrees here come from the *anti self dual* and *self dual* character of the components, via cohomology. The amplitudes are expressed in terms of basic invariants for the Lorentz group. These are

$$[\bar{\lambda}_1 \bar{\lambda}_2] \equiv \epsilon^{ij} (\bar{\lambda}_1)_i (\bar{\lambda}_2)_j \quad \langle \lambda_1 \lambda_2 \rangle \equiv \epsilon^{ij} (\lambda_1)_i (\lambda_2)_j \quad (132)$$

for the antisymmetric tensor ϵ . That is, one is in terms of W coordinates and the other in terms of Z . In the amplitudes these invariants are often abbreviated to $[12]$ and $\langle 12 \rangle$, for particles 1 and 2. A Mandelstam variable takes the form $s = \langle 14 \rangle [14]$, and so on.

An n particle amplitude is abbreviated to $M(123 \cdots n)$. The first non trivial $M(123 \cdots n)$ have two negative (resp. two positive) helicities, and these are known as MHV (resp. $\overline{\text{MHV}}$) amplitudes [101]. We write $M(- - + \cdots +)$ for the helicity configuration. For the minimal three point $\overline{\text{MHV}}$ configuration $(+ + -)$, the amplitude is given by

$$M(+ + -) = \frac{[12]^3}{[13][23]} \delta(\lambda_1 \bar{\lambda}_1 + \lambda_2 \bar{\lambda}_2 + \lambda_3 \bar{\lambda}_3) \quad (133)$$

including the momentum conservation delta function. Ignoring the delta function, the four point MHV amplitude

$$M(- - ++) = \frac{\langle 12 \rangle^4}{\langle 23 \rangle \langle 34 \rangle \langle 41 \rangle} \quad (134)$$

indicates the general MHV pattern. For k extra negative helicities, we have the $N^k \text{MHV}$ amplitudes. The first interesting six gluon MHV amplitude $(- - + + + +)$ equals simply

$$\frac{\langle 12 \rangle^4}{\langle 23 \rangle \langle 34 \rangle \langle 45 \rangle \langle 56 \rangle \langle 61 \rangle}$$

There is also a delta function for momentum conservation here, but this is understood. Observe how the negative helicity homogeneity $|2s - 2| = 4$ appears in the numerator for the particles 1 and 2, giving the required phase scaling. For a general MHV amplitude, the numerator is the same and there are $n - 1$ invariants on the denominator. Note how the MHV amplitudes are easily written in the Z variables, while the $\overline{\text{MHV}}$ ones use W .

These expressions for the MHV amplitudes originally arose from scrutinising concrete calculations using the Feynman method, when in the 1980s Parke and Taylor [102] were surprised to find such a simple answer. More recently, it has become clear that the twistor definition of the amplitudes is vastly simpler than the original Feynman form [103]. The modern advantage is our willingness to disallow spacetime locality its separate existence, and focus instead on unitarity.

In [104], scattering was considered in terms of on shell processes, which do not permit arbitrary momenta in internal loops. A *BCFW shift* selects two legs, $n - 1$ and n , and interpolates the twistor variables for these legs. For n particle tree amplitudes, this results in a rule [104][105]

$$M(123 \cdots n) = \sum_{+,-} \sum_{i=1}^{n-3} M_{\pm}(\bar{n}123 \cdots i) \frac{1}{P(n,i)^2} M_{\mp}((i+1) \cdots (n-2)(\overline{n-1})) \quad (135)$$

where $P(n,i)$ is the sum of momenta $p_n + p_1 + p_2 + \cdots + p_i$. In other words, there is a recursion rule that factorises an n point amplitude into a sum over products of amplitudes for a smaller number of particles. The two particles $n - 1$ and n have been singled out in this expression, breaking the cyclic invariance. In a twistor diagram [106], the two legs obtain a BCFW bridge.

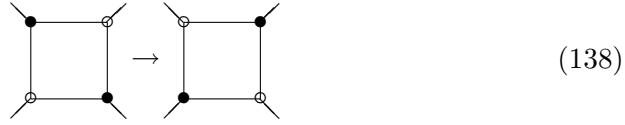


The black dots will stand for the Z variables and the white dots for the W [96]. In a general twistor diagram, the twistors define ribbon vertices [107]



where the anticlockwise and clockwise vertex orientation is given respectively by the permutations (312) and (231). The boundary of an amplitude diagram is again cyclic. The permutations (12) and (21) are also now ribbon strips, with an orientation. A modern twistor diagram with n legs defines a *decorated permutation* $\sigma \in S_n$ [23][107]. For four legs, there is a kind of

crossing flip



(138)

of Z and W nodes. A permutation in S_4 defines four paths through the diagram disc, giving 8 edges on the four legs of a planar ribbon graph. The identity (1234) can be drawn with no crossing points



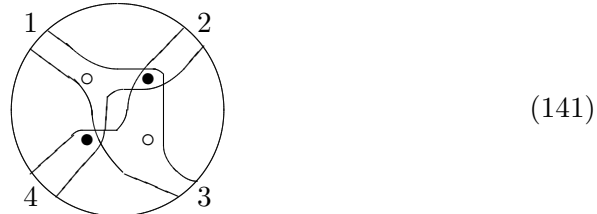
(139)

using ribbon edges that loop back to the same vertex. Thus the S_2 permutations are given by the pictures



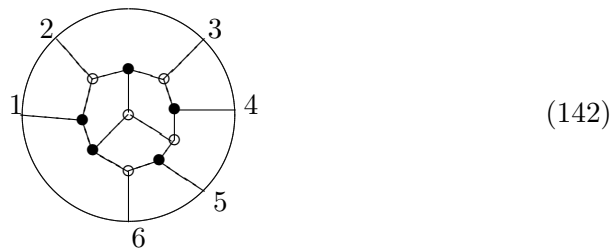
(140)

This is a crucial reinterpretation of the identity ribbon strip, because as we will see in the next two chapters, the usual planar pictures for S_2 are precisely the other way around. This existence of a dual representation for S_2 suggests a study of interpolations between (21) and (12), giving elements in a group algebra $\mathbb{F}S_2$. In another example, the permutation (3412) requires a twistor square.



(141)

By convention, we choose to turn left at the white dots and right at the black, and each leg has one incoming and one outgoing path. Then there is always a ribbon segment associated to each edge of the internal diagram. The permutation is uniquely determined by such a set of ribbon edges. An S_6 example is



(142)

where we see the six pentagons and three squares of the A_4 associahedron, except that the twistor object has 16 vertices and not 14.

These decorated permutations give a natural choice of Grassmannian variables for a $(k+2) \times n$ matrix [107]. These are the $G(k+2, n)$ Grassmannian homogeneous coordinates, where a $(k+2) \times (k+2)$ submatrix is fixed at I_{k+2} . This generalises the Minkowski space $G(2, 4)$ coordinates, which now correspond to 4 particles in a $(--++)$ configuration. Reducing the number of legs with a BCFW type cut, a Minkowski point could be drawn as a two leaved tree

$$\begin{array}{c}
 - \quad + \\
 \diagdown \quad / \\
 \quad \quad \quad | \\
 \quad \quad \quad || \\
 \quad \quad \quad -+
 \end{array}
 \tag{143}$$

with a double edged root. Recall that the unsigned tree stands for the unique associahedron point A_1 . All sign configurations can be given by a tree so that left leaning leaves get a minus sign and right leaves a plus. In other words, the MHV rule, which says one must have at least two negative helicities, comes down to the emptiness of associahedra below the fundamental point. The three particle trees that are required for gravity then reduce to a diagram with only one leaf, either left or right leaning, and this gives two distinct representations of the empty set.

The columns of the Grassmannian matrix span a planar subspace of n dimensional space. The homogeneity sets $k+2$ columns to the identity matrix, as in

$$M_{13} \equiv \begin{pmatrix} c_{12} & 1 & c_{32} & 0 \\ c_{14} & 0 & c_{34} & 1 \end{pmatrix}
 \tag{144}$$

for the Minkowski space configuration $(+ - + -)$. M_{ij} is indexed by the column choices, so that the remaining indices are used for the rows. In total, there are

$$m = \binom{n}{k+2}$$

such matrix minors, the full set giving coordinates M_{ij} for the projective space \mathbb{P}^{m-1} via the Plücker map. The Plücker relation (126) holds between the determinants of the six minors in the four point case. The interesting part of the Grassmannian is *positive* [108][109], meaning that all minors are positive.

For these Yang-Mills diagrams, there is a globule reduction rule known as *bubble deletion*. This is the categorical rule (274)

$$\begin{array}{c}
 | \\
 \circ \\
 | \\
 \bullet \\
 |
 \end{array}
 =
 \begin{array}{c}
 | \\
 | \\
 |
 \end{array}
 \tag{145}$$

often used for two distinct bases in a symmetric monoidal category. Finally, the full recursion rule for an n particle l loop amplitude is given by a sum over BCFW bridge tree factorisations along with on shell loop terms

The diagram shows a large circle representing a loop. A horizontal line segment connects two points on the top of the circle, labeled n on the left and 1 on the right. A vertical line segment extends downwards from the left side of the circle, labeled $l-1$. A small loop is attached to the top of the large circle, between the two points where the horizontal line segment meets the circle. To the right of the diagram is the label (146).

where the little loop has an ingoing $\lambda_j \bar{\lambda}_j$ momentum and outgoing $-\lambda_j \bar{\lambda}_j$ one.

6.2 $N=8$ Supergravity

In the twistor formalism, there is a close link between the $N = 4$ theory and $N = 8$ supergravity. The spin 2 tensors required for gravity are, in a suitable sense, squares of the Yang-Mills ones [110][111]. This is known as *color kinematic duality*. First, let the numerator of a term in a Yang-Mills tree amplitude be expressed as $c_j n_j$, where c_j are color factors related to the structure constants of the Lie algebra. Duality imposes a relation between the c_j and n_j . That is, given three terms that are related by the Jacobi rule

$$\perp\perp - \underline{X} = \underline{Y} \quad (147)$$

a relation $c_1 \pm c_2 \pm c_3 = 0$ implies that $n_1 \pm n_2 \pm n_3 = 0$ [111]. The supergravity amplitudes have numerators like n_j^2 , namely two kinematic factors. The three particle spin 2 amplitude is just M^2 , where M is the spin 1 Yang-Mills amplitude. The four point graviton amplitude [112] is

$$M(++--) = G_N \frac{\langle 34 \rangle^4 [12]^4}{\langle 14 \rangle [14] \langle 12 \rangle [12] \langle 13 \rangle [13]} \quad (148)$$

where G_N is Newton's constant. The denominator is an stu factor, using the convention above. This is clearly a product of Yang-Mills $M(- - ++)$ and $M(++--)$ amplitudes, whereas the three point case

$$M(- - +) = \frac{\langle 12 \rangle^6}{\langle 13 \rangle^2 \langle 23 \rangle^2} \quad (149)$$

does not mix Z and W invariants.

Physical localisation in twistor scattering comes from the observation that factors in internal propagators, such as $(p_1 + p_2 + p_3 + p_4)^{-1}$, give

singularities precisely when the internal particle is real. This is now an *extra* condition on the amplitudes, and a strong constraint on the spin s . For spin 2 there was an stu factor in the four point case. The only other solution for a fixed s theory is a factor $s^{-1} + t^{-1} + u^{-1}$, appearing in a spin zero ϕ^3 scalar field theory [112].

There is also a straightforward recursion rule for the gravity amplitudes. Recent results include an exact tree level formula for the $N = 8$ theory. In [21][23], the N^k MHV kinematic invariants are defined by an $n \times n$ matrix $K(k+2)$. This is paired with a matrix \overline{K} for dual variables. We mention the MHV case only. Define the phases [23]

$$\begin{aligned}\phi_{ij} &= \frac{[ij]}{\langle ij \rangle} & i \neq j \\ \phi_{ii} &= - \sum_{j \neq i} \frac{[ij]\langle jx \rangle \langle jy \rangle}{\langle ij \rangle \langle ix \rangle \langle iy \rangle}\end{aligned}\tag{150}$$

which are independent of the choices x and y , for momentum conservation on the n points. Now let

$$c_{ijk} = (\langle ij \rangle \langle jk \rangle \langle ki \rangle)^{-1}.\tag{151}$$

Then the n point amplitude is expressed in terms of the c_{ijk} and ϕ_{ij} as a new kind of determinant for the symmetric matrix K_{ij} , which has entries ϕ_{ij} . One needs to delete 3 rows and 3 columns from K_{ij} , namely ijk and a complementary rst . These yield a $(n-3) \times (n-3)$ minor, called $\Phi_{rst,ijk}$. Let $\sigma_{rst,ijk}$ be the permutation in S_n sending $(ijk12 \cdots n)$ to $(rst12 \cdots n)$. Then the important part of the gravity amplitude is just

$$M'(12 \cdots n) = (-1)^{n+1} \text{sgn}(\sigma_{rst,ijk}) c_{ijk} c_{rst} \Phi_{rst,ijk}.\tag{152}$$

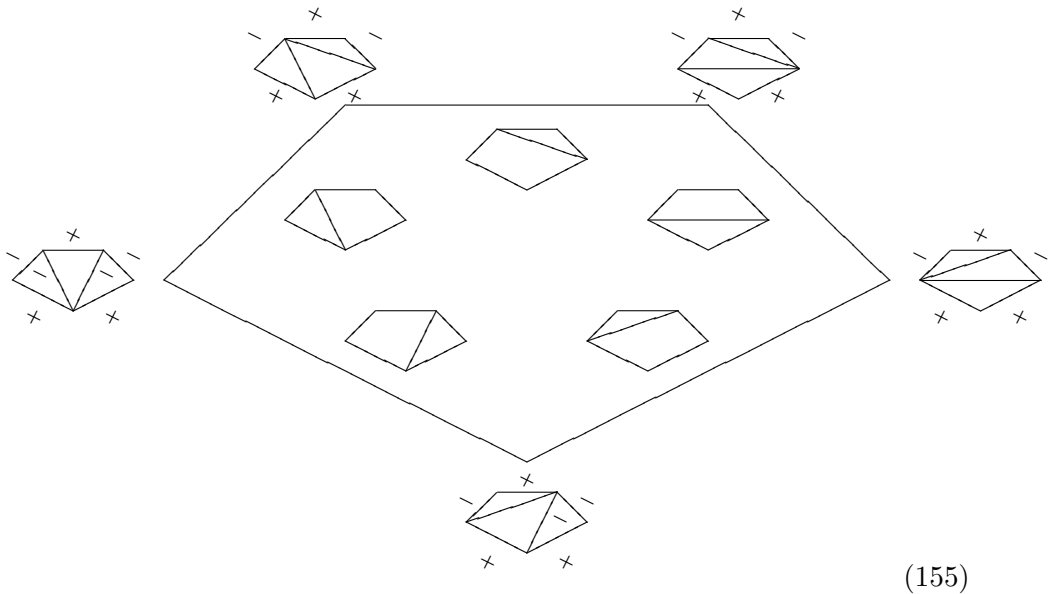
Despite appearances, it does not depend on the permutations. The full amplitude $M(12 \cdots n)$ is essentially a product $\det(\overline{K}) \det(K)$ of such reduced determinants [21]. The reduced determinant at N^k MHV requires $n - k - 3$ contractions.

As a ribbon graph, the Jacobi rule 147 is similar to the braid skein diagrams when the internal propagators are cut out. The two propagator edges are replaced by joins along the ribbons, and this looks like three S_2 moves, one for each diagram. A similar thing happens for the point particle line diagrams, except that the internal edge is only replaced by the endpoints. In this way, the Jacobi rule is dual to the Jones skein relation.

6.3 Grassmannians and Associahedra

With two rows in a $k = 0$ $\overline{\text{MHV}}$ Grassmannian matrix, there are $(d-1)(d+2)/2 + 1$ minors M_{ij} , for $d = n - 1$. Recall that $(d-1)(d+2)/2$ counts the

correspond to labeling both outer edges and chords, so that all triangles in the chorded diagram have mixed sign sets. That is, no triangles of form $(- - -)$ or $(+ + +)$ are allowed. On the index hexagon for A_4 , this selects the two points that meet three pentagon faces and no squares. Since square faces will typically mark braid crossings, it is not surprising that they are trivial in the planar theory. Let us attempt to assign such signs to the pentagon of pentagons



The horizontal chord in the top right pentagon must be a $-$ by the triangle rule. This forces the one other chord to be marked with a $+$ sign. Moving around four sides of the large pentagon, all chord signs are fixed by associator edges. But then, as we return to the start, the last pentagon will have the wrong signs on an internal chord. The required additional sign flip suggests turning the pentagon into a hexagon; this is in general the extension to permutation groups.

Observe that only three vertices of the pentagon have some freedom in assigning signs to chords. These are all equivalent under cyclic shifts. In the end, there is only one vertex for the $(- - + - +)$ sequence and one for $(- - - + +)$, and these configurations are counted by the Catalan number C_2 , the vertices on an associator edge A_2 . As n increases, there are more possibilities for the chordings, but the correct count of sign configurations is always C_n .

Consider now the canonical leaf signs for helicity. Once again, let $k + 2$ be the total number of minus signs, and let r be the number of $+$ signs. For a given k , the number of terms in a scattering amplitude is given by the Narayana numbers. Recall from chapter 5 that the collection of Narayana numbers, for all possible k , sums to the Catalan number associated to n .

For n points,

$$C_{n-3} \equiv \frac{1}{n-2} \binom{2(n-3)}{n-3} \quad (156)$$

for $n \geq 3$. For example, at $n = 5$ we take the polygon with $n - 1 = 4$ sides, and this has two possible chordings, giving C_2 . The Catalan numbers are decomposed into Narayana numbers $N(k, j)$ with $C_k = \sum_{j=1}^k N(k, j)$. In terms of n and r ,

$$N(n, r) = \frac{1}{n-3} \binom{n-3}{r-1} \binom{n-3}{r-2} \quad (157)$$

so that $N(6, 3) = 3$ recovers the three internal vertices of the pentagon A_3 . The A_3 signs are given in (83). After choosing a root, the other helicity signs correspond to the direction of the leaves, with $-$ for a left branching and $+$ for right. Since these signs are canonical, all the higher dimensional cells of an A_d polytope are defined as usual.

6.4 Symbology and Polylogarithms

Multiple polylogarithms are ubiquitous in scattering theory. This large class of functions satisfies numerous functional relations. Symbology [114][115][116] is the process of mapping a given polylogarithm to a unique object in a categorical algebra so that the combinatorics of functional relations are respected by this algebra. Polylogarithms are defined [117] recursively in terms of complex parameters by

$$G(a_1, a_2, \dots, a_{n-1}; x) = \int_0^x \frac{dt}{t - a_1} G(a_2, a_2, \dots, a_{n-1}; t) \quad (158)$$

starting with $G(0) = 0$ and $G(x) = 1$ for $x \neq 0$, and then $G(0; x) = \log x$. This class includes the classical polylogarithms $\text{Li}_{n-1}(x) = -G(0, \dots, 0, 1; x)$ and nested sums such as

$$G(0, 0, \frac{1}{x_3}, 0, \frac{1}{x_2 x_3}, \frac{1}{x_1 x_2 x_3}; 1) = (-1)^3 \sum_{i_1 < i_2 < i_3} \frac{x_1^{i_1} x_2^{i_2} x_3^{i_3}}{i_1^1 i_2^2 i_3^3}.$$

Sometimes the shorthand 0_m is used for a string of m zeroes. In particular, the multiple zeta values $\zeta(s_1, \dots, s_k)$ [118][119] for $s_i \in \mathbb{N}$, called MZVs for short, are given by $G(0_{s_k-1}, 1, 0_{s_{k-1}-1}, \dots, 0_{s_1-1}, 1; 1)$. These MZVs occur in the basic n point Veneziano amplitudes, which may be obtained through cohomological integration on spaces described by the categorical polytopes [120][121]. A multiple zeta value of *depth* j and *weight* n is a function of the form

$$\zeta(k_1, k_2, \dots, k_j) = \sum_{n_1 > n_2 > \dots > n_k \geq 1} \frac{1}{n_1^{k_1} n_2^{k_2} n_3^{k_3} \dots n_j^{k_j}} \quad (159)$$

for positive integers k_1, k_2, \dots such that $n = \sum k_i$. Higher order classical polylogarithms [122] are defined iteratively as

$$\text{Li}_n(z) = \int_0^z \text{Li}_{n-1}(z) \frac{dz}{z}$$

and in particular $\text{Li}_n(1) = \zeta(n)$. The *symbol* $\mathcal{S}(G)$ associated to an MZV will always be zero, due to the parameters occurring in G . For instance, when some $s_i \geq 2$ the MZV symbol contains at least one term equal to 1, coming from a $(0, 1)$ subsequence in the arguments, and this forces a zero symbol.

By construction then, the symbol algebra is *torsion free*, meaning that any occurrence of a root of unity, such as 1 itself, kills the symbol. This reflects the simple fact that $\mathcal{S}(\log x) = x$ with $\log 1 = 0$. In particular, the pole of the Riemann zeta function at $s = 1$, which equals $-G(1; 1)$, has symbol 0.

Since $\mathcal{S}(\log x) = x$, we may think of the symbol $\mathcal{S}(G)$ as a kind of exponentiation map, which turns arithmetic sums into products. Moreover, since \mathcal{S} acts on functions, it might be viewed as a functor on a subcategory of functions on $\{\mathbb{C}^n\}$. The pointwise product $G_1 G_2$ of two functions should then be sent by \mathcal{S} to a product for the symbol algebra. At the level of universal algebra, the shuffle rule

$$x \sqcup\sqcup y \equiv x \otimes y + y \otimes x \tag{160}$$

interprets $x \sqcup\sqcup y$ as $\mathcal{S}(\log x \log y)$ in the target category. This becomes a functoriality law for the symbol algebra.

Given a vector $(a_1, a_2, \dots, a_{n-1})$ of complex singularities, a general polylogarithm function $G(a_1, a_2, \dots, a_{n-1}; x)$ of weight $n-1$ is referred to simply as a *polylog*. The symbol $\mathcal{S}(G)$ [114][115] of a polylog G is an object in a tensor algebra of functions in the parameters $(a; x) \equiv (a_1, a_2, \dots, a_{n-1}; x)$ of G . Words W of the form $w_1 \otimes \dots \otimes w_k$ in the tensor algebra form an algebra with respect to the shuffle product $W_1 \sqcup\sqcup W_2$ (see appendix C). In summary, the full symbol algebra satisfies the following axiomatic properties.

- **Functorality:** $\mathcal{S}(G(a_1, a_2, \dots, a_j; x)G(a_1, a_2, \dots, a_k; y))$
 $= \mathcal{S}(G(a_1, a_2, \dots, a_j; x)) \sqcup\sqcup \mathcal{S}(G(a_1, a_2, \dots, a_k; y)).$
- **Distributivity:** function products split, as in $U \otimes (xy) \otimes V = U \otimes x \otimes V + U \otimes y \otimes V.$
- **Scale Invariance:** since, for all $\lambda \in \mathbb{C}^*$, $G(\lambda a; \lambda x) = G(a; x)$ provided $a \neq 0$, the symbol must satisfy $\mathcal{S}(G(\lambda a; \lambda x)) = \mathcal{S}(G(a; x)).$
- **No Torsion:** for ω_n the n th root, $U \otimes \omega_n \otimes V = 0$, for all $n \in \mathbb{Z}.$

Functoriality implies that

$$\mathcal{S}(\log x \log y) = \mathcal{S}(\log x) \sqcup \mathcal{S}(\log y) = x \otimes y + y \otimes x. \quad (161)$$

Here the symmetric expression $x \otimes y + y \otimes x$ is associated to the concatenation xy , since the exponential of $\log x \log y$ is xy .

An example of a classical polylog is $\text{Li}_2(x) = -G(0, 1; x)$, which has symbol $-(1-x) \otimes x$. Another example will be determined in the next section by a set of three chorded, labeled polygons P . These new diagrams use a special *function assignment* f , which sends the simplest two variable globule diagram $P(y; x)$ to

$$f(P(y; x)) = 1 - x/y \quad (162)$$

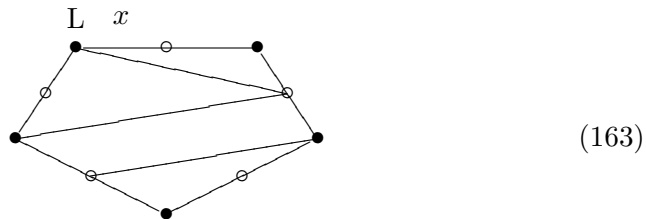
when $y \neq 0$, and to x otherwise [114][115][116]. Why this particular function? Firstly, the ratio x/y enforces scale invariance on all $\mathcal{S}(G)$. When $y = 0$, $P(0; x)$ must recover $\mathcal{S}(\log x) = x$. The basic polylog $-\text{Li}_1(x) = G(1; x)$ has symbol $(1-x)$, since this is just $\log(1-x)$.

6.5 Decorated Polygons for Symbols

Decorated trees [80] appeared in section (5.3). Their dual polygons are used to construct the symbol for a polylog. To each polylog G we assign a decorated, rooted polygon $P(G)$ following [80][123].

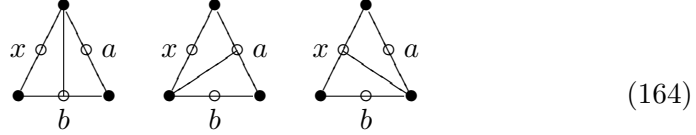
For an n argument polylog $G(a_1, a_2, \dots, a_{n-1}; x)$ there is an n -gon with halved sides, forming a $2n$ -gon with alternating black and white vertices, such that the white vertices mark the midpoints on the sides of the original n -gon. The sides of the n -gon are labeled with the arguments of $G(a_1, a_2, \dots, a_{n-1}; x)$, so that x marks a root edge. The *orientation* of $P(G)$, left or right, is specified by choosing a vertex at either the left or right hand side of the root edge.

A *maximal chord diagram* is a set of $n-2$ non intersecting chords on the $2n$ -gon, with each chord joining one black and one white vertex, but not an adjacent vertex, as in the figure



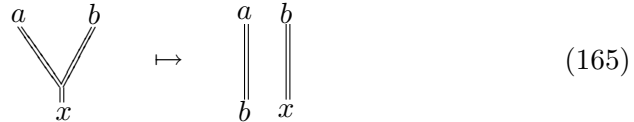
where the top edge is a left oriented root edge, holding the x variable. The symbol $\mathcal{S}(G)$ is constructed from the set of all maximal chord diagrams

for $P(G)$. To start with, at $n = 3$, there are three chorded triangles for $G(a, b; x)$.



In what follows, we assume a left orientation for the polygons, so that labels are read in an anticlockwise direction. The chording turns the $2n$ -gon into a polygon chopped into squares. Observe that this $2n$ -gon is dual to a tree with ternary vertices. So accounting for the root, a hexagon for $n = 3$ would become a tree with five leaves, and two ternary nodes.

The polygon is decomposed using the splitting contraction of (5.3) on the edge at the head of a chord. Thus the first chorded triangle, drawn dually as trees, becomes

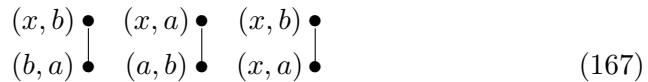


a forest. The top label is taken from the root side of the globule. Using trees dual to hexagons, and remembering the root, the three triangles for $n = 3$ are labeled by the three square faces



of the A_4 associahedron. For any n we obtain index diagrams for certain codimension $n - 2$ faces of A_{2n-2} , which are always of dimension $n - 1$. There are $n!/2$ such faces, which can be seen inductively. Fixing one initial chord, there are $(n - 1)!/2$ ways to cut the remaining $(2n - 2)$ -gon by the remaining chords. There are then n rotations of each such diagram.

Given a maximal chord diagram, there are associated linear orders with $n - 1$ vertices. These are the internal orders of the dual decorated tree. Each vertex is labeled with a pair (u, v) of variables from the decorated diagram, representing a rooted globule with sides u and v . For the triangles, there are two vertices in the unique order,



with globule labels determined as above, by contraction. Observe that each vertex on a linear order is a node on the dual tree. The orders are simply paths through the dual tree, with the root node at the top.

There remains only a sign problem in the symbol construction. This uses the orientation that was required for the differential on trees, as in chapter 5.

The symbol obtains a factor of $(-1)^k$, where k is the number of backwards arrows, as follows. Orient every chord on the polygon with an arrow head at the white vertex. An arrow is backwards if its tail starts at a vertex to the right of its head, with the string of edges read clockwise from the root vertex and ending with the root edge. For example, only the first triangle has a backwards chord. Finally, the symbol for $G(a, b; x)$ is

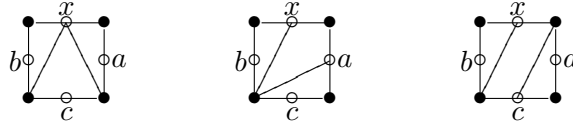
$$\mathcal{S}(G(a, b; x)) = -(1 - \frac{x}{b}) \otimes (1 - \frac{b}{a}) + (1 - \frac{x}{a}) \otimes (1 - \frac{a}{b}) + (1 - \frac{x}{b}) \otimes (1 - \frac{x}{a}), \quad (168)$$

reading the function assignments, as in (162), from the linear orders. For general polygons, the symbol is obtained via a sum over all maximal sets P ,

$$\mathcal{S}(G) = \sum_P (-1)^k \sum_{\text{orders}} f(u_1, v_1) \otimes \cdots \otimes f(u_{n-1}, v_{n-1}) \quad (169)$$

using the above algorithm.

Example 6.2 The 12 octagons for $G(a, b, c; x)$ are given by chord rotations of the three diagrams



There are three diagrams with V shaped linear orders, which have symbol terms of the form

$$\begin{aligned} & -f(b, x) \otimes f(a, b) \otimes f(c, b) - f(b, x) \otimes f(c, b) \otimes f(a, b) \\ & -f(c, x) \otimes f(a, x) \otimes f(b, c) - f(c, x) \otimes f(b, c) \otimes f(a, x) \\ & f(b, x) \otimes f(a, x) \otimes f(c, b) + f(b, x) \otimes f(c, b) \otimes f(a, x) \end{aligned}$$

and the other 9 diagrams contribute terms like $f(a, x) \otimes f(b, a) \otimes f(c, b)$.

In general, there is also a contraction differential that defines a differential graded algebra of polygons with a \wedge product, where the symbol belongs to the associated \otimes coalgebra. This is known as the *bar construction* [124][80][125]. Polygon differentials are closely related to the comultiplication for the Hopf algebra of rooted trees, underlying renormalisation theory. In the symbol calculus, the polygon label set $(a_1, \dots, a_{n-1}; x)$ defines a polygon *cocycle*. With both algebra and coalgebra structures, the polygons form a commutative Hopf algebra. It is commutative because the disjoint union of trees is taken to be commutative, but this could be modified to noncommutative forests.

Only a few basic function types occur in symbol terms. Essentially, these are listed by the permutation group S_3 [123],

$$\begin{aligned}
x &= \begin{pmatrix} 1 & 0 & 0 \\ 0 & 1 & 0 \\ 0 & 0 & 1 \end{pmatrix} & \frac{1}{x} &= \begin{pmatrix} 0 & 0 & 1 \\ 0 & 1 & 0 \\ 1 & 0 & 0 \end{pmatrix} \\
\frac{1}{1-x} &= \begin{pmatrix} 0 & 1 & 0 \\ 0 & 0 & 1 \\ 1 & 0 & 0 \end{pmatrix} & \frac{x}{x-1} &= \begin{pmatrix} 0 & 1 & 0 \\ 1 & 0 & 0 \\ 0 & 0 & 1 \end{pmatrix} \\
1 - \frac{1}{x} &= \begin{pmatrix} 0 & 0 & 1 \\ 1 & 0 & 0 \\ 0 & 1 & 0 \end{pmatrix} & 1 - x &= \begin{pmatrix} 1 & 0 & 0 \\ 0 & 0 & 1 \\ 0 & 1 & 0 \end{pmatrix}
\end{aligned} \tag{170}$$

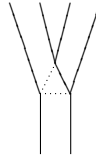
where function substitution is the group operation. For example, substituting $1/x$ into the variable in $1/(1-x)$ gives $x/(x-1)$. This means that $(231)(321) = (213)$. The sum of all six functions gives the ordinal 3, just like the sum over S_3 determines the 3×3 representation of 3. The coidentity $1/x$ is the inverse of x as an up down matrix reflection, and similarly for the other functions. Recall that such a matrix symmetry is captured by the permutation signature classes, with signature string reversal and sign flipping. In terms of logarithms, this symmetry is the additive inverse between $\log x$ and $-\log x$.

This substitution form of S_3 is the same as the S_3 action on the argument z of the j -invariant for elliptic curves [126]. That is, each function in z is also a ratio in terms of roots of a cubic polynomial. For example, for (312) we can take $z/(z-1) = (e_2 - e_3)/(e_2 - e_1)$. Recall that the ribbon graph for the j -invariant is the two loop curve in the complex plane with trivalent nodes at ω_6 and its conjugate. There are also special bivalent points on the real line, defining a triangle on $\mathbb{R} \cup \infty$. This is the source of the S_3 symmetry.

Remark 6.3 In one complex dimension, a closed string diagram is a surface of genus g . Surfaces with n marked points may be viewed as ribbon diagrams. An abstract conformal field theory is defined as a categorical structure for ribbon graphs [24][25], requiring mainly the pentagon and hexagon laws. These are most easily understood by turning the surface diagrams into line graphs [127], where the number of loops in the graph corresponds to the genus g . The pentagon rule is then the basic associahedron rule for four leaved trees, cut out of the surface graphs. In a conformal field theory, one labels the tree edges with graph data. This extends the composition on the pentagon and hexagon to matrix rules.

As smooth surfaces, ribbon graphs have no automatic internal edges, but we permit branched surfaces, defined using ribbon vertices. Chords drawn

on a ribbon strand across a vertex



(171)

secretly turn the ribbon back into a tree graph, using associated lines. Such ribbon vertices may be glued into branched surface diagrams, and these are interesting as universal templates for knots, removing the need for a third dimension.

7 The Ribbon Particle Spectrum

In the Standard Model, the Higgs mechanism [128] introduces mass generation for both the electroweak gauge bosons and all fermions appearing in the Lagrangian. A particle with the properties of a Higgs boson was discovered in 2012 by the ATLAS [129] and CMS [130] experiments at the LHC.

Yet despite this success, we know that the correct description of electroweak symmetry breaking is not entirely a local one. We expect both spacetime and gauge symmetries to emerge from a richer arithmetic structure for the information of quantum states. In this chapter, ribbon graphs are used to list the fundamental particles. Unlike diagrams for a local field theory, these graphs are not meant to be directly associated to a spacetime or momentum space.

Fortunately, ribbon graphs retain some aspects of gauge symmetry, as representations of finite groups. But the representation types that appear can differ from those of the local Lagrangian, which one imagines is reconstructed in the world of infinite dimensional matrices, where the continuum resides. The ribbon graphs make both left and right handed fermions into adjoint representations, in analogy to the bosons. This highlights a novel kind of supersymmetry [131], for which the Standard Model fermions correspond one to one to boson states under a quantum Fourier transform.

The best evidence for this ribbon structure lies in the Koide phenomenology for rest masses. Although there is no immediately obvious representation of the Higgs boson as a ribbon graph, it is possible that a composite description of the Higgs exists, as favoured in many approaches. Note that the observed Higgs mass $m_H = 126$ GeV was predicted some years ago by Dharwadker and Khachatryan [132] using the simple formula

$$m_H = \frac{1}{2}(m_{W^+} + m_{W^-} + m_Z) = m_W + \frac{m_Z}{2}, \quad (172)$$

which is discussed below. The running of mass under renormalisation does not prohibit algebraic relations between the masses. We expect the emergent theory to pick out special scales in a different way to the Standard Model, wherein mass values depend on empirical parameters. Yukawa couplings for the Lagrangian are then, in principle, secondary to the ribbon description of Koide mass matrices, wherein rest mass appears as an eigenvalue of a circulant Hermitian matrix. That is, although the simple Lie symmetries of the Standard Model require spontaneous symmetry breaking, nature has already selected the broken symmetry, and this may be amenable to another description.

There are $U(1)$ charges appearing explicitly in the diagrams below, in the twists of ribbon strands. We start with the assumption that this represents electromagnetic charge, but the interplay of different $U(1)$ symmetries turns up naturally in ribbon networks. In James Clerk Maxwell's original paper

on electromagnetism [133], such twist loops were supposed to define vortices in the aether. This classical aether is absent when the ambient ribbon space is no longer associated to space itself, but vortices remain a useful insight into gauge construction.

The ribbon spectrum [93] represents the most fundamental set of localised IR states, according to observation rather than the rules of classical geometry. The only additional states that must be considered are mirror neutrino states. These occur naturally within the basic ribbon set, which uses braid crossings in order to distinguish matter from mirror matter. Although a full zoo of mirror particles is possible in the braid scheme, and gravitationally interacting mirror matter is a leading candidate for dark matter, a natural ansatz does not permit localisable mirror matter. If it exists as dark mass, as discussed in the final chapter, it is not an independent entity. On the contrary, the mirror world is supposed to balance our thermodynamic arrow of time with its contracting universe. Both halves of this cosmos define the true vacuum, and rest mass itself requires the pairing of one baryonic and one mirror state. Chirality for massive particles is then maintained by the handedness of the baryonic component.

One intriguing possibility is to view the mirror matter as the proton sector: electrons are mirrored by antiprotons, positrons by protons, and quarks by the components of leptons. In this case, the ribbon set gives exactly the observable low energy states, and there can be no particle-like dark matter or dark energy. This means that general relativity fails to describe the cosmos on large scales, a possibility quite consistent with current observations.

To begin with, we ask the simple question: what happens with the neutrinos? Due to neutrino oscillations, there are up to 24 possible states, including generation, mirror, flavor and antiparticles. Most simply, we assume that the four electroweak states for a given flavor give standard Dirac mass terms [134] using the right handed states. Since neutrinos are massive, these right handed states must exist. In the ribbon diagrams, as for the charged leptons, these are not singlet states, which is interpreted to mean that mirror neutrinos participate in the non local weak interaction, and are not truly sterile.

7.1 Braids and Ribbons

We consider both the Burau representations for B_n , particularly B_3 and B_6 , and also matrix representations arising directly from the diagrams.

The special knots in B_3 are the non identity odd cycles for S_3 , which do not reduce to B_2 or B_1 objects. We choose the writhe zero knots in the set $\{\tau_1\tau_2^{-1}, \tau_2\tau_1^{-1}, \tau_1^{-1}\tau_2, \tau_2^{-1}\tau_1\}$. The alternative is to consider braids with only positive or negative crossings, which correspond to unlinked knots. This option doubles the braid set considered below, but without substantially altering the construction.

Since a given B_3 braid is only permitted positive or negative charges, but not both, the mirror particle set is defined by switching the B_3 crossings. The $w = 0$ condition on the selected braids may be viewed as a restriction to rotations out of the page, from the symmetric point where the crossings are fused.

Our braided ribbons will always be double knots in B_{2n} , meaning that there is an underlying knot in B_n . Since ribbon twists are separated from the braiding in B_n , the reversal of crossings in B_n can occur while maintaining the direction of the ribbon twist, and this gives the mirror states. Full ribbon twists will define a unit of electromagnetic charge [93]. The sign convention

$$+ \begin{array}{c} \text{---} \\ \text{---} \\ \text{---} \\ \text{---} \end{array} \quad \begin{array}{c} \text{---} \\ \text{---} \\ \text{---} \\ \text{---} \end{array} - \quad (173)$$

follows the B_2 convention, and the magnitude of charge q on each strand is set at $1/n$, where n is the total number of ribbon strands in a diagram. At a basic interaction vertex, at most $\Delta q = \pm 1$ is exchanged between particles. Note that whereas B_2 is generated by a half twist, charge generates $\mathbb{Z} \simeq B_2$ with a full twist. It would be better to label a half twist with the integer 1, and let a full set of three twists stand for $q = 6$. However, this disagrees with the physical convention.

Ribbons appear because we need the structure of a tortile tensor category [135], or more general structures of this kind. These are braided \otimes categories for which the braiding is compatible with the existence of dual objects. Some definitions are given in appendix A.

Recall the Burau matrix

$$\tau_2 = \begin{pmatrix} 1 & -t & 0 \\ 0 & -t & 0 \\ 0 & -1 & -1 \end{pmatrix}, \quad (174)$$

in B_4 , which is similar to the central τ_n generator for all B_{2n} . Note that the top two rows look like τ_2 in B_3 and the bottom rows like τ_1 . There is a transformation that sends τ_2 in B_4 to τ_2^{-1} by shifting the B_3 τ_2 down to its mirror τ_1^{-1} and similarly shifting the B_3 τ_1 up. That is, crossing flips are related to actual matrix flips in this algebraic representation. This is the kind of behaviour that we demand from any algebra associated to constructive diagrams. In what follows, crossing flips are usually reduced to complex conjugation, as in the 1×1 Burau representation.

Particle ribbons naturally use two phase parameters, in analogy to the two variable homflypt polynomial (121) or its related ribbon graph invariants. We think of the particle braids as a basis for all ribbon diagrams.

7.2 The Single Generation Spectrum

In the Koide phenomenology, rest masses will emerge algebraically from the operators attached to ribbon diagrams. One set of ribbon particle diagrams looks like one generation of massless fundamental states.

Historically, the important Lie groups are $SU(n)$ for $n = 1, 2, 3$, and their fundamental, adjoint and trivial representations. For an $SU(2) \times U(1)$ symmetry, the four dimensions of the adjoint representation predict the existence of four gauge bosons. When the symmetry is appropriately broken by the Higgs mechanism, these bosons become the photon γ and the massive W^+ , W^- and Z^0 bosons.

This traditional formulation considers gauge freedom for all points in the continuum spacetime used to specify field operators. In the contrasting modern view, locality is the secondary consideration, and spacetime geometry should emerge from the quantum information of processes in an abstract circuit space. So we first ask, what is a basic axiomatic analogue of the important Lie group representations?

Cayley's theorem [136] for groups, relying only on the basic group axioms, says that every finite group has a representation in permutations, through action on itself by (right) multiplication. This is the discrete analogue of an adjoint representation.

The permutation groups S_n also have the usual fundamental representation in $n \times n$ matrices. Consider the first few permutation groups. S_1 is the trivial group, given by the 1×1 matrix with entry 1. Then S_2 has a 2×2 fundamental representation. Since S_2 has only two elements, this is also an adjoint representation. The two special representations first split for S_3 . It's fundamental representation is 3×3 , while the adjoint is in S_6 , given by 6×6 matrices.

To see what happens in S_6 , consider the diagrams for S_3 . Recall that S_3 is generated by two basic crossings, (21) and (32), subject to the rule $(\tau_i)^2 = 1$ for each generator. Since we allow a braiding to relax this symmetry condition, we begin straight away with braided ribbon diagrams, in B_n . The underlying S_3 permutation is maintained as a string map from three points to three points. A (32) generator and the identity, in S_6 , look like

$$(23) \quad \begin{array}{c} \text{U} \quad \text{U} \quad \text{U} \\ \text{U} \quad \text{U} \quad \text{U} \\ \text{U} \quad \text{U} \quad \text{U} \end{array} \quad \begin{array}{c} \text{U} \quad \text{U} \quad \text{U} \\ \text{U} \quad \text{U} \quad \text{U} \\ \text{U} \quad \text{U} \quad \text{U} \end{array} \quad (123) = 1 \quad \begin{array}{c} \text{U} \quad \text{U} \quad \text{U} \\ \text{U} \quad \text{U} \quad \text{U} \\ \text{U} \quad \text{U} \quad \text{U} \end{array} \quad (175)$$

for a suitable choice of basis. Observe that the ribbons *must* be twisted for S_3 to be correctly represented. A matrix for the (32) diagram in S_6 is given

by

$$M(32) = \begin{pmatrix} 0 & 0 & 0 & 1 & 0 & 0 \\ 0 & 0 & 0 & 0 & 0 & 1 \\ 0 & 0 & 0 & 0 & 1 & 0 \\ 1 & 0 & 0 & 0 & 0 & 0 \\ 0 & 0 & 1 & 0 & 0 & 0 \\ 0 & 1 & 0 & 0 & 0 & 0 \end{pmatrix} \quad (176)$$

in a basis with 3×3 blocks. The twist on the left hand ribbon appears in the M_{41} and M_{14} flip, while the larger ribbon crossing is given by a flip on 2×2 blocks. For S_4 , the adjoint representation would have 24 dimensions. Each string in S_4 is turned into six strands in S_{24} , and each set of six strands is limited to an S_3 diagram. In this way, any S_n element is turned into a diagram that respects the factors of $n!$.

Returning to S_3 , we must extend the 6×6 permutation matrices to braid group objects. Each diagram crossing corresponds to a flip map in S_2 , but the block size of the flip depends on the level of the crossing within the S_n hierarchy. So for S_3 we need two crossing labels, say ω and $\sqrt{\phi}$. The seven single crossings of the (32) diagram become seven label pairs, which we insert into the matrix as in

$$M(32) = \begin{pmatrix} 0 & 0 & 0 & \omega & 0 & 0 \\ 0 & 0 & 0 & 0 & 0 & \omega\phi \\ 0 & 0 & 0 & 0 & \omega\phi & 0 \\ \omega & 0 & 0 & 0 & 0 & 0 \\ 0 & 0 & \omega\phi & 0 & 0 & 0 \\ 0 & \omega\phi & 0 & 0 & 0 & 0 \end{pmatrix}. \quad (177)$$

It is convenient to consider these labels as complex phases, so that the conjugate phases $\bar{\omega}$ and $\bar{\phi}$ represent under crossings. Then the symmetry rule of S_n is recovered when all phases equal ± 1 . That is, there is a sign ambiguity in the usual permutation representation, since we are free to include a factor of -1 in the generators.

An irrational phase might give a representation of the full braid group, because ω^d never returns to 1. One may verify that the flip generators in places i and $i + 1$ satisfy $\sigma_i \sigma_{i+1} \sigma_i = \sigma_{i+1} \sigma_i \sigma_{i+1}$. However, $(\sigma_i \sigma_{i+1} \sigma_i)^2$ is a multiple of the identity, namely $\omega^4 I$. At an eighth root of unity ω_8 we then have a reduction to the modular group. For now we work with the rational truncations.

A rational phase sets a limit on the allowed number of full twists in a ribbon, at any level. Starting with S_3 , we only allow one full ribbon twist, since this is sufficient to represent all elements in S_3 . To distinguish an over from an under double twist, we require that ω^2 is distinct from ω^{-2} . The choice of sixth root ω_6 for all crossings would make a full twist equal either ω_3 or $\bar{\omega}_3$. But then the half twist $-\omega_6$ is the same as a full twist $\bar{\omega}_3$.

Since this disrespects the underlying permutation, we go to the 12th root ω_{12} instead.

In [93], the set of odd A_3 diagrams in S_3 is used, as it is here. These are the true B_3 braids. The cycle (231) is called left handed, while (312) is right handed. The annihilation of such fermion braids, one left and one right handed, gives the identity (123), which is a photon. When all three ribbon strands have a double twist, the particle is a charged lepton, with electromagnetic charge given by the direction of the twist. If all ribbons in the B_3 identity are twisted, we have the W^\pm bosons. With this S_6 representation, all particle representations have become self acting adjoint ones.

The trivial representation is always a single strand from B_1 . In principle, any braid becomes a B_1 braid when all the strands are grouped together by the association operation. This suggests, loosely speaking, that a doublet for the Lagrangian is joined to a singlet in a pairing map $B_n \times B_n \rightarrow B_1$.

In [131] it was shown that the fermions $\{e^\pm, \nu_L, \nu_R\}$ may be considered a (twisted) Fourier transform of the electroweak bosons $\{W^\pm, \gamma, Z\}$. The twist carries braiding information for B_3 , while the 3×3 quantum Fourier transform essentially acts on the underlying permutations, carrying the charge information as a constant. This perfect Fourier supersymmetry introduces no new particles to the Standard Model zoo, except for the right handed neutrinos. Traditional supersymmetry does not contribute local states, and enters only in the mathematics of the division algebras.

So for the (312) braid in B_6 , with phases for both the B_3 and B_2 components, a positron matrix is given by

$$\begin{pmatrix} 0 & 0 & 0 & 0 & 0 & \omega\phi \\ 0 & 0 & 0 & \omega & 0 & 0 \\ 0 & 0 & 0 & 0 & \omega\bar{\phi} & 0 \\ 0 & 0 & \omega\phi & 0 & 0 & 0 \\ \omega & 0 & 0 & 0 & 0 & 0 \\ 0 & \omega\bar{\phi} & 0 & 0 & 0 & 0 \end{pmatrix}. \quad (178)$$

For the neutrinos, we take $\omega = \pm 1$. The quarks [93] are given by diagrams with a mixture of twisted and untwisted ribbons, which correctly accounts for quark charge and color. If we untwist the 3×3 block in (178) by the twist factor

$$\begin{pmatrix} \bar{\phi} & 0 & 0 \\ 0 & 1 & 0 \\ 0 & 0 & \phi \end{pmatrix} \quad (179)$$

on the left, we return to the underlying circulant matrix [131].

In summary, with ordered sign lists denoting ribbon charges, a single generation may be given by the following list of braids from B_6 . One is free

to flip the B_3 crossings to obtain an equivalent set of mirror states.

$$\begin{aligned}
e_L^- &= [\tau_2 \tau_1^{-1}, (- - -)] & e_R^+ &= [\tau_1 \tau_2^{-1}, (- - -)] & (180) \\
e_L^+ &= [\tau_2^{-1} \tau_1, (+ + +)] & e_R^- &= [\tau_1^{-1} \tau_2, (+ + +)] \\
\bar{\nu}_L &= [\tau_2^{-1} \tau_1, (000)] & \nu_R &= [\tau_1^{-1} \tau_2, (000)] \\
\nu_L &= [\tau_2 \tau_1^{-1}, (000)] & \bar{\nu}_R &= [\tau_1 \tau_2^{-1}, (000)] \\
u_L &= [\tau_2 \tau_1^{-1}, (+ + 0)] & \bar{u}_R &= [\tau_1 \tau_2^{-1}, (- - 0)] & \mathbf{R} \\
u_L &= [\tau_2 \tau_1^{-1}, (+ 0 +)] & \bar{u}_R &= [\tau_1 \tau_2^{-1}, (- 0 -)] & \mathbf{G} \\
u_L &= [\tau_2 \tau_1^{-1}, (0 + +)] & \bar{u}_R &= [\tau_1 \tau_2^{-1}, (0 - -)] & \mathbf{B} \\
\bar{d}_L &= [\tau_2^{-1} \tau_1, (00 +)] & d_R &= [\tau_1^{-1} \tau_2, (00 -)] & \mathbf{R} \\
\bar{d}_L &= [\tau_2^{-1} \tau_1, (0 + 0)] & d_R &= [\tau_1^{-1} \tau_2, (0 - 0)] & \mathbf{G} \\
\bar{d}_L &= [\tau_2^{-1} \tau_1, (+ 0 0)] & d_R &= [\tau_1^{-1} \tau_2, (- 0 0)] & \mathbf{B} \\
W^- &= [I_2, (- - -)] & W^+ &= [I_2, (+ + +)] & \gamma = [I_2, (000)] \\
Z_1 &= [I_2, (- + 0)] & Z_2 &= [I_2, (+ 0 -)] & Z_3 = [I_2, (0 - +)]
\end{aligned}$$

In the above, we have decomposed the neutral Z boson into three pieces, as in [131]. Although the mixed charges are forbidden for observed states, this splitting permits the introduction of the right handed neutrino, since the three right handed leptons may be transformed to these Z boson preons. In other words, the three lepton singlets from the Standard model Lagrangian become a triplet associated to B_3 . In this way, we might view the unique boson mass as a sum of three equivalent preon masses. This scheme balances to an equal boson fermion count, under the Fourier supersymmetry. The mirror neutrinos are the only extra states required. A left and right pair of fermion matrices, along with a multiple of the annihilation photon, will specify a Koide Hermitian mass matrix.

Since the ribbon twists are an essential part of the permutation representation, we would like to build *all* fundamental states out of the charged lepton states. We allow the neutrinos, since these are obtained by selecting opposite charges on the even cycle components. They are also easily obtained by composing a charged lepton braid with a W^\pm boson diagram. Note also that the neutrinos could be given by the fundamental representation in B_3 , rather than in B_6 . Neutrality is then enforced by the shrinking of a ribbon to a line, and then no braid compositions have been employed in the definition of either leptons or their Fourier transform, the electroweak bosons. This completely covers the local observable electroweak spectrum, using exactly the trivial, fundamental and adjoint representations for S_3 . In summary, a basic set of four (left handed) leptons on (231) may be assigned phases:

e^-	e^+	$\bar{\nu}$	ν_m
ω, ϕ	$\bar{\omega}, \bar{\phi}$	$1, \bar{\phi}$	$1, \phi$

where the subscript m denotes the mirror state. There is a similar right handed set using the permutation (312).

It is the mixing of twisted and neutral strands for quarks that remains to be clarified. The up quarks have two charged strands and one neutral one. The known algebraic structure of quarks uses the nonassociative octonions, as in appendix D. If we use instead the braid association operation to reduce neutral ribbons to a line, as for the B_3 neutrinos above, then all quarks reduce B_6 objects to braids in B_4 or B_5 .

Given the hierarchy of S_n representations, such an association operation is actually essential for maintaining the levels within complicated diagrams for S_n , when $n \geq 3$. By so bracketing the ribbon edges in B_6 , we can turn any B_6 braid back into a B_3 one. For neutral particles, no information is lost. With the quark reductions to B_4 and B_5 , all braid groups up to B_6 occur in the fundamental state information.

Quarks may be assigned the appropriate matrix in either B_6 or in a lower dimensional representation. In contrast to the lepton case, the quark braids of [93] and [131] do not have a Fourier transform that is a braid matrix. Nonetheless, the known quark phases of mass matrix phenomenology are simple fractions of the charged lepton phases [137][138][139][140], which are noted below. This suggests that all Koide phases arise from the ribbon diagrams.

7.3 CPT and the Higgs Mechanism

Hypothetically, if the quark CKM mixing matrix is a function of the circulant mass operators, as in [141], one might have a unique factorisation into circulants, which may then be used to create asymmetric Yukawa matrices from the diagonal of Koide values. However, the braid picture suggests that we should begin with higher dimensional matrices. In electroweak symmetry breaking, there is a 4×4 adjoint representation required for the 2×2 rotations by $\theta_W \sim 0.5$ and $\pi/4$ [142]. In the finite permutation groups, S_4 has its ribbon adjoint in dimension 24, which is then the minimal braid dimension for studying the Higgs mechanism. Each of the four strands in B_4 become six strands, as (Z, γ) and (W^+, W^-) are each represented by a pair of B_6 braids.

On such 24×24 matrices, θ_W and the $\pi/4$ rotation each act on 12×12 blocks. There is an 18×18 block for the massive bosons (W^+, W^-, Z) . If this boson triplet is projected to a scalar triplet, there should be a 3×3 manifestation of Dharwadker's Higgs boson underlying the Koide matrices. Although its connection to the full gauge theory still requires clarification, the observation is noteworthy. Consider the decomposition of the Hermitian

matrix

$$M = \mu_b \begin{pmatrix} x & 1 & 1 \\ 1 & x & 1 \\ 1 & 1 & x \end{pmatrix} + i\mu_f \begin{pmatrix} 0 & y & -y \\ -y & 0 & y \\ y & -y & 0 \end{pmatrix} \quad (181)$$

into real and imaginary parts. The real part specifies a (W^+, W^-, Z) degenerate mass triplet, with $x = \sec \theta_W$. The imaginary part represents an annihilation triplet, with the massless photon on the diagonal. Since photons are the only massless states, this is an essentially unique way to view the Koide matrix.

In general, a 3×3 Hermitian matrix requires one real and one phase parameter, up to the scale factor. We would like to understand how the Koide phases arise from the ribbon graph representations. Since the bosons all arise from the twisted Fourier transform [131], it suffices to consider the triplet mass splittings of the fermions. The universal $2/9$ phase for the leptons must be associated to the underlying B_3 braid, since this is the only common element between neutrinos and charged leptons.

How do the braid crossings relate to the important discrete symmetries of the theory? In the Standard Model, a discrete symmetry acts on spacetime, and has certain consequences for different fields. Here, however, the diagram is supposed to represent either material or spatial degrees of freedom, since these are not independent. Thus we allow basic moves on the ribbon diagram to directly specify special discrete transformations.

The conjugation of all phases, whatever their quantitative origin, denotes charge conjugation symmetry C . This is why the B_3 crossings for the positron are the opposite from the electron ones, allowing for the existence of the mirror set. Parity P should be associated to the left to right transformation. With the mirror neutrinos, full parity symmetry is restored. The $\pi/12$ phase that distinguishes neutrinos from charged leptons must come from a cancelation of left right phases in the charged lepton case. This special neutrino phase is like a minimal braid phase for S_4 states, counting the 24 dimensions of a simple state space. It distinguishes the mass matrices of neutrinos and mirror neutrinos [143].

The flip of B_3 crossings, while maintaining charge, should be a time reversal operation T , because this conjugation is achieved when reading the diagram upside down, noting that microscopic time flows down braid strands in quantum processes. This time, however, is not to be identified with the usual coordinate time. Now given a **CPT** exactness, the combination of the C flip and the T flip implies some association between P and the ribbon charge phases. This is expected, since the three strands in B_3 do abstractly index the spatial directions X, Y and Z . Since T itself swaps particles for mirror particles, the abstract time reversal presumably has a cosmological origin.

In summary, the low energy phase assignments for the leptons are given

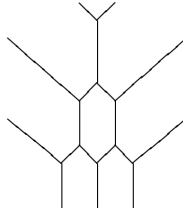
in the table.

lepton	projectors	Koide phase
e^-	$+-$	$-2/9$
e^+	$-+$	$+2/9$
ν	$--$	$-2/9 - \pi/12$
$\bar{\nu}$	$++$	$+2/9 + \pi/12$
ν_m	$++$	$-2/9 + \pi/12$
$\bar{\nu}_m$	$--$	$+2/9 - \pi/12$

At this point, the name *projector* is somewhat arbitrary. These signs might be taken from the octonion operators of appendix D, but alternative mechanisms should occur in the braid context. Here, parity non conservation has prevented the secondary phase cancelation for the neutrinos. The given phases recover the empirical rest mass triplets, with a separate choice of scale factor for the charged and neutral cases [137][138][139][140].

Note that the left and right electrons appear to take on canceling $\pi/12$ phases, while there is only one such phase for a neutrino. The dimension 24 also counts the basic particle list in Dharwadker's scheme [132]. When the total phase differs only by a sign there is no difference in the rest mass triplet, accounting for both particles and antiparticles. That is, a conjugate pair of phases determines the Hermitian matrix.

Although it is still unclear, the universal $2/9$ phase most likely stands for a count of 6 out of 27 qutrit paths on the tetractys, such as the paths that contain all three directions X , Y and Z . Recall that these six paths themselves form a copy of S_3 . When three particle ribbons come into a vertex with nine ribbon strands, one finds this internal hexagon



at the centre of the ribbon picture. Such a ribbon diagram would replace the basic massless vertex of twistor diagrams, which uses only one ribbon strand per leg. The tripling of ribbon strands is essential to both the electroweak $SU(2)$ symmetry and the color degree of freedom.

Since the tetractys nodes represent the commutative reduction of 27 noncommutative paths for three qutrits, and the hexagon covers the $2/9$ fraction at the central vertex, we take seriously the idea that this qutrit path object is somehow responsible for the Koide phase. Recall that the 27 paths in the letters X , Y and Z are the three dimensional analogue of the

matrix index

$$\begin{pmatrix} XX & XY & XZ \\ YX & YY & YZ \\ ZX & ZY & ZZ \end{pmatrix} \quad (182)$$

underlying the Koide circulants. For example, concatenation by X on the left gives the block

$$\begin{pmatrix} XXX & XXY & XXZ \\ XYX & XYY & XYZ \\ XZX & XZY & XZZ \end{pmatrix}, \quad (183)$$

coming from a two qutrit corner of the word simplex. In this matrix there are only two paths, XYZ and XZY , on all three letters. But taking the three distinct concatenations, we cover all off diagonal entries in a 3×3 matrix using S_3 . These paths represent the six paths around a cube, which replaces the S_3 hexagon in dimension 3.

In appendix D we note the special role of the 3×3 matrix Jordan algebras. It is interesting to compare our 27 qutrit paths with the basis for the 27 dimensional octonion algebra. The qutrit paths provide a ternary analogue of the two noncommuting variables for the quantum plane. The octonion units are usually put onto a qubit cube, which sits along one edge of the tetractys graph. But these three edges meet at the corner vertices, forcing us to mix the 1 and e_7 units for the three copies of \mathbb{O} , and to borrow paths from the central vertex. This is exactly what happens in the octonion particle scheme [1].

A more symmetrical way of selecting eight basis paths is to use the concatenations in (183), eliminating the XXX path. This puts XXX , YYY and ZZZ on the diagonal of the Jordan matrix. The quarks are then shared around a pair of sides on the tetractys. This has interesting phenomenological consequences.

Our so called CPT transformations are associated to phases that don't match the π rotations of actual ribbons in the diagram. This might be interpreted as a conic deficiency for a point on the central line through a ribbon strand, as the ribbon edges rotate. Such phase deficiencies stand for curvature in three dimensional gravity, as described by braid diagrams [144][13]. From a holographic perspective, this is the correct dimension for spacetime. However, the ambient braid space should not be identified with a macroscopic kind of spacetime, since it does not play this role in modern scattering theory. Instead, macroscopic spacetime comes from a pairing between our baryonic world and the mirror world, starting with a six dimensional pair of braid spaces.

Any network of knotted ribbon particles with internal loops then specifies an observable. Ribbon graphs are categorically dual to polytope axioms for categories of roughly three dimensions. We need nonassociative braid

diagrams in order to keep track of the levels, and so both the ribbon surface and the ambient space are expected to play a role in determining emergent geometry.

In the Koide matrix picture, the Higgs expectation value should be responsible for the scale factor μ_b/μ_f of (181). Dharwadker et al [132] correctly predicted such a Higgs boson mass $m_H = 126$ GeV in 2009, with the relation

$$m_H = \frac{1}{2}(m_{W^+} + m_{W^-} + m_Z) = \frac{m_Z}{2}(1 + 2 \cos \theta_W), \quad (184)$$

where θ_W is the Weinberg angle. This is a Koide eigenvalue with parameter $x = 1$ and a zero boson phase. The geometry of [145] is hypothesised to come from a particular *Steiner system* [146] known as the Witt design. This special set, called $S(5, 8, 24)$, is a collection of 759 length 8 subsets, known as octads, of a 24 letter alphabet, such that every 5 element subset of $S(5, 8, 24)$ is contained in exactly one octad. It may be constructed using the 24 dimensional parity cube, which is associated to a state space for 24 qubits, where 0 and 1 give the characteristic function for subsets of 24.

First, put all the length 24 binary strings in lexicographic order. Then, from the top, delete any string that does not differ in at least 8 places from any previous one. The resulting 4096 strings form the extended binary Golay code [147]. The strings with exactly 8 plus signs are the $759 = 3 \times 253$ octads. Later on, we will consider this code in the guise of the permutoassociahedron axiom.

This geometry is thought to be related to the four color mapping theorem, which states that any proper map in two dimensions requires no more than four colours. Mathematicians have hypothesised [148] that this maximum of 4 corresponds to the quantum algebra limit given by the braid parameter δ^2 at t a root of unity. Since this parameter can be expressed in the form $4 \cos^2 \theta$, it clearly has a maximal value of 4.

A rest mass quantum number is viewed via a Stern-Gerlach type experiment, analogous to the measurement of spin [121]. A mass spectrometer separates a fixed velocity beam of mixed mass particles into three streams, separated by the ambient magnetic field. These streams have become the three strands that label the three points of our discrete braid space. Mass and spin together define a six point basis for the particle diagrams.

All this hinges on the assumption that the unbroken $SU(2) \times U(1)$ gauge symmetry of the Standard Model Lagrangian also has a description in terms of braid algebras.

7.4 Electroweak Quantum Numbers

Let us consider the electroweak quantum numbers, algebraically [149]. Start with B_3 , or rather the underlying S_3 . Take the group algebra for S_3 , with complex coefficients. The matrix representation for the odd cycles is given

by the circulant permutations (123), (231) and (312). An element of the subgroup algebra is then

$$G_1 = \begin{pmatrix} a/2 & b & c \\ c & a/2 & b \\ b & c & a/2 \end{pmatrix} \quad (185)$$

for $a, b, c \in \mathbb{C}$, such that $c = \pm b$ for a left right pair. As above, we work with the assumption that such circulant matrices are fundamental to electroweak symmetry breaking [150]. The even permutations in S_3 stand for an operation that fixes one object. To maintain invariance between the three directions, all three 2-circulant coefficients must be equal. This is then another 1-circulant. They can then contribute to the electroweak quantum numbers only using

$$G_2 = \frac{u}{3} \begin{pmatrix} 1 & 1 & 1 \\ 1 & 1 & 1 \\ 1 & 1 & 1 \end{pmatrix}, \quad (186)$$

for a parameter $u \in \mathbb{C}$. The copy of S_2 underlying B_2 has objects σ_X and I_2 . These may be used to create a 6×6 element of the Hopf algebra $\mathbb{C}S_6$,

$$G \equiv G_1 \otimes I_2 + G_2 \otimes \sigma_X, \quad (187)$$

where two copies of G_1 form the diagonal blocks. From [149], we impose the measurement projector condition $G^2 = G$ to obtain equations for a, b, c, u . The solutions give exactly the weak hypercharge $Y = a$ and weak isospin $T_3 = u$ for the leptons and quarks, such that the $U(1)$ charge quantum number is given by the Gell-Mann Nishijima formula

$$q = T_3 + \frac{Y}{2}. \quad (188)$$

	Y	T_3		Y	T_3
e_L^-	-1	-1/2	e_L^+	+1	+1/2
e_R^-	-2	0	e_R^+	+2	0
ν_L	-1	+1/2	$\bar{\nu}_L$	+1	-1/2
ν_R	0	0	$\bar{\nu}_R$	0	0
u_L	+1/3	+1/2	\bar{u}_L	-1/3	-1/2
u_R	+4/3	0	\bar{u}_R	-4/3	0
d_L	+1/3	-1/2	\bar{d}_L	-1/3	+1/2
d_R	-2/3	0	\bar{d}_R	+2/3	0

7.5 The Burau Representation and Mirror Circulants

In B_3 , an $e_L^- e_R^+$ annihilation



$$(189)$$

occurs in either the baryonic or mirror sector, both diagram sets being required for massive states. Including left and right handed particles, there are then *eight* possible braid diagrams associated to charged lepton annihilation. How do these objects interact algebraically?

Consider the simplest possible 2×2 Burau representation for both e_L^- and its mirror partner. Formally, these objects add

$$\begin{pmatrix} 1 - 1/t & -t \\ 1 & -t \end{pmatrix} + \begin{pmatrix} -t & 1 \\ -t & 1 - 1/t \end{pmatrix} = \begin{pmatrix} 1 - t - 1/t & 1 - t \\ 1 - t & 1 - t - 1/t \end{pmatrix} \quad (190)$$

to a basic 2×2 circulant. In other words, rather than viewing such a circulant as a sum of permutations in S_2 , we could view it as a braid sum for B_3 . Then when 2×2 objects appear in B_3 , they have a truly three dimensional representation.

Any mirror pair gives such a circulant in the group algebra $\mathbb{C}S_2$. The scalar $\delta^2 - 1 = 1 - t - 1/t$ defines an interesting choice of braid parameter $\delta = i(t^{-1/2} - t^{1/2})$. With the substitution $t \mapsto -t$, this becomes $\delta = t^{1/2} + t^{-1/2}$. At a root of unity t , this parameter corresponds to unitary representations of B_3 [84].

The circulant was constructed with one choice for t , but the conjugate \bar{t} should play an equivalent role in any crossing symmetric diagram. Taking all four possibilities together, we obtain instead

$$- \begin{pmatrix} 2(t^{1/2} - t^{-1/2})^2 + 2 & (t^{1/2} - t^{-1/2})^2 \\ (t^{1/2} - t^{-1/2})^2 & 2(t^{1/2} - t^{-1/2})^2 + 2 \end{pmatrix}. \quad (191)$$

Circulants are also constructed for the larger representation below. As an $R_2(r)$ rotation matrix, the circulant (190) corresponds to a parameter $r = i(1 - t - 1/t)/(1 - t)$, so that

$$t = \frac{1}{2} \pm \frac{1}{2} \sqrt{1 - 4/(1 - ir)}. \quad (192)$$

In particular, at the identity value $r = 0$ we have $t = \omega_3$. At such a modular group value $t \in \{\omega_6, \omega_3\}$, the I_2 component can be either 0 or 2, and the off diagonals reduce to multiplicative generators of the cyclic group C_6 , which can be embedded in S_6 . As permutations, C_6 rightfully requires a 6×6 representation. Actually, the (234561) matrix can be decomposed into the form $H_1 \otimes I_2 + \otimes H_2 \sigma_X$, with

$$H_1 = \begin{pmatrix} 0 & 1 & 0 \\ 0 & 0 & 1 \\ 0 & 0 & 0 \end{pmatrix} \quad H_2 = \begin{pmatrix} 0 & 0 & 0 \\ 0 & 0 & 0 \\ 1 & 0 & 0 \end{pmatrix}. \quad (193)$$

These are not circulant, but insisting on a nearby 2-circulant for H_2 and a 1-circulant for H_1 uniquely defines a dual permutation (651324) in S_6 ,

such that the group algebra sum $(234561) + (651324)$ is the matrix $H \equiv (231) \otimes I_2 + (321) \otimes \sigma_X$. This matrix has the nice property that H^2 is the binary negation of H , meaning that all zeroes and ones are interchanged.

The ribbon twists require a representation of $B_2 \simeq \mathbb{Z}$. Let the Burau representation generate $m \in \mathbb{Z}$ with $(-Q)^m$, where Q is a one half ribbon twist. Then a full twist is Q^{2m} , and the strand charge is $m/3$. We now need to identify strands in the matrices, but this occurs naturally in the full $n \times n$ representation for B_n , where generators are given by 2×2 crossing blocks. For charge, the twist generator becomes

$$\begin{pmatrix} 1-Q & Q \\ 1 & 0 \end{pmatrix}^{2m} \quad (194)$$

where $m \in \{0, \pm 1\}$. Three charges form three blocks of a 6×6 matrix for the double knot. The two copies of B_3 must also use the 3×3 representation. The canonical choice is to select rows and columns to match the double knot strands, so that the braid b is embedded as $b \otimes I_2$. Alternatively, permuting with (142536) , we can place two copies of b along a diagonal, as $I_2 \otimes b$. This is easier to work with. For example, the e_L^+ mirror B_3 braid is

$$\tau_2 \tau_1^{-1} = \begin{pmatrix} 1 & 0 & 0 \\ 0 & 1-t & t \\ 0 & 1 & 0 \end{pmatrix} \begin{pmatrix} 0 & 1 & 0 \\ 1/t & 1-1/t & 0 \\ 0 & 0 & 1 \end{pmatrix} \quad (195)$$

and the full 6×6 particle operator should be

$$\begin{pmatrix} 1+Q^2-Q & 0 & 0 & Q-Q^2 & 0 & 0 \\ 0 & 1+Q^2-Q & 0 & 0 & Q-Q^2 & 0 \\ 0 & 0 & 1+Q^2-Q & 0 & 0 & Q-Q^2 \\ 1-Q & 0 & 0 & Q & 0 & 0 \\ 0 & 1-Q & 0 & 0 & Q & 0 \\ 0 & 0 & 1-Q & 0 & 0 & Q \end{pmatrix} \times (196)$$

$$\begin{pmatrix} 0 & 1 & 0 & 0 & 0 & 0 \\ 1/t-1 & 2-t-1/t & t & 0 & 0 & 0 \\ 1/t & 1-1/t & 0 & 0 & 0 & 0 \\ 0 & 0 & 0 & 0 & 1 & 0 \\ 0 & 0 & 0 & 1/t-1 & 2-t-1/t & t \\ 0 & 0 & 0 & 1/t & 1-1/t & 0 \end{pmatrix}$$

so that charge acts on the ribbons at the base of a braid. The charge operators are

$$(+) : \begin{pmatrix} 1+Q^2-Q & Q-Q^2 \\ 1-Q & Q \end{pmatrix} \quad (-) : \begin{pmatrix} 1/Q & 1-1/Q \\ 1/Q+1/Q^2 & 1+1/Q^2-1/Q \end{pmatrix}. \quad (197)$$

When $Q = 1$, we get the 6×6 identity, and when $t = 1$ the permutation (231) . Note that we can also use $Q = \infty$ as a valid charge operation, letting

Q take values in \mathbb{CP}^1 . The 6×6 particle determinant has no dependence on the parameter t .

Now consider the 2×2 circulants constructed from the larger representation. The mirror matching works by exchanging τ_i for τ_{n-i}^{-1} . The 2×2 generators τ and τ^{-1} give circulants

$$\begin{pmatrix} 1-t & 1+t \\ 1+t & 1-t \end{pmatrix} \quad \begin{pmatrix} 1-1/t & 1+1/t \\ 1+1/t & 1-1/t \end{pmatrix}. \quad (198)$$

The first matrix corresponds to an $R_2(r)$ matrix for the root of unity

$$t = \frac{-ir - 1}{ir - 1}. \quad (199)$$

That is, $t = \cos 2x + i \sin 2x$ when $r = \tan x$. Let $\phi_r = \tan^{-1}(1/r)$. Then the special braid parameter $\delta_t \equiv t^{1/2} + t^{-1/2}$ equals $-2 \sin \bar{\phi}_r$ and $\delta_{-t} = -2 \cos \bar{\phi}_r$. Summing the positive and negative contributions of (198), we obtain the circulant

$$\begin{pmatrix} \delta_{-t}^2 & \delta_t^2 \\ \delta_t^2 & \delta_{-t}^2 \end{pmatrix} = \begin{pmatrix} (1-t)(1-1/t) & (1+t)(1+1/t) \\ (1+t)(1+1/t) & (1-t)(1-1/t) \end{pmatrix}. \quad (200)$$

The products $(1 \pm t)(1 \pm 1/t)$ are *perfect polynomials*, because like the number four, their product equals their sum. One can substitute any polynomial into t , and δ^2 remains perfect. At the trigonometric values this matrix is a probability matrix, when multiplied by a factor of $1/4$. The Schur square root is the unitary circulant

$$\frac{-i}{2} \begin{pmatrix} \cos \bar{\phi}_r & i \sin \bar{\phi}_r \\ i \sin \bar{\phi}_r & \cos \bar{\phi}_r \end{pmatrix} = -i \sin \bar{\phi}_r R_2(-r). \quad (201)$$

Observe that (199) is the fractional linear transformation $-F_2$ on ir , where F_2 is the Hadamard gate [27]. It sends $r \in \{0, 1, \infty\}$ on the line \mathbb{R}^+ to $\{0, \pi/2, \pi\}$ on the unit circle.

7.6 Neutrino and Quark Mixing

The charged leptons, in increasing order of mass, are the electrons (e^\pm), muons (μ^\pm) and tau (τ^\pm) particles. To each of these electroweak states there is a corresponding neutrino state, namely ν_e , ν_μ and ν_τ , but the neutrino mass states are a mixture of the electroweak states. That is, neutrinos are observed to oscillate as they propagate [151][152]. The mass states are called ν_1 , ν_2 and ν_3 . Neutrino mixing between the electroweak and mass states is given by a non trivial 3×3 unitary transformation, in analogy to the quark CKM mixing matrix.

The propagating mass states supposedly transition from one to the other with a probability that depends on the distance L from the source, and

the energy E . For two or three states, using reasonable assumptions, the probability $P_{i \rightarrow j}$ is expressed as the square of an amplitude, such as

$$A_{i \rightarrow j} = \sum_{k=1}^3 V_{ik}^* V_{jk} \exp(-im_i^2 L/2E), \quad (202)$$

given a complex mixing matrix V_{ij} . The unitary 3×3 MNS matrix for neutrinos gives the observed transition amplitudes for the three known states [153]. In contrast, the unitary CKM matrix for quarks [154] contains amplitudes

$$\begin{pmatrix} V_{ud} & V_{us} & V_{ub} \\ V_{cd} & V_{cs} & V_{cb} \\ V_{td} & V_{ts} & V_{tb} \end{pmatrix} \quad (203)$$

that depend on both the up and down quark triplets. We usually write $V = U_u U_d^\dagger$, for left handed states. It is the factors of V and its right handed complement that diagonalise the Yukawa matrices for the Standard Model Lagrangian.

The Jarlskog invariant $J(V)$ [155] measures **CP** violation in terms of the complex entries of the CKM matrix, in a phase convention independent way. It is usually derived from a given four parameter form for the matrix, but in [141] it was noted that the rotation parameters alone come close to giving the correct empirical values for both J and other physical phases. Since this agrees with the cyclic ansatz for mass operators, we note here some empirical results.

Each 3×3 mixing matrix must respect unitarity, whereby the sum of norm squares for each row and column equals 1, conserving probabilities [156]. That is, $\sum_i V_{ij} V_{ik}^* = \delta_{jk}$ and $\sum_j V_{ij} V_{kj}^* = \delta_{ik}$. We write each rotation factor $R_2(r)$ as a 3×3 circulant, essentially a *phase locked* element of $SU(2) \times U(1)$. As a one parameter matrix, it specifies a $U(1)$ element. Each factor belongs to the group algebra $\mathbb{C}S_3$, coming from the underlying braids.

The determinant condition on an $SU(2)$ matrix is the same as the unitarity condition. Thus the only way to select an $SU(2) \times U(1)$ matrix that is a circulant sum is as the sum of a real diagonal and an imaginary off diagonal 2-circulant. The required 3×3 R_2 factors are then of the form

$$R_{12}(r) = \begin{pmatrix} r & i & 0 \\ i & r & 0 \\ 0 & 0 & 1 \end{pmatrix} \quad R_{23}(r) = \begin{pmatrix} 1 & 0 & 0 \\ 0 & r & i \\ 0 & i & r \end{pmatrix} \quad R_{31}(r) = \begin{pmatrix} r & 0 & i \\ 0 & 1 & 0 \\ i & 0 & r \end{pmatrix} \quad (204)$$

giving a three parameter mixing matrix

$$V = N R_{12}(a) R_{23}(b) R_{31}(c), \quad (205)$$

where a , b and c are real, and

$$N^{-2} = (a^2 + 1)(b^2 + 1)(c^2 + 1) \quad (206)$$

is the required normalisation factor. As a circulant sum, V then takes the form

$$V = N \begin{pmatrix} abc & -a - c & -b \\ -b & abc & -a - c \\ -a - c & -b & abc \end{pmatrix} + iN \begin{pmatrix} bc & ac - 1 & ab \\ ac - 1 & ab & bc \\ ab & bc & ac - 1 \end{pmatrix}. \quad (207)$$

This is the general form for the cyclic decomposition, because one is always free to scale the imaginary entries of R_{ij} to unit norm. Such matrices are always magic, in the sense that rows and columns have a constant sum.

Neutrino mixing is close to, but not equal to, the tribimaximal probability matrix [157][158]

$$\begin{pmatrix} 1/3 & 1/3 & 1/3 \\ 1/6 & 1/6 & 2/3 \\ 1/2 & 1/2 & 0 \end{pmatrix} \quad (208)$$

This matrix has many complex representations, including F_3F_2 . It takes circulant mixing parameters $(a, b, c) = (1, \sqrt{2}, 0)$. When one parameter is zero there is necessarily a zero probability. Observationally, for both neutrinos and quarks, all the parameters a , b and c are observed to be non zero, and thus there will be **CP** violation in both sectors [141].

Using the mirror circulant construction, each mixing parameter has a corresponding braid parameter $t = \pm(r - i)(r + i)$, which is a root of unity. This phase converts a mixing factor to a determinant 1 matrix. The overall phase for all three factors is

$$\phi_V \equiv \sqrt{\frac{(a + i)(b + i)(c + i)}{(a - i)(b - i)(c - i)}}. \quad (209)$$

For the CKM quark mixing matrix, the conjugate numerator and denominator are near to $\pm\pi/24$, so that $\phi_V = \pi/12 + x$ for a small parameter $x \sim 0.0035$.

Neutrino experiments are not yet sufficiently accurate to pinpoint the parameters precisely. However, strong evidence for a non zero θ_{13} in neutrino mixing has come to light in recent years [159][160][161]. The accurate Daya Bay result [161] corresponds to an angle of around 9° . Current estimates for the other two angles are $34.0^\circ \pm 1.1$ (θ_{12}) and $45^\circ \pm 7$ (θ_{23}) [162]. Current constraints, including the Δm^2 values, are:

$$\begin{aligned} \Delta(m_{12})^2 &= 7.59 \pm 0.2 \times 10^{-5} \text{ eV}^2 \\ \Delta(m_{31})^2 &= 2.43 \pm 0.13 \times 10^{-3} \text{ eV}^2 \\ \sin^2 2\theta_{13} &= 0.092 \pm 0.017 \\ \sin^2 2\theta_{23} &> 0.92 \end{aligned}$$

Observe that $\theta_{13} + \theta_{12} \simeq \theta_{23}$. If the large mixing phase is $47 = 90 - \theta_{13} - \theta_{12}$, then the three phases satisfy a cyclic set of additive relations

$$\begin{aligned} 9 + 34 &= 47 \\ 47 + 9 &= 34 \\ 34 + 47 &= 9 \end{aligned} \tag{210}$$

under the 90° tangent rule. Thus the three phases give a 1-circulant, where the third column vector is considered a sum of the first two. A more cyclic representation in terms of the total angle

$$90 = 9.0 + 34.0 + 47.0 \tag{211}$$

sums all three vectors to obtain the democratic probability matrix. With these angles, all in agreement with the data, the neutrino mixing probabilities from V are roughly given by

$$|V_\nu|^2 = \begin{pmatrix} 0.01 & 0.48 & 0.51 \\ 0.60 & 0.17 & 0.23 \\ 0.39 & 0.35 & 0.26 \end{pmatrix}. \tag{212}$$

Consider now the quark CKM matrix. Recent experimental estimates [154] of the unsquared CKM amplitudes, for a complex matrix V_{CKM} , are given by

$$\begin{pmatrix} 0.97427 \pm 0.00015 & 0.22534 \pm 0.00065 & 0.00351 \pm 0.00015 \\ 0.22520 \pm 0.00065 & 0.97344 \pm 0.00016 & 0.0412 \pm 0.0011 \\ 0.00867 \pm 0.00030 & 0.0404 \pm 0.0011 & 0.999146 \pm 0.000046 \end{pmatrix} \tag{213}$$

which is closely approximated by the three parameter product

$$V_{\text{CKM}} = N R_{12}(a) R_{23}(b) R_{31}(c) \tag{214}$$

for $a = -0.231$, $b = 24.3$ and $c = 0.00347$. These parameters correspond to the Euler angles of the standard parameterisation, but are now also responsible for crucial phases.

Since a product of two rotation matrices is unordered, we interpret the three factor ordering as a noncommutative aspect of triality, directly responsible for **CP** violation. Note also that *all* unitary matrices in $U(3)$ have a neat parameterisation using magic matrices. In [163], Gibbs proved that any 3×3 unitary matrix U could be written in the form

$$U = \begin{pmatrix} \psi_1 & 0 & 0 \\ 0 & \psi_2 & 0 \\ 0 & 0 & \psi_3 \end{pmatrix} V \begin{pmatrix} \phi_1 & 0 & 0 \\ 0 & \phi_2 & 0 \\ 0 & 0 & \phi_3 \end{pmatrix} \tag{215}$$

for a magic matrix V along with phase diagonals. Since rephasing has no effect on the Jarlskog invariant J , a magic matrix must somehow determine **CP** violation. A more general proof was considered for unitary matrices in any dimension by S. Lisi [164], using braids.

7.7 The Koide Rest Mass Phenomenology

The leptons and quarks have the observed rest masses [165] as given in the table.

	m (MeV/ c^2)
e^-	0.510998910(13)
μ^-	105.6583668(38)
τ^-	1776.84(17)
d	4.1 - 5.7
u	1.7 - 3.1
s	100 ± 30
c	1290 ± 110
b	4190 ± 180
t	172900 ± 1500

and the neutrino states satisfy the current bounds noted above [162].

As a triplet of real numbers, a diagonal rest mass matrix is Fourier transformed to a Hermitian circulant. Alternatively, a Hermitian circulant matrix gives directly a triplet of rest mass eigenvalues. The off diagonal entries, responsible for mass splitting, are characterised by a single complex phase. We assume that the (231) phase comes from a baryonic state, while the conjugate (312) phase is due to a mirror partner.

First, recall the inverse pair of 3×3 circulant mutually unbiased bases

$$R_3 = \frac{1}{\sqrt{3}} \begin{pmatrix} 1 & \omega_3 & 1 \\ 1 & 1 & \omega_3 \\ \omega_3 & 1 & 1 \end{pmatrix} \quad R_3^{-1} = \frac{1}{\sqrt{3}} \begin{pmatrix} 1 & 1 & \bar{\omega}_3 \\ \bar{\omega}_3 & 1 & 1 \\ 1 & \bar{\omega}_3 & 1 \end{pmatrix}. \quad (216)$$

Note that R_3^2 , which is the natural increment from R_3 in the cyclic group, is the inverse only up to a factor of i . Thus R_3 is really a 12th root of I_3 . However, bases are equivalent up to multiplication by a complex scalar. Along with I_3 and F_3 , these are the 3×3 analogues of the Pauli unbiased bases, appropriate for describing real measurements with three outcomes. We need a Hermitian matrix, so one must sum R_3 and R_3^{-1} with the same coefficient, to obtain the simplest mass matrix

$$H = \begin{pmatrix} 2 & \omega_6 & \bar{\omega}_6 \\ \bar{\omega}_6 & 2 & \omega_6 \\ \omega_6 & \bar{\omega}_6 & 2 \end{pmatrix}. \quad (217)$$

The Schur square root of H

$$H_S = \begin{pmatrix} \sqrt{2} & \omega_{12} & \bar{\omega}_{12} \\ \bar{\omega}_{12} & \sqrt{2} & \omega_{12} \\ \omega_{12} & \bar{\omega}_{12} & \sqrt{2} \end{pmatrix} \quad (218)$$

contains the basic arithmetic phase $\pi/12$, along with the basic r parameter $\sqrt{2}$. Using any multiple of I_3 and conjugate phase multiples of R_3 and R_3^{-1} , we have a general Hermitian circulant. Note that the special matrix H is fixed under the projection operation $H \mapsto H^2$. Testing a general diagonal parameter x and phase $\phi \neq 1$, simple algebra shows that only the sixth roots have fixed points, at $x \in \{2, -1\}$ for ω_6 and $x \in \{-2, 1\}$ for ω_3 . However, if we let ϕ vary on iteration, then $x = x(\phi)$ can be fixed by maps $H \mapsto H^n$, in which case ϕ will eventually return to itself. At the special value $x = \sqrt{2}$, $\phi \simeq 4\pi/23$ rad fixes $H \mapsto H^3$. Although perhaps irrelevant, this phase $4/23$ appears in chapter 10 as an entropic probability for three unary fermion states.

The well known Koide formula [137][138] for the three charged lepton rest masses at low energy correctly predicted the τ mass in the 1980s, and has since been applied to neutrino triplets and hadrons by Brannen [139]. This formula arises from a triplet of eigenvalues for a circulant \sqrt{M} at some scale μ ,

$$\sqrt{M} = \sqrt{\mu}(I_3 + z(231) + \bar{z}(312)) = \sqrt{\mu} \begin{pmatrix} x & \phi & \bar{\phi} \\ \bar{\phi} & x & \phi \\ \phi & \bar{\phi} & x \end{pmatrix}, \quad (219)$$

where z is complex, $x^{-1} = |z|$ and $\phi = \arg(z)$. The eigenvalues are then

$$\sqrt{m_i} = \sqrt{\mu}(1 + 2|z| \cos(\arg(z) + \frac{2\pi i}{3})), \quad (220)$$

for $i = 1, 2, 3$. The square root best displays the following empirical data. Both charged leptons and neutrinos have mass triplets fitted with $x \simeq \sqrt{2}$. As discussed in [139][166] and previous sections, the charged lepton phase is $2/9$, while the neutrino states are assigned a phase $2/9 + \pi/12$. Although the meaning of low energy masses for quarks is unclear, we also consider Koide fits for the quark data. In fact, the minimal scale of observation for the quarks could be considered a quark analogue of the low energy regime. This idea is justified by the data.

The charged quark triplets are roughly fitted using phases $2/27$ for the up triplet and $4/27$ for the down triplet. Since the universal $2/9$ came from the B_3 braiding of the neutrinos, and *not from charge*, we obtain the $2/27$ from the single neutral strand that is required for an up quark. The quark $|z|$ value is related to the lepton value by basic trigonometry [167][168], with the lepton triangle inscribed inside the up quark one. This is

$$f(4/27) \equiv |z| = \frac{1}{\sqrt{2}} \frac{\sin(\omega_{12}^5 - 4/27)}{\sin \omega_{12}}.$$

Moreover, the natural charged lepton scale is given by $\mu_l = 313.8$ MeV, which equals the dynamical quark mass $m_p/3$. More recently it was observed

[140] that the alternative (b, c, s) quark triplet fits the lepton value of $x = \sqrt{2}$ with a phase close to $6/9$. This suggests three copies of a neutrino, and indeed there is a tripling of scales to $3\mu_l = m_p$, the proton mass, now directly paired to the tripling of the $2/9$ phase. What is the origin of the (b, c, s) selection? One possibility is the subdivision of the tetractys into three pentagons, which each sit about a corner of the tetractys, so that (b, c, s) gives the quark vertices for one pentagon. The other pentagons would then be the (u, d, s) and (d, b, t) triplets, and the first of these is included in the table below.

The fundamental Koide scale parameters are empirically related to the proton mass m_p , except for the neutrinos. Including mirror neutrinos, the table below summarises the Koide parameters and theoretical mass values that best match the empirical data. We choose as a basic scale the proton mass m_p . All triplets fit current observational constraints, and the Koide eigenvalues would therefore suggest precise predictions for these masses if a basic set of triplets could be selected.

	$2/x$	ϕ (rad)	μ	m
e^-	$\sqrt{2}$	$2/9$	$m_p/3$	0.51095
μ^-				105.65
τ^-				1776.82
u	$f(4/27) = 1.76$	$2/27$	$24m_p$	2.0
c				1249
t				171546
b	$\sqrt{2}$	$2/3$	m_p	4190
c				1356
s				92
u	$f(2/9) = 1.92$	$1/3$	$24m_p/1836$	2.5
d				5.0
s				97.4
ν_1	$\sqrt{2}$	$2/9 + \pi/12$	$10^{-11}m_p$	0.00038
ν_2				0.0087
ν_3				0.0497
ν_1^m	$\sqrt{2}$	$2/9 - \pi/12$	$10^{-11}m_p$	0.0006
ν_2^m				0.00117
ν_3^m				0.0581

Although the Koide relation holds at the scales considered, it is not yet clear how the parameters evolve with scale running. Observe that these triplets suggest a neat pattern at both low energy and the pole mass, with one charge accounting for the low energy phases and another for the best quark triplets. The inscribing length $f(2/9)$ replaces the $4/27$ phase with the phase $2/9$. The product $\sqrt{3}f(\sqrt{2})$ of up and down parameters is roughly 3.049, which is the side length of the Koide up quark triangle in the (r, ϕ)

plane [167]. The lepton triangle has side length $\sqrt{6}$, which is similarly a product of the $\sqrt{2}$ and $\sqrt{3}$. The 1836 is of course chosen to resemble the proton electron mass ratio, for a scale of $24m_e$. In the eigenvalue space \mathbb{R}^3 , the lepton Koide vector is rotated by $\pi/4$ from the $(1, 1, 1)$ vector [169]. This $(1, 1, 1)$ vector sits at the centre of the word monoid tetractys, when it is viewed as a simplex.

A total phase conjugation does not alter the rest mass triplet, so only two mismatched phase components can generate distinct mirror states. The mirror neutrino \sqrt{M} has a $2/9 - \pi/12$ mirror phase. With this phase, one easily verifies that the central mirror mass state corresponds precisely [170][143] to the current CMB temperature of 2.725 K, at 0.00117 eV. As discussed in the final chapter, in a quantum universe the CMB is not merely a cosmic relic of essentially arbitrary temperature, but a concrete observation of photon partners to the mirror neutrinos. Wherever they arise in the sky, the photons must have an energy near the rest mass peak. Thermodynamic equilibrium exists for the mirror neutrinos, perhaps because in our early universe the mirror world was coming to its end.

The columns of the tribimaximal matrix (208) may be used to list the Koide eigenvalues (220) for the $\sqrt{2}$ parameter, in the form

$$1 + \sqrt{2} \cos\left(\theta + \frac{2\pi k}{3}\right) \quad (221)$$

for $k = 1, 2, 3$, using the cosine rule for two phases. With a normalisation of $\sqrt{3}^{-1}$ we have

$$\begin{aligned} \lambda_1 &= \frac{1}{\sqrt{3}} - \frac{1}{\sqrt{6}} \cos \theta - \frac{1}{\sqrt{2}} \sin \theta \\ \lambda_2 &= \frac{1}{\sqrt{3}} - \frac{1}{\sqrt{6}} \cos \theta + \frac{1}{\sqrt{2}} \sin \theta \\ \lambda_3 &= \frac{1}{\sqrt{3}} + \frac{\sqrt{2}}{\sqrt{3}} \cos \theta + 0. \end{aligned} \quad (222)$$

for any phase θ . This is an interesting connection between Koide masses for the $\sqrt{2}$ parameter and mixing phenomenology. We can view the tribimaximal matrix as a concrete link between neutrino mixing and mass, in the case that **CP** violation and dynamics in general are neglected. This matrix has long been considered in a chiral limit [171], where it arises in association with rank one mass matrices $M = aF_3DF_3^\dagger$, for D the democratic matrix and F the Fourier transform. Letting ψ_i , for $i = 1, 2, 3$, be the democratic eigenstates, one has lepton mass states [171]

$$\begin{aligned} e &= \frac{1}{\sqrt{2}}\psi_1 - \frac{1}{\sqrt{2}}\psi_2 \\ \mu &= -\frac{1}{\sqrt{6}}\psi_1 - \frac{1}{\sqrt{6}}\psi_2 + \frac{\sqrt{2}}{\sqrt{3}}\psi_3 \end{aligned} \quad (223)$$

$$\tau = \frac{1}{\sqrt{3}}\psi_1 + \frac{1}{\sqrt{3}}\psi_2 + \frac{1}{\sqrt{3}}\psi_3$$

in terms of the transpose of the form above. Observe that the signs are the same in both forms, so that these eigenstates justify the Koide rest mass formula. Moreover, as explained in [171], these lepton states are essentially the same as those for the chiral limit of the neutral pseudoscalar mesons, in terms of the (u, d, s) quark triplet. In the table above, this triplet neatly bounds the charged lepton triplet with the scale ratio $f(2/9)$.

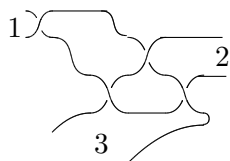
8 Knots and Ribbon Graphs

The aim of motives is to find a category **Mot** that describes a special class of spaces. Motives should provide a universal type of homology and cohomology, so that for any category of spaces there is an arrow that sends the universal cohomology to the usual one. Unfortunately, this universality is usually discussed in a 1-categorical sense. To a physicist, however, motives are about the emergence of classical geometry from quantum information, which takes place in arbitrary dimension. We need to consider noncommutative and nonassociative geometries, which appear to be essential for building classical spaces.

To start with, we seek the right diagram categories. Algebras for knots are a big clue about the structure of **Mot**. In the following few sections we look at the Temperley-Lieb category **TL** of planar diagrams, and its connection to twistor diagrams.

A Temperley-Lieb generator on two points is a diagram in (140). However, the arc diagram represents (21) in the Temperley-Lieb algebra, while it gives the identity (12) in the planar twistor diagrams [106][107]. And (21) for twistors is the identity for the Temperley-Lieb algebra. This basic confusion between (12) and (21) is fundamental to the construction of knot invariants from algebras of this type.

The planar twistor diagrams for $n > 2$ are built with $4(n - 2)$ ribbon vertices, including the boundary legs. An extension to true braided ribbon diagrams will require a cyclic structure for braids. A particle braid in B_3 is usually drawn acyclically with three top inputs and three bottom outputs. But a cyclic trace could be used to create open ribbon legs. For example, $\tau_1^{-1}\tau_2$ on the points $\{1, 2, 3\}$ is paired with two extra crossings to create a zero writhe ribbon vertex out of the figure eight knot.

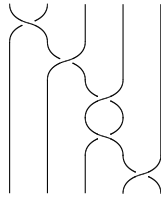

(224)

This is not a twistor vertex, because the edge paths are no longer cyclic, due to the half twist on leg 1. A three crossing vertex can only create a trefoil knot in B_2 . As a traced braid on B_3 , this would lead to a separated loop at one leg. Since knotting should be related to the essential entanglement of particle states, the figure eight knot is a minimal three way linking diagram.

The figure eight knot is hyperbolic, in contrast to the trefoil knot, which is a torus knot [172]. Its complementary space in dimension three may be constructed from two ideal hyperbolic tetrahedra. This knot gives the smallest of all hyperbolic volumes. The complement of the figure eight knot also has the property that its ribbon template diagram contains *all* knots, as

a branched surface. This is the so called universal template of Ghrist [28], which uses four letters for knot monomials, just like DNA.

The figure eight knot is a writhe zero knot. Consider again the writhe zero links in the standard braid group presentation. For $a \in \mathbb{Z}$, consider the $w = 0$ braid words $t_{i,a}^\pm \equiv \tau_i^a \tau_{i\pm 1}^{-a}$ in B_n . This includes the fundamental particle braids at $a = \pm 1$. In B_n , there are $4(n - 2)$ braids of the form $t_{i,\pm 1}^\pm$. Observe that all $w = 0$ links in B_n are given as words in the $t_{i,a}^\pm$, since a general braid word $\tau_{i_1}^{a_1} \tau_{i_2}^{a_2} \dots \tau_{i_k}^{a_k}$ satisfies $\sum a_i = 0$. For instance, $\tau_1^2 \tau_3^{-1} \tau_2^{-1}$ is expanded to $\tau_1^2 \tau_3^{-2} \tau_3^1 \tau_2^{-1}$. Another example is $\tau_1 \tau_4^{-1}$ in B_5 .



(225)

Double knots in B_{2n} can have the writhe augmented by any $n \in \mathbb{Z}$ via the addition of a ribbon twist within B_{2n} . Therefore any link in B_n has a $w = 0$ ribbon representation.

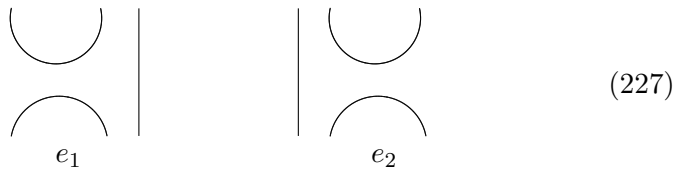
8.1 The Temperley-Lieb Algebra

The Catalan numbers C_d , which enumerate the vertices of the associahedra, also give the dimension of the Temperley-Lieb algebra TL_{d+1} [173]. The diagram representation of TL_{d+1} has d generators e_i , $i = 1, \dots, d$, such that

$$\begin{aligned} e_i^2 &= \delta e_i & e_i e_{i\pm 1} e_i &= e_i \\ e_i e_j &= e_j e_i & |i - j| &\geq 2 \end{aligned} \quad (226)$$

for $\delta \in \mathbb{C}$. The first relation is a weak projection rule, and the last relation is an orthogonality rule for such projectors, perhaps thought of as acting on some Hilbert space [26]. This connection to quantum mechanics was the original clue that algebras of this kind could be used to build knot invariants.

An element of TL_{d+1} is a string diagram from $d + 1$ points to $d + 1$ points in the plane, such that non crossing arcs and loops are permitted. Composition in TL_{d+1} is given by the vertical gluing of diagrams, as for braids. The generators of TL_3 are



(227)

When a loop is created in a diagram, it acts as the scalar δ . This can be seen in the relation $e_i^2 = \delta e_i$. The identity 1 is, by definition, the same as

a braid identity. The other two loop free diagrams in TL_3 are

$$(228)$$

The pair e_1e_2 and e_2e_1 define a basis for TL_3 , since for instance $e_1e_2 \cdot e_2e_1 = \delta e_1$. This basis is enumerated by $C_2 = 2$.

Compare this to the $d + 1$ leaved trees that define the vertices of A_d . We use the permutations in S_d to determine a diagram word. For example, (231) is mapped to $e_2e_3e_1$. Now observe how (132) and (312) reduce to the same Temperley-Lieb diagram on the A_3 pentagon.

$$(229)$$

The TL_d pictures correspond directly to trees. Place a node on each downward arc in the picture, as it is built from generators. These are the tree nodes. Then one only needs to draw lines connecting nodes to other nodes on arcs below it, and include the arc segments going to the top.

Altogether there are 14 loop free pictures in TL_4 . This equals C_4 , the vertex number for the next associahedron, A_4 , just as there were $C_3 = 5$ diagrams in TL_3 . In other words, there is a second way to match trees to arc pictures, so that A_3 comes from TL_3 , rather than TL_4 .

The algebra TL_d is generalised to arc pictures from d to k points, for distinct d and k . Let $TL_{d,k}$ denote the vector space with basis given by all possible arc diagrams, equipped with formal addition of diagrams. We restrict the coefficients to rational functions in Laurent polynomials in δ , with coefficients in \mathbb{Z} .

It is easy to check that the algebra TL_d gives a representation of the *positive* braids in the braid group B_d under the correspondence

$$\tau_i \mapsto \delta e_i - 1 \tag{230}$$

as follows. Plug $\tau_i = f(t)e_i - 1$ into the braid group relation $\tau_i\tau_{i+1}\tau_i = \tau_{i+1}\tau_i\tau_{i+1}$. Comparing the two sides forces $f(t)^2 = \delta f(t)$, so that $f(t) = \delta$ unless $f(t) = 0$. The negative generators τ_i^{-1} appear to require an inverse $(e_i^2 - 1)^{-1}$, but this is not obviously in TL_d . Inverses are discussed further below.

A nice choice of parameter is $\delta = (t^{1/2} + t^{-1/2})$, so that $\delta^2 = 2 + t + 1/t$, wherein we see the Alexander determinant for the writhe zero unknots in B_3 . When $t = \omega_n$ there is a unitary representation of B_d , and then $\delta^2 = 4 \cos^2 \pi/n$ [84].

Observe that the identity diagram in TL_2 and the generator e_1 look like the arc pictures in the Kauffmann bracket (120). This is important, because the Kauffmann bracket motivates a categorification of polynomial knot invariants. What does it mean to categorify polynomials? Recall that a categorification of a number was a set, or vector space. The polynomial invariant should be derived from diagram spaces, just as numbers give cardinalities of sets. This idea is the basis of *Khovanov homology* for links [174][175].

But we already have a space of planar diagrams associated to knots, namely TL_d . Actually, it is better to think in terms of a category \mathbf{TL} , which has ordinal objects $d \in \mathbb{N}$ and arrow sets given by TL_d , along with algebras $TL_{d,k}$ giving arrows $d \rightarrow k$, which are arc pictures from d to k . Then we can also work with the union $\coprod_d B_d$ of all braid groups.

Let us look for obvious diagram inverses within a single TL_d . Consider an arrow $2 \rightarrow 2$ which uses $TL_{2,4}$ and $TL_{4,2}$ to cancel the half loops of e_2 in TL_4 .

(231)

It provides an inverse for e_2 , but only via conjugation, and one obtains I_2 rather than I_4 . One always obtains an identity I_n , where n is the number of through strands in a diagram. This n grades the Temperley-Lieb algebras into subalgebras $TL_{d,k,n}$ for $n \geq 0$. In order to obtain an identity arrow $4 \rightarrow 4$, we might conjugate with elements of $TL_{4,2}$ and $TL_{2,4}$, but even this cannot provide a true inverse.

Since we have large categories, we look for inverses in another copy of the Temperley-Lieb algebra. In a category, we can invent products between distinct algebras. This large category is now permitted to contain TL_d algebras for distinct values of δ .

Consider B_3 , for which the two generators e_1 and e_2 give the positive generators τ_1 and τ_2 . In the Burau representations, the inverse τ_1^{-1} came from a distinct generator τ_2^* , using a $t \mapsto 1/t$ transformation for the matrix. This suggests working with two mirror copies of TL_3 , so that the second copy provides the correct site for the inverse braid crossing. Let the mirror category \mathbf{TL}^* be the union of all $TL_{d,k}^*$, so that e_i^* exists as a generator object in it. Then we choose the correct maps

$$\tau_i^{-1} \mapsto \delta(1/t)e_{n-i}^* - 1 \tag{232}$$

into \mathbf{TL}^* , which is equipped with the mirror parameter $\delta(1/t)$. The condition $\tau_i \tau_i^{-1} = I$ now states that

$$I = (\delta(t)e_i - 1)(\delta(1/t)e_{n-i}^* - 1). \tag{233}$$

A product between a **TL** and **TL*** object has been used here. With this product, the full braid group B_n is formally represented by crossing free diagrams. At the unitary values, where $\delta(t) = \delta(1/t)$, we have the simple rule

$$\delta e_i e_{n-i}^* = e_i + e_{n-i}^* \quad (234)$$

for the mixed algebra product. In $B_2 = \mathbb{Z}$, for the symmetric value $\delta = 2$, the group then collapses down to \mathbb{F}_2 .

In general, the mirror conjugation shifts the Burau matrix τ_i to τ_{n-i}^{-1} , just as it transforms the corresponding braid diagram. Using the **TL** and **TL*** product, for any B_n ,

$$(\delta(t)e_{n-j}^* - 1)(\delta(1/t)e_j - 1) \quad (235)$$

must pick out n identity strands. To each term we apply a Kauffman bracket (120), using the $t \mapsto 1/t$ inversion on the second term. By design, the resulting braid rule occurs at one generator site. Substituting the two brackets into the product, we have

$$f(t)I_2 = g(t) \begin{array}{c} \diagup \quad \diagdown \\ \diagdown \quad \diagup \end{array} + h(t) \begin{array}{c} \diagdown \quad \diagup \\ \diagup \quad \diagdown \end{array} \quad (236)$$

with

$$\begin{aligned} f(t) &= 2 + \delta(t)^{-1}t^{1/2} + \delta(1/t)^{-1}t^{-1/2} \\ g(t) &= t^{-1/4} + \delta(t)^{-1}t^{1/4} \quad h(t) = t^{1/4} + \delta(1/t)^{-1}t^{-1/4} \end{aligned} \quad (237)$$

At the special unitary values $\delta = t^{1/2} + t^{-1/2}$, f becomes $\delta + 2$. This is a local Jones type skein rule.

Remark 8.1 Let $q = t^{1/2} = \exp(2\pi i/r)$ be a root of unity braid parameter, so that $\delta^2 = 4 \cos^2 \pi/r$. The set $\{0, 1, \dots, r-2\}$ may be considered a set of spin labels for the ribbon functor that describes quantum computation [176]. This functor associates a k qubit state space to a disc marked with $3k$ points, where a basic set of three points represents a trivalent vertex. Such vertices are pieced together to form spin networks [177].

8.2 B_n and Khovanov Homology

In Khovanov homology [174][175] one has two choices for replacing each knot crossing, namely the two Kauffman uncrossings in TL_2 . Under the above TL to tree algorithm, e_1 is the unique two leaved tree, which is the 1-ordinal 1. The identity gives an empty tree, because there is nowhere to draw a node. Then an arrow $I_2 \rightarrow e_1$ represents the fundamental inclusion of the empty set in a one point set. It is often written $0 \rightarrow 1$, so that multiple crossing choices are denoted by sequences like 001 or $- - +$. These are vertices on a parity cube.

Remark 8.2 The tree differential of (5.3) also reduces the number of leaves by 1. It creates disjoint unions of rooted trees, and these underlying forest objects naively belong to multiple copies of the associahedron. However, in chapter 5 we saw that *noncommutative* forests are also counted by the Catalan numbers C_d .

8.3 Chorded Braids

Consider the (codimension 1) faces on A_{2m} for $2m = w + 1$, where w is the writhe of a positive knot with w crossings. These faces are specified by the two node trees with node valency $m + 2$.

To a positive writhe w knot in B_2 there is associated a chorded braid diagram [92]. This is essentially a Feynman diagram with w loops, created as follows. For the trefoil knot, insert two horizontal chords on the braid, connecting the first strand with the second.

(242)

Ensure that at least one crossing lies between a pair of chords. The traced knot defines a planar loop with the two chords attached, forming a three loop diagram. Start at a_1 and trace a path along the braid to determine the positions of the vertices. There are two possible chordings on the trefoil. For harder knots, crossed chords are necessary [92]. For B_2 torus knots of odd writhe, there are $m = (w + 1)/2$ chords. This corresponds to the leaf count of $m + 1$ at *one* node on the A_{2m} tree. These leaves count the loops in the Feynman diagram, or rather the number of cuts required to reduce it to a tree.

Such knotty Feynman diagrams are associated to the numerical zeta value $\zeta(w)$. This is also obtained from A_d using motivic methods, as discussed below.

8.4 Ribbons and Moduli Spaces

The pointlike nature of arrow sources and targets is associated to the pointlike nature of particles in the Feynman formalism. But lines are thickened to ribbons in the twistor formalism. The Riemann sphere \mathbb{CP}^1 with three

punctures is drawn as the interior of the flat ribbon diagram



where the outside line is a loop about ∞ , and the other loops traditionally mark the points 0 and 1. Although the continuum appears to be packed into the ribbon picture, we view ribbons as abstract geometric objects, prior to the existence of \mathbb{C} itself.

There is a fundamental reason for introducing ribbon graphs. Recall that for the associahedra A_d , the tree nodes correspond to the bracketing of letters in a word, such as $(a \otimes (b \otimes c))$. Consider the basic associator $(12) \rightarrow (21)$ of section (5.5). Ideally, this associator should be a *loop* rather than an edge, because it describes a homotopy. Using the ribbon diagram



the cyclic plat trace gives a picture of a Riemann sphere \mathbb{CP}^1 with 5 punctures, imagining the inside of the ribbon as the surface. What does this have to do with the associahedra?

Consider the complex equivalence classes of 5-punctured Riemann spheres, allowing for the degenerate cases where punctures collide. This defines a compactified *moduli space* $\mathcal{M}_{0,5}$ [178]. Now the real number points of the moduli space $\mathcal{M}_{0,5}$, which is a combinatorial gadget associated to points on the circle \mathbb{RP}^1 , define a two dimensional space that is tiled [179] by 12 copies of the A_3 pentagon. In general, there are $(d+1)!/2$ copies of the A_d polytope in the moduli space tiling.

But the A_3 pentagon is the basic axiom for associativity in monoidal categories! In other words, the shape of our punctured sphere is encoding information about the structure of *all* punctured spheres. With the tree line diagram, the cyclic trace would yield only a tetrahedron.

Similarly, the cyclic trace for the unique two leaved diagram $(1) \rightarrow (1)$ gives a picture of a 3-punctured sphere, and $\mathcal{M}_{0,3}$ is a point. This point is the A_1 associahedron. The empty polytope A_0 now corresponds to a basic ribbon strip, traced into a single loop. As a complex space, this is the disc, which models open regions of a complex curve. So in thickening trees to

ribbons, we obtain actual pictures of complex spaces, but in some sense their decomposition into ordinary open sets is completely empty!

The real points of the moduli compactification looks at configurations of points on \mathbb{RP}^1 . It smooths the moduli by adding points that represent the limiting case of collisions between points, which work to reduce the number of points in the configuration. These collisions are drawn as bubble offshoots of the original \mathbb{RP}^1 , introducing strings of loops or, rather, glued polygons. And glued polygons may be viewed as chorded polygons. This is where the A_d associahedra come in [179].

This polytope tiling for moduli spaces is used to describe relative cohomology invariants that happen to correspond to the n point Veneziano amplitudes [120][121]. These quantities are expressed in terms of the multiple zeta values. The chords of the n -gon are labeled (ij) and each chord indexes a variable u_{ij} , which is a function

$$\mathcal{M}_{0,n} \rightarrow \mathbb{CP}^1 \setminus \{0, 1, \infty\}$$

derived from simplex coordinates t_i . These are cross ratios

$$u_{ij} \equiv [ii + 1 | j + 1j] = \frac{(z_i - z_{j+1})(z_{i+1} - z_j)}{(z_i - z_j)(z_{i+1} - z_{j+1})} \quad (245)$$

such that the first three points z_1, z_2 and z_3 are sent to $1, \infty$ and 0 respectively, and the remainder are relabeled as t_i . So for n points there are $n - 3$ simplex coordinates, where a simplex is chosen with $0 < t_1 < \dots < t_m < 1$.

Example 8.3 For $n = 5$, there is an edge simplex with coordinates t_1 and t_2 . The five chords give

$$u_{13} = 1 - t_1 \quad u_{24} = \frac{t_1}{t_2} \quad u_{35} = \frac{t_2 - t_1}{t_2(1 - t_1)} \quad u_{41} = \frac{1 - t_2}{1 - t_1} \quad u_{52} = t_2$$

defining an affine space of dimension $n(n - 3)/2 = 5$.

Each u_{ij} determines a differential form $\omega_{ij} = d \log u_{ij}$. The face of the associahedron A_{n-2} is given by an equation $u_{ij} = 0$. This polytope correspondence creates pullbacks of differential forms on the lower dimensional associahedra, so that integrals are decomposed into an iterated expression. These multiple zeta value invariants form a rational algebra [118].

Let $s_i = (p_1 + \dots + p_i)^2$ give the sum of external momenta p_j . We introduce new coordinates x_i defined by $t_i = x_i x_{i+1} x_{i+2} \dots x_{n-3}$ [120], and also hyperplanes $\alpha_{ij} \equiv x_i - x_j$. The Veneziano integrals then take the form

$$B_n = \int_0^1 \prod_{i=1}^{n-3} dx_i \ x_i^{-\alpha(s_{i+1})-1} \prod_{1 < i < j < n} (1 - x_{i-1} x_i \dots x_{j-2})^{-p_i p_j} \quad (246)$$

where the $\alpha(s_i)$ and the $p_i p_j$ are integers.

Example 8.4 Consider seven point amplitudes. This requires 14 affine coordinates u_{ij} representing the chords of a heptagon.

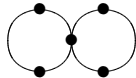
$$\begin{aligned}
u_{13} &= 1 - t_1 & u_{14} &= \frac{1 - t_2}{1 - t_1} & u_{15} &= \frac{1 - t_3}{1 - t_2} & u_{16} &= \frac{1 - t_4}{1 - t_3} \\
u_{24} &= \frac{t_1}{t_2} & u_{25} &= \frac{t_2}{t_3} & u_{26} &= \frac{t_3}{t_4} & u_{27} &= t_4 \\
u_{35} &= \frac{t_3(t_1 - t_2)}{t_2(t_1 - t_3)} & u_{36} &= \frac{t_4(t_1 - t_3)}{t_3(t_1 - t_4)} & u_{37} &= \frac{(t_1 - t_4)}{t_4(t_1 - 1)} \\
u_{46} &= \frac{(t_1 - t_4)(t_2 - t_3)}{(t_1 - t_3)(t_2 - t_4)} & u_{47} &= \frac{(t_1 - 1)(t_2 - t_4)}{(t_1 - t_4)(t_2 - 1)} \\
u_{57} &= \frac{(t_2 - 1)(t_3 - t_4)}{(t_2 - t_4)(t_3 - 1)}
\end{aligned}$$

The full motivic integral is

$$B_7 = \int_0^1 \prod_{i=1}^4 dx_i \ x_i^{-\alpha(s_{i+1})-1} (1 - x_i)^{\beta_i} \prod_{1 < i < j < n} (1 - x_{i-1} x_i \cdots x_{j-2})^{-p_i p_j}$$

Here, β_i gives an integer ghost term. Such ghost elimination is crucial to the derivation of the dimension $d = 26$ for bosonic string theory. As in appendix C, dimension 26 in M theory becomes the dimension of the traceless Hermitian elements of the exceptional 3×3 Jordan algebra over the octonions. Alternatively, it is the 27 paths of the three qutrit simplex under a rule of the form $XXX + YYY + ZZZ = 0$.

If the \mathbb{RP}^1 punctures stand for ribbon legs, a basic four leg vertex has a one dimensional moduli space tiled by three associator edges A_2 , forming a triangle $\{0, 1, \infty\}$. These A_2 are given by the S_2 trees, now described by Temperley-Lieb diagrams with the edge extrapolating between I_2 and e_1 . The bubble graph


(247)

for four points on \mathbb{RP}^1 has three places to put the second circle, representing the collision of two points. This is like putting two legs together in a BCFW type factorisation, reducing the four valent particle graph to two trivalent factors.

9 Bootstrapping Adjoint Actions

Ribbon graphs can create a powerful range of algebraic structures. Networks of such graphs define observables for a field theory, in which propagators can concretely represent the state information for a real particle. The diagrams may be interpreted geometrically, algebraically or logically. Since QCD tells us that particles are not fundamental, we imagine zooming in and out of the diagram, perhaps blowing up a strand to include further information.

We see that the crucial structures have representations in dimension 3, where polytopes of arbitrary complexity and genus may be drawn. Usually, with the ordinals for instance, the dimension of the underlying category is lifted with n . An infinite sequence of polytopes in increasing dimension turns a category like **Set** into an infinite dimensional category, rather than a zero dimensional one. But with braids, a dimension is encoded in the number of strands in the diagram. The hierarchy of adjoint representations for S_n in $B_{n!}$ may be used to build complicated nonassociative link diagrams, all in dimension 3.

On the basic permutohedron polytope, a point vertex $\sigma \in S_n$ has no structure. What we would like is for each vertex to concretely depict the ribbon permutation that it represents, so that a polytope is more self referential than a collection of trees. This seems feasible, except that the number of legs n on a twistor graph gives a valency one higher than the dimension of the polytope. But then everything is blown up into a trivalent graph in dimension 3, suggesting that for $n = 3k$ one could group particle legs onto an edge of the graph. Starting with S_4 in dimension 3, there are then 8 strands grouped onto an edge of a trivalent vertex, hinting at a concrete representation of triality.

We think of link and ribbon invariants for these diagrams as motivic invariants. Instead of tetrahedral simplices, a tetrahedron is modeled by a nonassociative link shaped into a tetrahedron. Everything should be modeled by links and ribbons, and their canonical representations.

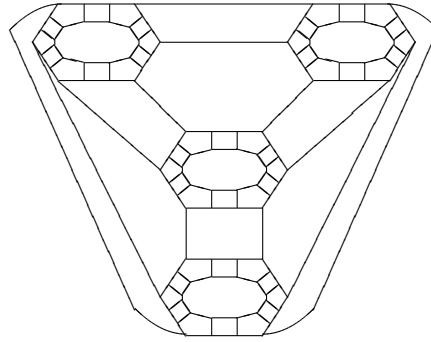
Here we merely introduce a few more self referential aspects to the geometry of permutations. The next section indicates how even S_2 can smooth out the basic diagrammatic representation of duality, and the following sections move on to the critical dimension 3.

9.1 Duality with S_2

For S_2 , the adjoint representation has two elements. The identity sends every $\sigma \in S_2$ to itself, while the flip σ swaps elements of S_2 . These four

9.2 The Permutoassociahedron

The polytopes of interest might be constructed recursively as follows. In the edge S_2 , replace each endpoint with a triangle. This results in two possible polytopes: the triangular prism in dimension 3 or the 4-valent octahedron in dimension 4. Stick with the octahedron, because each face is a triangle. Now replace each vertex of the octahedron with a square. This gives the S_4 permutohedron in dimension 3, with 24 vertices. Replacing each vertex of S_4 with a pentagon, we obtain the permutoassociahedron



(250)

in dimension 3. The true S_5 polytope in dimension 4 has the same vertices, but requires extra edges to make the graph 4-valent. The permutoassociahedron is not merely S_5 , since the pentagons have introduced nonassociativity as an axiom.

It is easy to construct an S_6 type polytope in dimension 3, replacing every vertex of the permutoassociahedron with a hexagon, since trivalent vertices may always be replaced by hexagons using the tetractys dual. This means placing three strands on every edge of the original polytope. If these strands are ribbons, we can cover this polytope with particle diagrams.

On the 4-valent octahedron, each vertex becomes a four leg ribbon graph, with an internal square loop. This square loop *itself* gives the square that we needed to blow the octahedron up into the permutohedron S_4 . But on S_4 each trivalent vertex cannot give us four ribbon legs, which is why we need, say, 24 strands in three groups of 8.

9.3 The Klein Quartic and S_5

The permutoassociahedron (250) on the tetrahedron may be used to visualise the genus 3 Klein quartic. First, let us count the vertices, edges and faces. The 24 vertices of the Klein quartic are the 24 heptagons created by gluing the 24 pentagons to neighbouring squares.

The genus 3 quartic has 84 edges and 56 faces, as follows. Each of the four large tetrahedron corners carries 21 edges and 14 points, because

$$21 = \frac{18}{2} + \frac{12}{2} + 6, \quad 14 = \frac{12}{2} + \frac{12}{2} + \frac{6}{3}.$$

That is, each edge on the inner or outer ring of heptagons will contribute twice, when the 8-gons are shrunk to nothing and the remaining 12-gons and 9-gons are glued pairwise. The internal heptagon edges are removed so that only six edges remain on the ring. The 12-gons are glued so that bivalent vertices meet trivalent ones. In this way, the resulting surface is entirely trivalent. Most vertices contribute twice. However, at a given tetrahedron corner, the six points that meet at the heptagon ring, an 8-gon and a 12-gon, will count three times, since the 8-gon brings two points together and the gluing adds another point. These points resemble the triple pentagon points on an A_4 associahedron, and the other points on the heptagon ring are like the other 12 points of A_4 .

In order for trivalency to be maintained, the four tetrahedron rings must be misaligned. The shrinking of an 8-gon brings together one bivalent and one trivalent vertex, at each of the two interior joins. Similarly, the resulting 9-gon has alternating bivalent and trivalent nodes, so it is twisted in its gluing to another 9-gon.

The Klein quartic is helpful in constructing the large Mathieu group M_{24} [181]. This large finite group is generated by only two permutations of the 24 heptagons. These permutations respect the symmetries of a cuboctahedron. This shape is easy to find on the 120 vertex tetrahedron. It has six squares (s), eight triangles (t) and six octagons (o), but in our dual setting these all appear at vertices on the heptagon rings, where each vertex is a triangle on a chorded polygon: six for an octagon, and so on. The heptagons come in two types: either the hidden pentagon peaks on a 12-gon or an 8-gon. These alternate around the loop of heptagons. On this loop we superimpose another two type sequence $abbaab$: type a has vertices in the order (ooosot), and type b the order (oosoot). The M_{24} generating permutations are

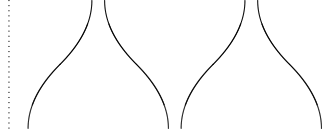
1. flip all diagonals on the o and s polygons
2. a three cycle permutation on 21 heptagons, such that $s^7 = 1$. This fixes three heptagons, or rather one vertex on the glued graph. This is one of the two generators for $PSL_2(2, 7)$. The other one, also in M_{24} , is a rotation by $2\pi/3$ about the same point, with eight cycles of length three.

The group M_{24} is closely related to the binary Golay code, and the Steiner system, that was mentioned in chapter (7) in relation to the Koide Higgs matrix.

9.4 Nonassociative Braids

If points and lines are blurred beneath duality, what of faces in a *triality* with points, lines and faces? For ribbons in an ambient space, nonassociativity

of the strands is able to swap the interior of the ribbon for the outside, as in the process



where the dashed lines here denote a boundary to the braid region, or a gluing to a cylinder. A nonassociative braid group is given by the standard generators σ_i along with a second set a_i that denote the bracketing of two strands. The additional relations are [180]

$$\begin{aligned} \sigma_i a_j &= a_j \sigma_i & a_i \sigma_{j-1} \sigma_j a_i & & a_i a_{j-1} &= a_j a_i & (251) \\ \sigma_{i+1} \sigma_i a_{i+1} &= a_i \sigma_i & \sigma_i \sigma_{i+1} a_i &= a_{i+1} \sigma_i \end{aligned}$$

when $j \geq i+1$. General nonassociative braid diagrams can partition a region into the interior and exterior of the ribbon graph. For example, a ribbon tetrahedron (with no twists) can send its vertices to its faces by regrouping the strands, since there are both four vertices and four faces. This sends open strings (the ribbons) to closed strings (on a 4 punctured sphere).

The nonassociative braid groups underlie categories that are governed by permutohedra axioms. These are true 2-ordinal polytopes, mixing the S_d and A_d polytopes.

10 Entanglement and Entropy

The black hole qubit correspondence [18][19] is a detailed relationship between black hole entropy formulas in M theory and measures of entanglement for multiple qudits. For example, extremal BPS solutions have eight charges, a magnetic (p^0, p^1, p^2, p^3) and an electric (q_0, q_1, q_2, q_3) . These correspond to the eight coefficients of an unnormalised three qubit state ψ_{ijk} , so that the black hole entropy is given by

$$S = \frac{\pi}{2} \sqrt{-\Delta(\psi_{ijk})} \quad (252)$$

where $\Delta(\psi)$ is Cayley's hyperdeterminant [73]. The hyperdeterminant is a natural generalisation of a matrix determinant for the $2 \times 2 \times 2$ qubit tensor cube. In the next section, we see how this invariant is connected to twistor geometry [182].

An acceptable measure of quantum entanglement must respect the equivalence relations of the physical system. These are taken to be either the local operations with classical communication (LOCC), or stochastic local operations (SLOCC). Here locality means that transformations act on each qudit separately [183]. For an n qubit system we usually consider a SLOCC group $GL_2(\mathbb{C})^{\otimes n}$, where GL_2 acts locally on each qubit. For a general mixed qudit Hilbert space on n objects, the SLOCC group will be $GL_{k_1}(\mathbb{C}) \otimes \cdots \otimes GL_{k_n}(\mathbb{C})$. We are also interested in determinant zero matrices, which shift the entanglement class, and are related to the underlying categorical structure.

The axioms of category theory can direct certain choices for entanglement measures, which are by no means yet settled. In some schemes, an entanglement class can contain both separable states and maximally entangled ones! Here we consider only maximally entangled states, meaning n -partite n qudit systems. For example, for three qubits there are two tripartite classes, one bipartite and one totally separable class. For four or more qubits, an entanglement measure may require a free parameter, every value of which defines a distinct class. Insisting on restricted coefficient sets at least limits the cardinality of such entanglement groupings.

The interesting invariants may be constructed using *secondary polytopes* [73], introduced below. These polytopes are indexed by finite geometries, associated to the word monoid. For example, the two qudit word monoid simplex is geometrically a hexagon, and its allowed triangulations recover the associahedron A_4 via the usual chordings of hexagons.

10.1 Entanglement with Trees and Jordan Algebra

The lowest dimensional associahedron is the geometric point A_1 , which we draw as two leaves attached to a double root with two minus and two plus

signs.

$$(253)$$

This will be a symbol for the unique non trivial entanglement class for $n = 2$ particles from a two state system.

Recall that the $2n$ particle scattering amplitudes include helicity configurations with n negative and n positive helicities, for $n \geq 2$. Given $2n$ legs on a diagram, there are clearly $h = \binom{2n}{n}$ ways to assign these \pm signs to the legs. This is $n + 1$ times the Catalan number C_n . It is also the number of minors in the $n \times 2n$ matrix of Grassmannian coordinates, where an $n \times n$ block has been fixed at I_n . These minors are a basis for \mathbb{C}^h .

When $n = 2$, the Minkowski space Grassmannian gives a basis for $\Lambda^2(\mathbb{C}^4)$ and the six minors v_{ij} satisfy the Plücker relation

$$V = v_{12}v_{34} - v_{13}v_{24} + v_{23}v_{14} = 0. \quad (254)$$

In [182], the minors for $n = 2$ and $n = 3$ are used to study entanglement for n fermions with two single particle states ($-$ and $+$). When $n = 2$, there is only one true bipartite entanglement class, given by $V \neq 0$. A measure of this entanglement is given by

$$\eta \equiv 8|V| \in [0, 1]. \quad (255)$$

When $V = 0$, the two particle system is separable. This means that V can be written in the twistor form $v_{ij} = Z_i W_j - W_i Z_j$ for two 4-vectors Z and W .

When $n = 3$, there are $20 = 4C_3$ minors in the 3×6 Grassmanian matrix [182]. We call them V_{ijk} , where as before the index ijk labels the selected columns. The *triple root trees*

$$(256)$$

form an associator edge, with its MHV and $\overline{\text{MHV}}$ source and target. This $C_2 = 2$ will count the number of tripartite entanglement classes for $n = 3$. The first entanglement measure is $|T_{123}| \in [0, 1]$, defined as follows. Let V_{ijk} also denote the numerical coefficient of $v_i \wedge v_j \wedge v_k$ in the full state. Since the ijk index tracks the choice of \pm signs, let the source $s = V_{123}$ and target

$t = V_{456}$. The remaining 18 3-forms fit into two helicity conjugate 3×3 matrices [182],

$$A = \begin{pmatrix} V_{156} & V_{164} & V_{145} \\ V_{256} & V_{264} & V_{245} \\ V_{356} & V_{364} & V_{345} \end{pmatrix} \quad B = \begin{pmatrix} V_{423} & V_{431} & V_{412} \\ V_{523} & V_{531} & V_{512} \\ V_{623} & V_{631} & V_{612} \end{pmatrix}. \quad (257)$$

The measure is defined by

$$T_{123} = 4[(\text{Tr}(AB) - st)^2 - 4\sqrt{\det(AB)}^{-1}\text{Tr}(A^\dagger B^\dagger) + 4s \det A + 4t \det B]. \quad (258)$$

This is chosen to be twice the quartic form $q(x)$ for the *Freudenthal triple* system $\mathbb{C} \oplus \mathbb{C} \oplus J \oplus J$ associated to the 3×3 matrix Jordan algebra J , where

$$x = \begin{pmatrix} s & A \\ B & t \end{pmatrix} \quad (259)$$

and A and B are in J . Some definitions are given in appendix D. Consider now the special case of diagonal A and B . This gives eight dimensional vectors

$$V = V_{123} + V_{156} + V_{264} + V_{345} + V_{423} + V_{531} + V_{612} + V_{456}, \quad (260)$$

which specialise further to a three qubit state when indices from $\{1, 2, 3\}$ are replaced by 0, and $\{4, 5, 6\}$ by 1. In this case, the entanglement measure is given by Cayley's hyperdeterminant Δ for a $2 \times 2 \times 2$ three qubit tensor cube, to be discussed further in the next section [73]. Then $T_{123} = 4\Delta(V)$, where

$$\begin{aligned} \Delta(V) = & V_{123}^2 V_{456}^2 + V_{612}^2 V_{345}^2 + V_{531}^2 V_{264}^2 + V_{423}^2 V_{156}^2 \\ & - 2V_{123} V_{456} (V_{612} V_{345} + V_{531} V_{264} + V_{423} V_{156}) \\ & - 2(V_{612} V_{345} V_{531} V_{264} + V_{531} V_{264} V_{423} V_{156} + V_{423} V_{156} V_{612} V_{345}) \\ & + 4(V_{123} V_{345} V_{156} V_{264} + V_{456} V_{423} V_{531} V_{612}). \end{aligned} \quad (261)$$

Unlike for qubits, the three fermions are distinguishable by their indices using the six letter alphabet. Consider now an example where $T_{123} = 0$, but the entanglement is still tripartite [182]. Let Φ be the normalised state with $V_{123} = 1/\sqrt{3}$, $V_{456} = 0$, $B \equiv 0$ and

$$A = \frac{1}{\sqrt{3}} \begin{pmatrix} 1 & 0 & 0 \\ 0 & 0 & 0 \\ 0 & 0 & 1 \end{pmatrix}. \quad (262)$$

How do we distinguish this state, known as a $|W\rangle$ state, from a $T_{123} \neq 0$ one? With the Jordan algebra J , one can define a dual state \tilde{V} . This turns out to be

$$\tilde{V}_{ijk} = 3\epsilon^{abcdef} V_{ibc} V_{ajk} V_{def}, \quad (263)$$

which may be thought of as a triality inspired dual. In the example, $\tilde{\Phi}$ is non zero, and this counts as a second entanglement measure. Let $\tilde{\Phi}$, \tilde{s} , \tilde{t} and \tilde{A} all be zero, but \tilde{B} non zero. Let $C(A)^T$ by the transpose cofactor matrix of A . Then

$$\tilde{B} = 3sC(A)^T = \frac{3}{3\sqrt{3}} \begin{pmatrix} 0 & 0 & 0 \\ 0 & 1 & 0 \\ 0 & 0 & 0 \end{pmatrix}, \quad (264)$$

from $\tilde{V}_{531} = V_{156}V_{123}V_{345}$. The $1/3$ coefficient comes from the single nonzero C_{ij} determinant. We also have

$$T_{123} = -ce^{abcdef}V_{abc}\tilde{V}_{def}, \quad (265)$$

for a normalisation constant c . This shows the origin of the quartic terms in $\Delta(V)$. So $T_{123}(\Phi)$ is zero precisely because of the complementarity of A and its cofactor matrix, but it is constructed from two non zero components, and the existence of a dual signifies an entanglement class distinct from the $T_{123} \neq 0$ class.

We could also specialise T_{123} to a three unary state system, using $(1, 4) \mapsto X$, $(2, 5) \mapsto Y$ and $(3, 6) \mapsto Z$. This is a qutrit. The hyperdeterminant Δ then becomes an expression in the 1-circulant three qutrit words, say for XYZ the identity,

$$\begin{aligned} \Delta &= (1 - 4V_{XYZ}^2)(V_{ZXY}^2 + V_{YZX}^2) \\ &\quad - 2V_{ZXY}^2V_{YZX}^2 + 8V_{XYZ}^2V_{ZXY}V_{YZX}. \end{aligned} \quad (266)$$

If these 1-circulants are used as a basis for a 3×3 Hermitian matrix with diagonal $V_{XYZ} = xI_3$ and off diagonal complex phases ϕ and $\bar{\phi}$, then we have a normalised state such that $T_{123} = (4/3)(\tan^2 \phi)(4x^2 - 1)$.

For the three qubit state Υ with coefficients a_{ijk} , consider a coordinate fix of $a_{000} = 1$. Cayley's hyperdeterminant is then reduced to

$$\begin{aligned} \Delta(\Upsilon) &= a_{111}^2 + a_{100}^2 a_{011}^2 + a_{010}^2 a_{101}^2 + a_{001}^2 a_{110}^2 \\ &\quad + 4(a_{011}a_{110}a_{101} + a_{111}a_{100}a_{010}a_{001}) \\ &\quad - 2(a_{100}a_{011}a_{111} + a_{010}a_{101}a_{111} + a_{001}a_{110}a_{111} \\ &\quad + a_{100}a_{010}a_{101}a_{011} + a_{010}a_{001}a_{110}a_{101} + a_{100}a_{001}a_{110}a_{011}). \end{aligned} \quad (267)$$

In [184] it was noted that the entanglement condition $\Delta(\Upsilon) = 0$ is equivalent to an ordinary determinant $D = a_{111}$ for the 3×3 matrix

$$M(\Upsilon) = \begin{pmatrix} a_{100} & \sqrt{a_{100}a_{010} - a_{110}^2} & \sqrt{a_{100}a_{001} - a_{011}^2} \\ \sqrt{a_{100}a_{010} - a_{110}^2} & a_{010} & \sqrt{a_{010}a_{001} - a_{011}^2} \\ \sqrt{a_{100}a_{001} - a_{101}^2} & \sqrt{a_{010}a_{001} - a_{011}^2} & a_{001} \end{pmatrix}. \quad (268)$$

The entries are written so that the set of a_{ijk} are the six 2×2 minors. When $\Delta(\Psi) \neq 0$ the determinant D differs from a_{111} , which then characterises the entanglement. Note that this matrix is really a two qutrit rather than three qubit matrix. It matches the path array when the parity 110 terms are zero, as for the $|W\rangle$ state. In that case, the qutrit state is $(\sqrt{a_{100}}, \sqrt{a_{010}}, \sqrt{a_{001}})$, and none of the matrix entries are zero. The $|W\rangle$ state, with $D = 0$, characterises null twistors, as shown in [20]. This now follows directly from the 2×2 minors of the qutrit matrix, which are essentially the Minkowski elements in $SL_2(\mathbb{C})$. In contrast, the GHZ state is given by $M(\Upsilon) \equiv 0$, with $a_{111} \neq 0$. This requires the twistor variables Z and W to specify distinct null directions.

The two tripartite classes given above ($T_{123} \neq 0$ and $\tilde{V} \neq 0$) are known respectively as the GHZ and $|W\rangle$ states for three qubits [185]. A biseparable state is given by the example $1/\sqrt{2}(V_{123} + V_{156})$ and a GHZ state by

$$\Psi = \frac{1}{\sqrt{3}}(\sqrt{2}V_{135} + V_{246}). \quad (269)$$

The four entanglement classes for three qubits do not distinguish the three *labeled* biseparable sets, such as $(AB)(C)$.

10.2 Categorical Entanglement

Does the Catalan number C_{n-1} count the number of n -partite classes for n fermions? In terms of categorical structure, it was shown in [186] that the two tripartite classes for three qubits, W and GHZ , correspond to two kinds of commutative Frobenius algebras on \mathbb{C}^2 in the symmetric monoidal category of qudit Hilbert spaces. These give the two trees for C_2 .

Take trivalent nodes for the multiplication m and comultiplication Δ , and truncated strings

$$\begin{array}{c} \bullet \\ | \\ \bullet \end{array} \quad \begin{array}{c} \bullet \\ | \\ \bullet \end{array} \quad (270)$$

for the unit $\eta : I \rightarrow A$ and counit $\epsilon : A \rightarrow I$ respectively. The compatibility condition looks like

$$\begin{array}{c} \bullet \\ / \quad \backslash \\ | \quad | \\ \bullet \end{array} = \begin{array}{c} \bullet \\ \backslash \quad / \\ | \quad | \\ \bullet \end{array} \quad (271)$$

stating that the order of nodes does not matter. For diagrams with no loops one can then introduce the shorthand

$$S_{mn} = \begin{array}{c} \dots \\ \backslash \quad / \\ \bullet \\ / \quad \backslash \\ \dots \end{array} \quad (272)$$

for a vertex from m to n strings. In particular, S_{02} and S_{20} give the arc diagrams of duality, so that we may consider a straightening law

$$\begin{array}{c} \text{---} \\ \text{---} \end{array} \text{---} = \begin{array}{c} | \\ | \\ | \end{array} \quad (273)$$

involving an arrow $A \rightarrow A \otimes A \otimes A \rightarrow A$. This is part of the structure of a *compact* category [187], for which writhe pieces are unimportant. The category of finite dimensional Hilbert spaces is an example of a compact category, with duals A^* . This straightening law underlies the protocol for quantum teleportation [188]. Now the *GHZ* and *W* states may be given respectively by [186] the laws

$$\begin{array}{c} \bullet \\ | \\ \bullet \end{array} = \begin{array}{c} | \\ | \\ | \end{array} \quad \circ \begin{array}{c} \bullet \\ | \\ \bullet \end{array} = \begin{array}{c} \bullet \\ | \\ \bullet \end{array} \quad (274)$$

noting the scalar loop for the *W* state. A so called induced tripartite state is given by the diagram S_{03}

$$\begin{array}{c} \bullet \\ / \quad \backslash \\ / \quad \backslash \end{array} \quad (275)$$

which we see is just an A_2 index tree. The diagram calculus of such *GHZ* and *W* states in a symmetric monoidal category captures multipartite entanglement for *any* number of qubits. However, for qutrits and beyond, symmetric monoidal categories cannot be the whole story, since the A_n polytopes are expressing coherence laws for higher and higher dimensional categories.

10.3 Secondary Polytopes and Hyperdeterminants

The associahedra and permutohedra are examples of secondary polytopes [73]. In this section we see how secondary polytopes can generate the determinant type invariants.

For any finite set S of n points in an embedding space \mathbb{R}^k , let $C(S)$ be the convex hull of the set, possibly with points in its interior. We consider triangulations with vertices in S , including the hull edges. For example, four points in the plane with one central point define two possible diagrams.

$$\begin{array}{c} \triangle \\ \bullet \end{array} \quad \begin{array}{c} \triangle \\ / \quad \backslash \\ / \quad \backslash \end{array} \quad (276)$$

Observe that a square configuration of four points would not have allowed a central subdivision. For the square configuration, the triangulations would be the chorded source and target of A_2 . Thus the *geometry* of the points dictates the diagram set. We only allow certain nice triangulations, as indicated in the examples below.

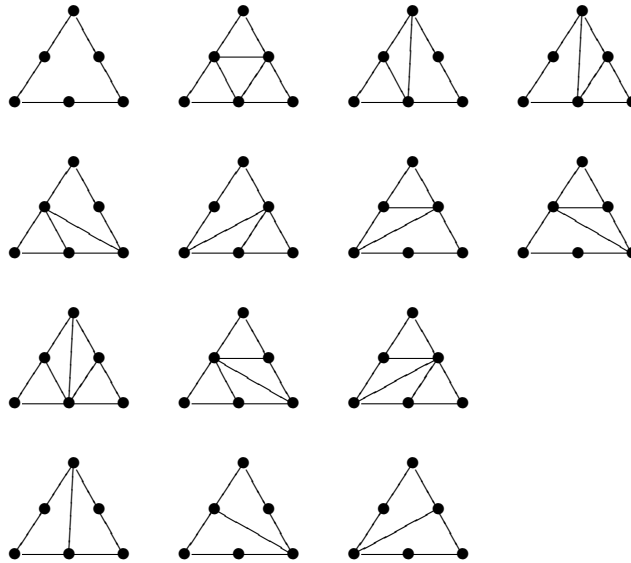
Given an allowed triangulation T for any S , let $\xi_T : S \rightarrow \mathbb{R}$ be the characteristic function defined by the sum

$$\xi_T(p) = \sum_{\{\sigma:p \in \sigma\}} \text{Vol}(\sigma) \tag{277}$$

over simplices σ in T . The volumes will be neatly normalised so that an underlying field is not crucial to the combinatorial arguments. Let \mathbb{R}^S be the vector space of all ξ_T for all T . The dimension of \mathbb{R}^S is just n .

The *secondary polytope* $\Sigma(S)$ is the convex hull in \mathbb{R}^S of all vectors ξ_T for all triangulations T . For the four point configuration above, the normalised volume vectors are $(3, 3, 3, 0)$ and $(2, 2, 2, 3)$, giving a secondary interval between these points. The dimension of $\Sigma(S)$ is $n - k - 1$, since every cone over T in \mathbb{R}^S shares a $k + 1$ dimensional subspace with every other, determining the codimension for $\Sigma(S)$.

Example 10.1 The A_4 associahedron polytope in \mathbb{R}^3 is determined by the 14 triangulations of the planar two qutrit simplex, which is a squashed hexagon.



The area of a minimal piece inside any triangulated configuration is normalised to 1. This procedure is dual to the one that assigns integral volumes to vertices, as in chapter 5. Zero area triangles are permitted along a simplex edge. These volumes take values $V \in \{2^{i_2} 3^{i_3} \dots l^{i_l}\}$ for $i_k \leq d - 1$, so that for A_4 , the volumes are 0, 1, 2 or 4.

Example 10.2 Consider the three qubit parity cube, at $n = 4$. Squashed into the path interval, it has four triangulations, matching the interval par-

titions $(1, 1, 1)$, $(1, 2)$, $(2, 1)$ and (3) . Recall from chapter 5 that these partitions label the vertices of the parity square. The four vectors of this secondary polytope are $(3, 3, 3, 3)$, $(1, 2, 2, 1)$, $(1, 3, 2, 2)$ and $(2, 2, 3, 1)$.

Example 10.3 The permutohedra S_d are secondary polytopes for the triangular prism $\Delta^1 \times \Delta^{m-1}$ in \mathbb{R}^m , for a simplex Δ^{m-1} [73], where Δ^1 is the interval. The prism clearly has $2m$ points, so the secondary polytope is of dimension $m - 1$, for $d = m$. For example, the hexagon S_3 of dimension 2 comes from the six point prism $\Delta^1 \times \Delta^2$. The ξ_T vectors form $2 \times m$ matrices, using the prism decomposition. For the permutation $(d(d - 1) \cdots 1)$ in S_d , one may take a triangulation such that the ξ_T vectors are $(d - k + 1, k)$, and the other ξ_T are permutations of these vectors. This is the simplest example that uses a product of basic simplices.

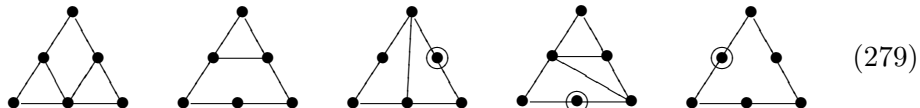
Recall that divided simplices are canonically coordinatised. For example, the two qutrit labels from the word monoid give its coordinates: $(2, 0, 0)$, $(0, 2, 0)$, $(0, 0, 2)$, $(1, 1, 0)$, $(1, 0, 1)$ and $(0, 1, 1)$. Coordinates in \mathbb{Z}^d come from the monomial indices of the word monoid [73]. The homogeneity of a monomial means that all points lie in a hyperplane

$$x_1 + x_2 + \cdots + x_n = d. \quad (278)$$

Let S sit in the integral lattice \mathbb{Z}^k , so that $p \in S$ is a commutative monomial $X_p = X_1^{i_1} \cdots X_k^{i_k}$ with k variables. That is, the integer vectors have become exponent vectors. When $k = 2$ let S be the monomials $X^i Y^j$ for $i \in \{1, 2, \dots, m_i\}$ and $j \in \{1, 2, \dots, m_j\}$. For any $m_i \times m_j$ matrix M defining a form $\sum M_{ij} X^i Y^j$, the S -discriminant is either 1, when $m_i \neq m_j$, or equal to the determinant $\det M$ when M is square. For the trilinear $X^i Y^j Z^h$ there is a *hyperdeterminant* for any form

$$\sum_{i=1}^{m_i} \sum_{j=1}^{m_j} \sum_{h=1}^{m_h} M_{ijh} X^i Y^j Z^h.$$

The Cayley hyperdeterminant $\Delta(V)$ for qubits is a $2 \times 2 \times 2$ example. Recall that $\Delta(V)$ is quartic by the triality of (263). Triality on A_4 itself is made manifest by the simplex triangulations. Look at the $21 = 3 \times 7$ edges, indicated by triangulations that may omit a boundary triangle. Two of these edge sets come with a left right reflection asymmetry, leaving only 5 diagram types.



Simplex volumes should take values $V_c \in \{2^{c_2} 3^{c_3} \cdots d^{c_d}\}$ for $c_k \leq n - 1$, as in chapter 5 [62]. Observe that the c vectors for $C_4 = 14$ are canonical

coordinates for four 4-dits. The tetrahedral four 4-dit simplex then contains an integral A_4 polytope, just as one corner of the tetractys contains the pentagon A_3 .

Let S be a generating set in the integer lattice \mathbb{Z}^k . The secondary polytope for S is known as the *Chow polytope* for the toric variety defined by S . In this case there is a *principal S -determinant* for S , such that a triangulation T is associated to a coefficient

$$c_T = \pm \prod_{\sigma \in T} \text{Vol}(\sigma)^{\text{Vol}(\sigma)}. \quad (280)$$

As noted in [73], the expression $\prod_i V^V$ is the same as

$$\exp\left(\sum V_i \log V_i\right) \quad (281)$$

where $\sum V_i \log V_i$ is in the form of a negative entropy, and V_i is a probability. Such a probability concretely measures the likelihood of ending up in a particular triangle, where this likelihood increases with volume.

Example 10.4 Consider the two qutrit word monoid simplex. When a minimal triangle is normalised to area 1, the 14 c_T take the values 1, 4 or 16. The renormalised probabilities over all 14 vertices of A_4 are then $1/92$, $1/23$ and $4/23$.

Planar square lattice paths in steps X and Y ending at a point (m, n) , and so of total length $m + n$, correspond to the (m, n) shuffles in S_{m+n} . The paths XY and YX therefore stand for the $(1, 1)$ shuffles in S_2 , which is all of S_2 . The *shuffle polytope* $N_{m,n}$ [73] has amongst its vertices all the (m, n) shuffles in the permutohedron S_{m+n} . Thus $N_{1,1}$ is the edge S_2 . The polytope $N_{3,3}$ determines an invariant for two cubic polynomials

$$f(z) = X_0 + X_1z + X_2z^2 + X_3z^3 \quad g(z) = Y_0 + Y_1z + Y_2z^2 + Y_3z^3 \quad (282)$$

whose coefficients X_i and Y_j define integral coordinates in \mathbb{R}^8 . The vertices of $N_{3,3}$ specify terms in the invariant.

11 Non Local Cosmology

The dark mass energy problem is unavoidable when one assumes that general relativity is the correct theory for gravity on cosmological scales. From the emergent viewpoint there is no reason to make a commitment to GR, but in this chapter we outline a mirror matter perspective in the context of standard cosmological techniques, for completeness. Observational data is typically analysed from the perspective of GR, or some small modification of it. At present, the empirical success of the Λ CDM model points to the correctness of GR only on small scales, where it has been tested in numerous experiments.

The Λ CDM model insists that the CMB dipole is due to our motion in the local galactic group, with respect to a CMB frame. But according to Mach's principle, there is only one special inertial frame: one for which the distant universe is not rotating [189]. The distant universe should be completely at rest with respect to us. This forces us to interpret the local dipole as the motion of a local photon source within the average CMB. But if all CMB photons arise from the same physical mechanism, these sources must tell us something fundamental about gravity. One might object that all photons must come from the distant universe, but this is an assumption of Λ CDM type cosmologies. The physical universe is quantum, and we only observe the photons when they are absorbed.

Here we interpret the CMB homogeneity in terms of the rest mass of a mirror neutrino. If the neutrinos set a mass unit, the ratio of different mass scales can change as we look back in cosmic time. That is, the ratio of baryon to neutrino scales will decrease with look back time, as the masses tend to zero at a conformal boundary. Since baryonic matter is then lighter in the past, photons are emitted with an observed redshift. This means that CMB photons can maintain their frequency in a *static* universe with no Big Bang, from any emission point within the observable universe, without contradicting the redshift of distant sources.

So we do not need to imagine an expanding spacetime. On the other hand, we can just as easily extrapolate the neutrino scale back to a hotter universe in sync with the usual temperature redshift dependence. The CMB photons are then redshifted, but only because the neutrino mass scale increases in step. If the galactic redshifts are then attributed entirely to expansion, we can say that the mass ratios are fixed for all time.

A novel viewpoint on the CMB might also be justified by holography, which takes all information internal to a classical spacetime and places it at a boundary. The mathematics of the AdS/CFT correspondence validates such a holographic principle for information in the twistorial $N = 4$ supersymmetric Yang-Mills theory, but the role of holography in emergent geometry remains unclear. In an observer dependent cosmology, where our Big Bang is unique only to our own teleological past, and is an illusion at

that, neither cosmological nor event singularities carry a universal existence. In this context, the underlying boundary may be viewed as a projection of observer constraints for the imagined interior space.

In a ribbon theory built with chiral particle graphs we naturally include matter and antimatter, and also the mirror set. It is important to understand that the mirror sector can have nothing to do with conventional supersymmetry, which completely ignores the concept of emergent geometry. There is no reason at all to attribute extra local states to the mirror braids. Rather, we may think of the mirror states as atoms of spacetime. The standard cosmology of mirror matter introduces an identical mirrored Lagrangian to that of the Standard Model, including a second bosonic sector [190][191], but the non local physics of ribbons tells us something different about mirror matter. The mirror world is intimately tied to our own, through the two directions of thermodynamic time that are responsible for the generation of local mass.

Initially, we can imagine mirror matter inhabiting a space behind our classical horizons, in a spacetime that contracts as ours expands, generating the true static, timeless universe. In this way, theories of black hole dark matter may approximate the behaviour of mirror matter using relativistic theories, and cosmic censorship becomes the rule that we do not inhabit the mirror world.

In particular, Riofrio [192] explains the CMB homogeneity using a variable speed of light picture, based on an FRW metric. This scheme couples particle pair creation with black hole dark matter to derive an exact baryonic mass fraction of $\Omega_b = 1 - 3/\pi$, as noted below. Penrose's conformal cyclic universe [193] is another relativistic cosmology that proposes a black hole dark sector. Its gluing of conformal boundaries requires a transformation of scale factors, which somewhat resembles the dualities of M theory. Although this classical picture requires each aeon in an infinite set of cycles to grow in scale, a quantum framework is free to loop back on itself, since a spectrum of energies is generated for each classical point. In the end, cosmology must be quantum.

Classically, one usually singles out a conformally flat spacetime such as de Sitter space. Although empty of traditional matter, we need not consider such metrics as empty spacetimes. As relativistic observers, we have only one cosmos, with one baryonic and one dark sector. We know from observation that the overall geometry is flat. This could be a de Sitter geometry or some other FRW geometry with a curvature $k = 0$, but it might not be possible to properly account for the mirror matter within the same geometry that is obeyed by the baryonic sector, in which case the dark component of the baryonic cosmos is merely an effective description for the mirror degrees of freedom. Given mirror contraction, it seems likely that a bimetric theory will have more success than GR.

Morally, the cosmological constant should be $\Lambda = 0$, because many argu-

ments tie Λ to a quantum deformation parameter. This is the case in [192]. However, Riofrio actually requires a varying \hbar over cosmic time, suggesting a sequence of Λ values, perhaps all canceled in some bimetric scenario.

We let M represent either a Planck mass or a total mass for the observable universe, and t is the cosmic time. As in the older steady state models, we will imagine that M increases with t , so that $M \rightarrow 0$ at a critical time in our cosmic past. Since $M \rightarrow 0$ is a condition that might apply anywhere, we consider it a quantum boundary condition, associated to the quantum vacuum from which all matter is born [192]. The universal mass that we observe is a reflection of our complexity as observers.

As noted by Dungworth [170], as our spacetime expands with respect to our cosmic arrow of time, the mirror world should contract. We observe this as a clumping of dark matter over time, generating gravitational entropy. This inclusion of a second world is necessary for the restoration of time symmetry in microscopic physics, for which there can be no absolute time direction [16]. Although microscopic time is reversible in the Standard Model, its usual application to cosmology introduces an essential arrow for time. Since the important dualities of M theory link the largest and smallest scales, there is then a basic inconsistency in the Λ CDM picture, between the time directed world and a time unordered one.

Mirror neutrinos are special, capturing the essence of the mirror time reversal, manifesting themselves as CMB photons. Short lived mirror neutrinos must have uncertain rest masses, but the corresponding photon energy is peaked at the theoretical rest mass under Wien's law, which is precisely the observed CMB temperature of $T = 2.725$ K [170][143].

The CMB is the perfect black body spectrum for bosonic states, whereby any fermionic aspect to the information has been squeezed out by its space-time restriction. The CMB represents the thermodynamic equilibrium that the mirror world reaches, as it bumps against our own. There is no need for inflation, because the homogeneity of the CMB is entirely due to the precise neutrino rest mass. There is no horizon problem. The slight lack of scale invariance can also be attributed to the light neutrino mass. Neutrinos mediate gravity non locally, and there are no gravitational waves. IceCube can observe high energy neutrinos, traveling extremely close to c , since zero velocity mirror neutrinos are partnered to light speed laboratory neutrinos. This specifies a characteristic acceleration of around cH_0 , assuming that our Hubble time is closely linked to neutrino gravity. This acceleration appears in the phenomenology of modified Newtonian dynamics.

11.1 Modified Newtonian Dynamics

Modified Newtonian dynamics [194][195] suggests that new forms of matter are not the correct resolution to the dark matter problem. Instead, there exists a fundamental constant a_0 , an acceleration, such that bodies on galactic

scales undergoing accelerations $a \ll a_0$ no longer obey Newton's law. These bodies instead obey the MOND rule

$$a = \frac{\sqrt{MGa_0}}{R}, \quad (283)$$

where M is a galactic mass, R the radius of the orbiting body and G is Newton's constant.

MOND theories usually assume that general relativity no longer holds for small accelerations. Here, however, we consider that relativity and Newtonian mechanics might still apply, at least in certain circumstances. The empirically successful MOND rule must then be viewed as a Newtonian law in disguise. This may be achieved by allowing the galactic mass M to evolve with large distances. This evolution of baryonic mass is meant only as a simple model for the inclusion of mirror mass. For a distant observer, the galactic mass appears to grow as a local observer recedes from its centre, just as our universal mass increases in cosmic time.

The observational evidence begins with galactic rotation curves, which exhibit peculiarly high velocities at outer radii [195]. The standard Λ CDM model cannot fit the details of rotation curves, and it also fails on many other points, such as the polarised nature of satellite galaxy groups and the variation of dark matter content within galaxies. These Tully-Fisher relations [197][195] give a tight correspondence between apparent dark matter content and galaxy luminosity.

In the baryonic form of the relations, there is a tight correlation $M_b \sim V^4$ between galactic baryonic mass and the flat limiting speed of galactic rotation. The only way [195] an FRW framework can accommodate the Tully-Fisher law is if the dark matter surface density *exactly* balances out the baryonic density at large radii. This coincidence really forces a close link (no pun intended) between the apparent baryonic and dark matter densities.

Under the evolving mass hypothesis, the MOND law (283) for a mass M_0 may be interpreted as a Newtonian law for a mass M_1 . Equating the two laws,

$$\frac{M_1 G}{R^2} = \frac{\sqrt{M_0 G a_0}}{R} \quad (284)$$

we find that

$$M_1 = \sqrt{\frac{M_0 a_0}{G}} R \quad (285)$$

in the MOND regime. This increase in apparent mass with radius mimics the relativistic behaviour of black hole mass. It suggests that the region interior to the body's orbit is filling up with mass as the body recedes, at least from the perspective of a distant observer. This is analogous to an $M \sim t$ rule for black hole cosmologies [198][192].

11.2 AdS, dS and FRW Cosmologies

In the standard Λ CDM picture, an FRW cosmology mixes dark energy, dark matter, radiation and baryonic matter components. Although almost certainly inadequate for dealing with the quantum universe, we augment this model in a brief discussion here. The Λ CDM model is empirically valid for small angular scales, where causal contact poses no observational dilemma. It fails most notably at large angular scales, where we might expect appreciable effects from the non local cosmology.

The anti de Sitter and de Sitter metrics play a special role in alternative cosmologies, contrasting with the usual power law relation for the FRW scale factor $a(t)$. The de Sitter geometry is neatly expressed as a five dimensional space in six dimensions, the dimension of twistor space. AdS space in dimension 5, on the other hand, appears in the bulk string theory associated to the four dimensional $N = 4$ supersymmetric Yang-Mills theory, with its superconformal symmetry. AdS space is of some interest here, because the inclusion of a Schwarzschild black hole in AdS space is a natural way to break conventional supersymmetry and to endow the boundary theory with a finite temperature [199]. For the four dimensional $N = 4$ theory [199] this temperature is equal to $\sqrt{3|\Lambda|^{-1}}/\beta$, where β is the period of the time coordinate τ in the string theory metric. In some sense, then, de Sitter space accounts for the imaginary temperatures of a mirror world. We are always working on the boundary, and not with string theory, but a pairing of the dS and AdS geometries is suggested as a mechanism for mass generation, breaking the conformal symmetry with the complex temperature.

In contrast, the standard Λ CDM model uses an FRW metric with a power law for the scale factor $a(t)$ as a function of time. It maintains flatness with a dark energy density Ω_Λ as well as an ordinary matter component, whose density falls off as R^{-3} as the universe expands. The total density Ω is set to 1 for a flat universe. The usual fractional densities are: Ω_γ for photons and neutrinos, Ω_b for baryons, Ω_Λ for dark energy and Ω_m for the sum of baryonic and dark matter. We will also allow a classically nonsensical $M \sim R$ evolving mass component Ω_R , which we employ as a means to obtain a flat geometry without any ordinary matter on large scales.

The FRW metric for a flat, homogeneous spacetime on the largest scales is given by

$$ds^2 = -c^2 dt^2 + a(t)^2 (dr^2 + r^2 d\Omega^2), \quad (286)$$

where the variable t denotes the cosmological passage of time and $a(t)$ is the scale factor. Define the t dependent Hubble parameter by $H \equiv \dot{a}/a$. One usually sets $a(t_0) = 1$ at the present time.

The basic equations governing standard cosmology [200] can either be derived from this metric, or from Newtonian mechanics. Including a space-

time curvature constant k , we have

$$\dot{a}^2 = -k + \frac{\lambda}{a} + \frac{1}{3}\Lambda R^2, \quad (287)$$

where λ is a constant, and Λ is the cosmological constant. At $k = \lambda = 0$, and with $\Lambda > 0$, one obtains the de Sitter solution,

$$a(t) = \exp(ct\sqrt{3\Lambda^{-1}}). \quad (288)$$

For this solution, the Hubble parameter H is the constant $c\sqrt{3\Lambda^{-1}}$. We consider an FRW density parameter ρ , as in

$$H^2 = \frac{8\pi G}{3}\rho, \quad (289)$$

where G is Newton's constant. For de Sitter space, ρ is essentially the inverse of the cosmological constant, meaning that it must remain constant in time.

The second classical equation for the density is the fluid equation, which assumes a locally reversible expansion,

$$\dot{\rho} + 3H\left(\rho + \frac{p}{c^2}\right) = 0 \quad (290)$$

for a pressure p . Whether a reversible $dS = 0$ expansion is an acceptable assumption for cosmic time is a debatable point. Anyway, here it merely specifies the hypothetical nature of pressure for various matter components. Using general relativity, the fluid equation follows from local energy conservation, which is classically beyond question. However, the existence of a thermodynamic arrow of time suggests taking at least two copies of FRW spacetime, as in the dS/AdS pairing.

In Friedmann's equation (289) we need to consider different density functions, for the different components of mass energy. The usual choices are the first three items on the list

1. non relativistic matter: $\rho \sim a^{-3}$, $a(t) \sim t^{2/3}$
2. radiation: $\rho \sim a^{-4}$, $a(t) \sim t^{1/2}$
3. cosmological: constant ρ , $\rho c^2 = -p$
4. evolving mass: $\rho \sim a^{-2}$, $a(t) \sim t$.

Ordinary matter was used in [192] to derive $\Omega_b = 1 - 3/\pi$, as follows. The critical density is

$$\rho = \frac{1}{6\pi G t^2}. \quad (291)$$

This is compared to an initial density $\rho_0 = M/V$ prior to baryonic matter creation, based on the universal mass M and the toric volume $V = 2\pi^2 a^3$.

We have $\rho_0 = (2\pi^2 G t^2)^{-1}$. The ratio ρ/ρ_0 gives $3/\pi$ for the dark sector density, in good agreement with WMAP. Note that $a(t) \sim t^{1/3}$ leads to a similar result.

In the fourth component, since $M \sim a$, the density inside a volume a^3 goes like a^{-2} . That is, $M \sim t$ again. Here the Hubble parameter goes like t^{-1} . This contrasts with the standard flat geometry, in which $a(t) \sim t^{2/3}$ contributes a scaling of $2/3$ to H . Note also that with $M \sim t$, the density behaves like a surface density. Although seemingly odd, this case is worth considering. Using (287), it leads to a very strong constraint on the cosmic time,

$$\Lambda t^3 - 3t + 3\lambda = 0. \quad (292)$$

This is a cubic with at most three distinct solutions for t , unless Λ is a function of time. Classically this is ridiculous, but phenomenologically we are quite free to step outside GR.

The equation of state parameter w is defined by $p = w\rho c^2$. For evolving mass, we then have $w = -1/3$. This contrasts with $w = 0$ for an ordinary matter component, and $w = -1$ in the case of a constant energy density. Note that before the observation of an apparent universal acceleration, and the requirement for Ω_Λ in the Λ CDM model, it was generally accepted that any type of matter should obey the strong energy condition: $\rho c^2 + 3p \geq 0$. The clear violation of this principle is itself a serious problem for the Λ CDM picture.

Under the evolving mass scenario, the age of the universe is measured directly by the inverse Hubble constant H_0^{-1} . When $a(t)$ is a power law, ρ always goes as t^{-2} , but the different matter components have distinct constant coefficients. In particular, we now have

$$\rho_R = \frac{3}{8\pi G t^2} \quad \rho_\gamma = \frac{3}{32\pi G t^2} = \frac{\rho_R}{4}. \quad (293)$$

In this scenario, when there is no standard matter component, the Hubble parameter takes the form

$$H = H_0 \sqrt{\Omega_\Lambda + \Omega_R(1+z)^2 + \Omega_\gamma(1+z)^4}, \quad (294)$$

where z is the spectral redshift and H_0 the present Hubble constant. When there is no Ω_Λ component, and we neglect radiation, this Hubble law reduces to $H = H_0(1+z)$. Up to numerical factors, this is just the temperature law $T = T_0(1+z)$ for the CMB. This form of Hubble evolution corresponds to the behaviour of a particle detector near the event horizon in de Sitter space [201].

For a relativistic, ideal gas at temperature T , $\rho \sim T^4$. When this applies to ρ_γ , then $a \sim T^{-1}$. In this case, the evolving mass must satisfy $M \sim T^{-1}$. This is just the behaviour of a black hole mass with respect to the

temperature of its Hawking radiation [202]. The Hawking law

$$\frac{8\pi GkT}{\hbar c^3} = \frac{1}{M}, \quad (295)$$

with Boltzmann's constant k and Planck's constant \hbar , is a strong motivation for relating rest mass to temperature. We now say that *all* mass is created by the quantum gravitational vacuum through pair creation in Hawking radiation. Either evolving mass or Riofrio's pair production [192] result in a $M \sim t$ law [192], indicating the $T \sim t^{-1}$ relation.

Combining (295) with (285) we infer a temperature dependence for the critical acceleration a_0 . Observationally, a_0 is indeed of the order cH_0 . For the critical acceleration $a_0 = 1.2 \times 10^{-10} \text{ ms}^{-2}$ the Hubble constant would be $4 \times 10^{-19} \text{ s}^{-1}$. Using the law $t \sim 1/H$ for evolving mass, this corresponds to a universal age of around 80 billion years. This is exactly four times the value of 20 billion years obtained for the evolving mass FRW metric.¹ Using this estimate, Newton's formula $M = a_0 r^2 / G$ for the universal mass gives $M \sim 10^{53} \text{ kg}$. This is equivalent to around 10^{12} galaxies, in agreement with observation.

Currently, the CMB data is analysed using the Λ CDM scheme. The recent Planck collaboration results [203] for this model obtain an optimal Ω_Λ of around 0.68. The six parameter model gives a very good fit for high multipoles in the CMB sky, but there is noticeable tension in the low multipole data, as previously predicted using evolving mass arguments [192][193].

Planck's Hubble constant H_0 also differs significantly from astrophysical estimates using the cosmic distance ladder. Models with further standard parameters do not greatly improve the fit. According to the Planck analysis, there are roughly three species of relativistic neutrino in the early universe, in agreement with the Standard Model of particle physics. It is reasonable to conclude that something like Λ CDM is a good empirical model for small angular scales, but that quantum cosmology will be required to obtain a clear understanding of the data.

The Hubble constant discrepancy might be alleviated by the evolving mass hypothesis. Observe that one can only underestimate H_0 for low z if the terms in (294) are low powers in $(1+z)$. In particular, for a true Hubble constant of $H_{0,A}$, the respective cosmologies give the ratio

$$\frac{H_0^2}{H_{0,A}^2} = \frac{\Omega_{\Lambda'} + (1 - \Omega_{\Lambda'})(1+z)^2}{\Omega_\Lambda + (1 - \Omega_\Lambda)(1+z)^3} \quad (296)$$

where we assume that Ω_Λ is roughly the same as $\Omega_{\Lambda'}$ and radiation is neglected.

¹A radiation epoch could lower this high age to something around 15 billion years, a little above the accepted Λ CDM value.

11.3 Observational Notes

Dark matter was not predicted by theorists, but observed first in the anomalous rotation of galaxies by Zwicky [204] in the 1930s. It has since become clear that basically all galaxies show a flat rotation curve at high radius [205], apparently in line with the hypothesis that extra mass lies in the galactic halo [206]. However, no dark mass has been detected in our own environment, except possibly in the form of black holes.

The dark energy component was hypothesised after the observation of dimming for distant supernovae, which act as standard candles for distance measurement [207][208]. It is now usually attributed to the cosmological constant term in Einstein's equations, responsible for Ω_Λ . However, the supernovae data are fitted without dark energy in Riofrio's scheme [192].

Another cornerstone of cosmology is the evolution of structure formation [209]. Traditionally, this is analysed with a strictly classical image of colliding galaxies and star formation in an a priori spacetime. Large scale structure is associated to the so called initial perturbations, seen in the cosmic microwave background radiation. In this framework, it takes billions of years from the Big Bang for complex spiral galaxies to form, and yet they are observed at high redshift.

Direct detection dark matter experiments have now ruled out many WIMP scenarios [210][211]. There remains the oscillation results of DAMA [212] and other experiments, which observe a variation in event rates with a phase that is correlated with Earth's relative galactic motion, rather than solar system motion. This might be explained with traditional mirror matter [190], but it now seems more likely that neutrino gravity is directly responsible for the keV scale nuclear recoils, via full neutrino absorption. In non local gravity, scattering is not a viable interaction between the dark and baryonic worlds.

Recently, Alexander obtained an interesting evolving equation of state w from a neutrino condensate ansatz [213]. An evolving w has the advantage of alleviating the evolving mass constraints, and is feasible provided that there is a long epoch of roughly constant w . This again suggests that neutrinos are closely related to the cosmic microwave background radiation [170][143].

11.4 Mirror Neutrinos and the CMB

Our cosmic time is measured by the temperature of the cosmic microwave background. Thus the increasing universal mass M is inversely proportional to a temperature T . This is a statement of Hawking's law, wherein a black hole mass M is inversely proportional to a Hawking temperature. This finite universal mass is now characterised by the rest mass of a mirror neutrino.

In chapter 7, the $\pm\pi/12$ Koide phase conjugation gave both a neutrino mass triplet and a mirror neutrino one. The central mirror state corresponds

precisely to the current CMB temperature $T_0 = 2.725$ K, equal to 0.00117 eV under Wien's law [170][143]. There are two other mirror mass states in the triplet, one at a future cosmic time and one in the distant past. That is, the mirror neutrinos mark out the minimal three time points required to describe the mass quantum number. All other Koide states correspond to temperatures that are hotter than the present CMB.

In principle, mirror neutrinos are inaccessible as fermions, but they are observed in the form of CMB photons. The CMB is a perfect black body distribution. The probabilistic state variables that determine Planck's bosonic law can always be interpolated to a fermionic regime by expanding the available set of states. In this way, the underlying statistical information is more fundamental than the boson fermion distinction, and fermions are just those particles with a sufficiently sparse state distribution. With the positions of mirror neutrinos strongly limited in our spacetime, only the bosonic states are observed.

The mirror neutrino hypothesis cures the so called horizon problem: CMB photons can arrive from anywhere within our universe, their temperature given precisely by the fermion rest mass. In the expanding picture, the temperature varies as $T = T_0(1 + z)$, and this law is well tested by astrophysical observation over a wide range of redshifts. This forces us to identify the Koide neutrino scale with the evolution of z , so that at least the mirror neutrinos are extremely heavy in our early universe, perhaps representing primordial black holes. However, when balancing expansion with contraction, so that the early universe is dominated by mirror mass, we can attribute spectral redshifts to the lower atomic masses at early times. That is, the temperature is considered constant. We do not need to imagine that spacetime stretches photons!

One usually uses the current constraints on Δm^2 values [160] for neutrinos to obtain the Koide phase $\phi_\nu = 2/9 + \pi/12$ as an empirical result. With the CMB hypothesis, however, we can fix the Koide scale using the present value of T_0 , and the exact arithmetical phases then predict precise masses for the ordinary neutrinos. This assumes that both neutrino triplets have the same mass scale of $\sum m_i = 0.06$ eV. Recalling Planck's derivation of the black body law, we have Wien's law

$$mc^2 = 4.965114 \cdot kT, \quad (297)$$

where the dimensionless constant comes from differentiating Planck's law as a function of wavelength and solving the transcendental equation $\exp(-x) = 1 - x/5$. The central mirror neutrino rest mass of 0.001166 eV agrees with the temperature T_0 , using accurate values for c and k . At this temperature, the standard neutrino rest masses take the values

$$\nu_1 = 0.0506 \text{ eV} \quad \nu_2 = 3.824 \times 10^{-4} \text{ eV} \quad \nu_3 = 0.0089 \text{ eV} \quad (298)$$

at $\mu_\nu = 0.009973$ eV. This gives the range

$$\Delta m_{\text{atm}}^2 = 2.478 \pm 0.002 \times 10^{-3} \text{ eV}^2 \quad \Delta m_{\text{sol}}^2 = 7.885 \pm 0.002 \times 10^{-5} \text{ eV}^2, \quad (299)$$

in rough agreement with current constraints. Recently, the MINOS experiment [160] has narrowed the range of Δm_{atm}^2 to very near $2.48 \times 10^{-3} \text{ eV}^2$. These oscillation results are open to clarification by future experiments, as is the question of a correlation between the CMB sky and anomalies in oscillation results.

11.5 Discussion

The holographic principle [214] places quantum information at horizons, which are typically one dimension lower than the spacetime they inhabit. In the non local cosmos, the distinction between interiors, exteriors and boundaries is complicated. Branched ribbon surfaces in dimension 3 can fill space without defining an interior or exterior. Their edge boundaries define an interior for the ribbon surface, but in braids on a cylinder, for instance, these interiors can be swapped for the exterior. Since these subtleties are tied to the space generating properties of matter, they cannot be ignored in attempts to draw the classical picture.

A mathematical foundation for non local cosmology must include the physical dualities of M theory. Duality arises firstly in the thickness of a ribbon strand, which introduces string diagrams to twistor physics. It is also the distinction between 0 and 1 for qubits. But these symmetric categorical structures require no braid crossing information. Physical duality, on the other hand, is a statement about energy scales. Whether a representative for distances or couplings, the only natural unit is that of energy. And it is when we take three dualities together that we begin to create dimension 3. These are the S, T and U dualities of M theory.

When $M \sim t$ is a cosmological law, cosmic time also displays dualities. We interchange our thermodynamic arrow of time for the one in the time reversed mirror world. Our long lived baryonic matter has sharp mass states, while short lived mirror states cannot be localised in our spacetime. Once both energy and time display duality, quantum mechanical uncertainty becomes the balance between dualities. Locally we see three spatial directions and one time direction, and the spatial directions correspond to the three dualities of M theory, but in twistor theory one can also consider three time directions.

An observer selects two natural clocks. The *cosmological* clock estimates the elapsed time since the observer's imaginary Big Bang, with a measurement of the CMB temperature T . The *laboratory* clock uses the local dynamics of a few massive objects to define an orbital tick. Each clock covers the full range of energy scales. Our cosmological clock measures time from

the timeless $M \rightarrow 0$ limit to the present, and possibly into the future. The laboratory clock keeps time for both low and high energy local experiments. Duality is not enough to account for the present, because it is triality that marks the past, present and future.

Implicitly, dual clocks occur already in black hole thermodynamics. In black hole complementarity [215][216], quantum information resides in both the particle states and in the local environment. For particles, one expects $m \sim T$, while Hawking radiation suggests an inverse T dependence. As Riofrio [192] notes, the $M \sim t$ rule is just Kepler's law for the universal mass M ,

$$GM = tc^3, \quad (300)$$

where t marks this passage of cosmic time. We might attribute the missing factor of π in Kepler's law to the difference between the cosmic radial time and the time defined by an orbital clock. This factor of π now differentiates the rational and non rational Koide phases for neutrinos.

When the observer's past universal mass M is interpreted as a black hole mass, then the Hawking temperature T , as a measure of cosmic time, appears in a modified form of (300),

$$\frac{1}{t} = \frac{8\pi kT}{\hbar} = \frac{c^3}{GM}, \quad (301)$$

with k Boltzmann's constant. At the CMB temperature, we then have $8\pi T \simeq 0.03$ eV, which is close to the tripled neutrino mass scale $3\mu_\nu$. This is the natural neutrino scale, since $3\mu_l$ is the proton mass. This is an additional coincidence between neutrinos and the CMB. The neutrino masses, in their thermal bath, define a limit for black hole evaporation.

A Category Theory

Categories are the foundation of relational mathematics. A *set* is a zero dimensional category, because everything in a set is an element, pictured as a pointlike object. A one dimensional category \mathbf{C} , or 1-category for short, has both zero dimensional *objects* and *arrows* between objects. If the head of an arrow meets the tail of another, they compose to form another arrow in \mathbf{C} . That is, an arrow f has *source* and *target* objects. Instead of equations relating elements of sets, categories relate arrows using commutative diagrams. For example, the square

$$\begin{array}{ccc} A & \xrightarrow{h} & B \\ f \downarrow & & \downarrow k \\ C & \xrightarrow{g} & D \end{array} \quad (302)$$

says that $gf = kh$, if it commutes, and A, B, C and D are source and target objects. Diagrams of any shape are possible. A 1-category \mathbf{C} is associative on arrows, so that $h(fg) = (hf)g$, and it always contains at least identity arrows $1_A : A \rightarrow A$ for every object A , that represent the object at the arrow level.

Since categories replace sets, we need maps between categories. A *functor* $F : \mathbf{C} \rightarrow \mathbf{D}$ sends objects A to objects $F(A)$ and arrows f, g to arrows such that $F(gf) = F(g) \circ F(f)$. This is the covariant rule. A contravariant functor satisfies $F(gf) = F(f) \circ F(g)$. We can also say that a contravariant functor is a covariant functor $\mathbf{C}^{\text{op}} \rightarrow \mathbf{D}$ from the *opposite category* \mathbf{C}^{op} , which is the same as \mathbf{C} with all arrows formally reversed.

Example A.1 $\mathbf{Vect}_{\mathbb{F}}$ is the category of vector spaces over the field \mathbb{F} . Every vector space V is an object in the category. The arrows are the linear maps between vector spaces.

Example A.2 \mathbf{Set} is the category of all sets, with functions as arrows. The empty set is an *initial* object, since it is included in any other set in only one way. A one element set is terminal. All one element sets A and B are equivalent, because the unique maps $!$ in the squares

$$\begin{array}{ccc} A & \xrightarrow{!} & B \\ 1_A \downarrow & & \downarrow 1_B \\ A & \xleftarrow{!} & B \end{array} \quad \begin{array}{ccc} B & \xrightarrow{!} & A \\ 1_B \downarrow & & \downarrow 1_A \\ B & \xleftarrow{!} & A \end{array}$$

ensure that they commute. The two element set $\Omega = \{0, 1\}$ in \mathbf{Set} gives it the structure of a *topos* [8]. In particular, Ω allows characteristic functions $A \rightarrow \Omega$, which send some elements of A to 1 and others to 0, thereby defining a subset of A using an arrow.

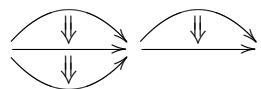
Note that two objects A and B are *equivalent* when there exist two arrows $f : A \rightarrow B$ and $g : B \rightarrow A$ such that both $fg = 1_B$ and $gf = 1_A$ hold. Arrows can be equal, but distinct objects can only be equivalent.

Why categories? Many familiar structures are already categories. For instance, a group is a 1-category with only one object. Arrow composition is the group operation and every arrow has an inverse. The axioms of a category have automatically given the group its identity, and a group homomorphism is nothing but a functor between two groups. A *groupoid* is any category in which every 1-arrow is invertible. This extends groups to categories with multiple objects.

So the category **Grp** of all groups is really a *category of categories*, containing all one object categories with inverses, and all functors between them. Now comes the interesting part. Categories of categories have another level of structure, namely 2-arrows between the 1-arrows. Let F and G be functors with the same source and target categories. These 2-arrows are *natural transformations* $\eta : F \Rightarrow G$, given by a collection of arrows η_A in the target category, such that for every f in the source category the squares

$$\begin{array}{ccc} F(A) & \xrightarrow{F(f)} & F(B) \\ \eta_A \downarrow & & \downarrow \eta_B \\ G(A) & \xrightarrow{G(f)} & G(B) \end{array} \quad (303)$$

all commute. The 2-arrows are two dimensional pieces of a diagram, filling an area between two 1-arrows. Such 2-arrows may compose both horizontally and vertically, as in a globule



$$(304)$$

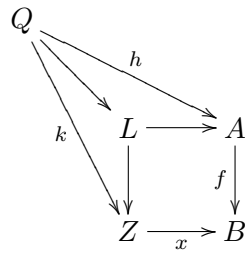
piece of a 2-category. Natural transformations were originally introduced for cohomology, since cohomology is a functor from a category of spaces to the algebraic category that gives the invariants. Now a 2-category is a collection of objects, 1-arrows, 2-arrows and identities, such that every equation on 1-arrows can be weakened by 2-arrows between the paths.

There is no reason to stop at dimension 2. Categories are naturally defined for any ordinal dimension n . Things get much more interesting in dimension 3, with the appearance of *tricategories* [9][65]. Up to dimension 2, all categories are essentially *strict*. This means that every bicategory is equivalent, at the level of 2-arrows, to an ordinary 2-category [66]. Bicategories will be discussed below.

A.1 Limits and Universality

As for sets, categories can have natural closure conditions, such as the existence of certain limiting objects [187][37]. A *limit* in a 1-category is defined over any diagram D in the category. It is an object L , with an arrow from L to each object in D , such that given any other object Q in the category, and arrows from Q down to D , there is always a unique arrow $Q \rightarrow L$ so that the whole diagram commutes.

Thus the *pullback* limit of a pair of arrows, f and x , if it exists, is a unique square in a set of diagrams

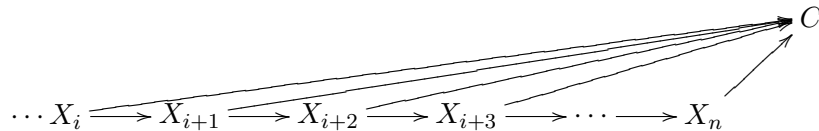


given by the following condition. For any pair of arrows h and k , there is a unique arrow $Q \rightarrow A$ such that the diagram commutes. Note that an arrow $L \rightarrow B$ also exists by composition.

Example A.3 Pullbacks characterise the behaviour of the differential form functor in the de Rham cohomology of manifolds. Given $f : \mathbb{R}^m \rightarrow \mathbb{R}^n$, there is a pullback f^* from 0-forms on \mathbb{R}^n to forms on \mathbb{R}^m , defined by $f^*(w) = wf$ [35]. The pullback f^* extends to all differential forms.

Similarly, a *colimit* is an object C , along with arrows from D to C , so that for any other object Q and arrows from D to Q , there is a unique $C \rightarrow Q$ making the diagram commute.

Example A.4 The direct limit of a sequence $\{X_i\}$.



Limits are instances of *universality*: the idea that a single object essentially contains the structure of a larger piece of the category. In particular, *motives* are supposed to be a universal cohomology theory in some category of functors. However, the 1-categorical limit concept is too limiting, not least because a category of functors is already a 2-category! We need higher dimensional limit concepts. On that note, observe that there is a unique

limit only in the sense that all limits must be equivalent. Let us look then at equivalences between categories.

Let $1_{\mathbf{C}}$ and $1_{\mathbf{D}}$ be the identity functors on two categories \mathbf{C} and \mathbf{D} . There is an *adjunction* $F \dashv G$, for functors $F : \mathbf{C} \rightarrow \mathbf{D}$ and $G : \mathbf{D} \rightarrow \mathbf{C}$, if there exist natural transformations $\eta : 1_{\mathbf{C}} \Rightarrow GF \Rightarrow$ and $\epsilon : FG \Rightarrow 1_{\mathbf{D}}$. It helps to draw out the arrows. In simple cases, F and G may compose to the identity itself.

Example A.5 F and G are both the same functor $\vee : \mathbf{Vect} \rightarrow \mathbf{Vect}$, namely the duality functor on a category of vector spaces. There is a natural equivalence $(V^\vee)^\vee \simeq V$ between the double dual of a vector space and itself.

Example A.6 Let K be a finite extension of the number field \mathbb{F} defined by the splitting property. For example, \mathbb{C} splits quadratics over the reals. Let S be some subset of K . The field $\mathbb{F}(S)$ closes S under the field operations. This gives a lattice of extensions between \mathbb{F} and K . To any such nice extension K/\mathbb{F} we consider the group of automorphisms of K which fix the elements of \mathbb{F} . This is the *Galois group* $\text{Gal}(K/\mathbb{F})$. For example, $\text{Gal}(\mathbb{C}/\mathbb{R})$ is the two element group, containing the trivial automorphism and complex conjugation. The subgroups of $\text{Gal}(K/\mathbb{F})$ are in one to one correspondence with the extensions between \mathbb{F} and K . This is an adjunction between the lattice of extensions and the subgroups.

A *monad* is an endofunctor $T : \mathbf{C} \rightarrow \mathbf{C}$ with natural transformations $\mu : T^2 \Rightarrow T$ and $\eta : 1_{\mathbf{C}} \Rightarrow T$ such that $\mu(T\eta) = \mu(\eta T)$ and

$$\begin{array}{ccc} T^3 & \xrightarrow{T\mu} & T^2 \\ \mu T \downarrow & & \downarrow \mu \\ T^2 & \xrightarrow{\mu} & T \end{array} \quad (305)$$

Note how this axiom resembles associativity for a binary product. Every adjunction defines a monad with $T = GF$. Monads define T -algebras, which are pairs (X, h) for X an object in \mathbf{C} and $h : TX \rightarrow X$ the algebra structure, so that $Th \cdot h = \mu_X h$ [66].

A *multicategory* allows arrows with multiple sources.



On such tree diagrams the arrow orientations are often omitted, and it is understood that processes occur downwards on the tree. An *operad* is a

multicategory on one object [217]. That is, for every $n \in \mathbb{N}$ there is an object $X(n)$, including an identity 1 in $X(1)$, so that the collection has a composition

$$X(n) \times X(k_1) \times X(k_2) \times \cdots \times X(k_n) \rightarrow X(k_1 + k_2 + \cdots + k_n) \quad (307)$$

given by an associative $x \cdot (x_1, x_2, \dots, x_n)$ such that $x \cdot (1, 1, \dots, 1) = x$. This last identity rule extends n leaves on a tree by a secondary leaf. Similarly, the generic composition uses the tree $X(n)$ as a base for grafting the other components. Special sequences of polytopes of real dimension n form operads, and these are an important theme of the book. Operads are often defined with a permutation group action, but the weaker definition is more suited to noncommutative geometries.

A.2 Monoidal, Braided and Tortile Categories

In category theory, *coherence* of a structure means providing a finite set of axioms that are sufficient to force commuting diagrams wherever necessary. The primary example is Mac Lane's proof of coherence for monoidal categories [66], which are examples of bicategories.

A *bicategory* \mathbf{B} is the general form for two dimensional axioms, as in categories of 1-categories, functors and natural transformations. Thus it contains 0-arrows, 1-arrows and 2-arrows, along with weak identities 1_A for all 0-arrows A , and a left identity λ_f and right identity ρ_f for all 1-arrows f . The 1-arrows and 2-arrows from A to B form a 1-category $\mathbf{B}(A, B)$. The identities satisfy

$$\begin{array}{ccc} & A & \\ & \swarrow f & \downarrow f \\ B & \xrightarrow{1_B} & B \end{array} \quad \begin{array}{ccc} & A & \\ & \swarrow 1_A & \downarrow f \\ A & \xrightarrow{f} & B \end{array} \quad (308)$$

It turns out that any bicategory is weakly equivalent to a 2-category, where all the λ_f and ρ_f are strictly identities. For objects A, B and C , there is a functor

$$\otimes : \mathbf{B}(B, C) \times \mathbf{B}(A, B) \rightarrow \mathbf{B}(A, C) \quad (309)$$

and associator 2-arrows $\psi_{fgh} : f \otimes (g \otimes h) \rightarrow (f \otimes g) \otimes h$ such that

$$\psi_{fg1}(f \otimes \rho_g) = \rho_{f \otimes g} \quad \psi_{1fg}\lambda_{f \otimes g} = \lambda_f \otimes g \quad \psi_{f1g}(f \otimes \lambda_g) = \rho_f \otimes g. \quad (310)$$

The *interchange law* for 2-arrows ψ, ϕ, ψ' and ϕ' states that $(\psi \otimes \phi)(\psi' \otimes \phi') = \psi\psi' \otimes \phi\phi'$, interchanging the two inner arrows. That is, the composition of

collection of arrows $\gamma_{AB} : A \otimes B \rightarrow B \otimes A$ such that the hexagon

$$\begin{array}{ccc}
 & A \otimes (B \otimes C) \xrightarrow{\gamma_{A(BC)}} (B \otimes C) \otimes A & \\
 \psi \nearrow & & \searrow \psi \\
 (A \otimes B) \otimes C & & B \otimes (C \otimes A) \\
 \searrow \gamma_{AB} \otimes 1_C & & \nearrow 1_B \otimes \gamma_{AC} \\
 & (B \otimes A) \otimes C \xrightarrow[\psi]{} B \otimes (A \otimes C) &
 \end{array} \tag{314}$$

and another hexagon with inverse associators ψ^{-1} , commute [49]. Braids are actually just that: knotted string diagrams. String diagrams are geometrically dual to the usual arrow diagrams, because a string stands for an object A , while a node on a string is an arrow. Thus a braid arrow γ_{AB} is a braid crossing

$$\begin{array}{cc}
 A & B \\
 & \diagdown \quad \diagup \\
 & \text{X} \\
 & \diagup \quad \diagdown \\
 B & A
 \end{array} \tag{315}$$

and γ_{BA} is the opposite crossing, taking B over A . A *tortile* braided monoidal category \mathbf{C} has a dual object A^* for every object A in \mathbf{C} , and twist maps $\theta_A : A \rightarrow A$ that twist the object pairs, now represented by ribbons. As explained in [135], ribbons are necessary to make a braiding compatible with the existence of duals. We can assume that A^* is a *right dual*, since in tortile categories this automatically makes it a left dual also. From the adjunction $A \dashv A^*$ there is a unit and counit

$$\eta_A : I \rightarrow A^* \otimes A \quad \epsilon_A : A \otimes A^* \rightarrow I \tag{316}$$

where I is the monoidal identity. These are drawn as arcs

$$\begin{array}{cc}
 \frown & \smile \\
 \eta & \epsilon
 \end{array} \tag{317}$$

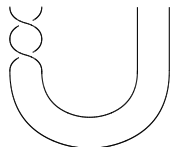
so that I is an empty diagram. The arrow $(1_A \otimes \eta_A)(\epsilon_A \otimes 1_A)$ should be the identity 1_A , as should $(\eta_A \otimes 1_{A^*})(1_{A^*} \otimes \epsilon_A)$. For every A , the twist θ_A satisfies the compatibility condition

$$\begin{array}{ccc}
 A \otimes B & \xrightarrow{\gamma_{AB}} & B \otimes A \\
 \theta_{A \otimes B} \downarrow & & \downarrow \theta_B \otimes \theta_A \\
 A \otimes B & \xleftarrow{\gamma_{BA}} & B \otimes A
 \end{array} \tag{318}$$

In string diagrams, this just says that the braiding of ribbons does not interfere with the ribbon twists. Tortile categories introduce both ribbons

and arc segments. Usually only full twists are permitted on ribbons, so that ribbon diagrams are doubled braids, with a unique underlying braid [135].

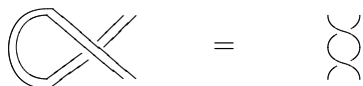
The definition of tortile tensor category includes the condition $\theta_{A^*} = (\theta_A)^*$. That is, if a ribbon A is twisted, the twisting on the dual object A^* must define the dual of the twisted A . This is because A and A^* are connected by a ribbon arc, and the twists can propagate along a ribbon


(319)

to the other side. A single braid crossing within a ribbon diagram, thought of as a double knot, adds ± 1 to the *writhe* of the braid. Recall that a braid's writhe w is the sum $j - k$, where j is the number of over crossings and k the number of under crossings. This quantity is important in the definition of knot and link invariants. For a double knot, the *twist number* is given by

$$\theta_K = \frac{1}{2}(j - k) \tag{320}$$

This is always an integer, since two ribbons create four braid crossings when they cross. The total number of twists n and w together give an equivalence between double knots, because $w/4+n$ is conserved under ambient isotopy in \mathbb{R}^3 . We can see this by observing that a writhe component on the underlying knot is turned into a full twist.


(321)

A *ribbon functor* is a functor between ribbon categories that preserves the essential structures. In particular, modular functors are used to model quantum computation [176].

In general, the categorical dimension is not restricted. Even the \otimes structure will be broken by physical considerations in dimension 3. It is too laborious to write out the rules for categories with more than two or three levels of arrow, so one must focus on basic geometric elements, namely trees, braids and ribbons.

A.3 Tricategories and Higher Dimensions

In 1995, Gordon, Power and Street found a coherence theorem for tricategories [9]. It shows that not every tricategory is triequivalent to a strict 3-category, with simple identity arrows. Although the definition is essentially unique, its precise form is still a mystery. One axiom is given by the

A_4 polytope, which generalises the Mac Lane pentagon to dimension 3. Instead of strict natural transformations, the category provides 2-arrows to fill in the squares. A convenient concept is the *pseudonatural transformation*, where the square filling arrows are assumed to be invertible. For example, given objects A, B, C and D and bicategories of arrows $T(A, B)$ between them, there is a pseudonatural transformation

$$\begin{array}{ccc}
 T(A, B) \times T(D, A) \times T(C, D) & \xrightarrow{\otimes \times 1} & T(D, B) \times T(C, D) \\
 \downarrow 1 \times \otimes & \Downarrow & \downarrow \otimes \\
 T(A, B) \times T(C, A) & \xrightarrow{\otimes} & T(C, B)
 \end{array} \tag{322}$$

on the \otimes composition functor. Since a tricategory has three dimensional arrows, diagrams of composed pseudonatural transformations are subject to *modification* 3-arrows. For example, the cube

$$\begin{array}{ccccc}
 & & T^4 & & \\
 & 11\otimes & \downarrow & \otimes 11 & \\
 T^3 & & & & T^3 \\
 & \otimes 1 & \downarrow 1\otimes & & \\
 & & T^2 & & \\
 1\otimes & & \downarrow 1\otimes 1 & & \otimes 1 \\
 & & T^3 & & \\
 & 1\otimes & \downarrow \otimes & \otimes 1 & \\
 T^2 & & & & T^2 \\
 & \otimes & \downarrow \otimes & & \\
 & & T & &
 \end{array} \tag{323}$$

is filled with a modification. A weak identity axiom is given by the (left) triangular prism 3-arrow

$$\begin{array}{ccccc}
 & & T^3 & & \\
 & \nearrow & \downarrow & \searrow & \\
 T^2 & \xrightarrow{\quad} & T^2 & \xrightarrow{\quad} & T^2 \\
 \downarrow & \nearrow & & \searrow & \downarrow \\
 T & \xrightarrow{\quad} & & & T
 \end{array} \tag{324}$$

with faces filled by 2-arrows. Although tricategories are not all strict, they are all triequivalent to a special tricategory **Gray** of 2-categories with a Gray tensor product [218].

A.4 The Crans-Gray Tensor Product

Distributivity is at least a three dimensional structure, because the two binary operations lift the axioms to dimension three. Thus categorical operations, like knots, guide us towards a three dimensional picture for the integers \mathbb{Z} . In [12], Crans noted that a natural tensor product for higher dimensional categories was not dimension preserving. In particular, the horizontal composition of two 2-arrows gives a 3-arrow, just as branched 2-surfaces contain three dimensional knots. A generic category of dimension ≥ 2 has such dimension raising compositions, so that beyond dimension 3, space is automatically generated from the algebra of surfaces.

To begin with, the Gray tensor product breaks interchange. Put two objects U in \mathbf{C}_1 and V in \mathbf{C}_2 into a formal pair (U, V) . Let g_i be a 1-arrow in \mathbf{C}_1 and f_j a 1-arrow in \mathbf{C}_2 . Then the formal pairs $(g_i, 1_{V_i})$ and $(1_{U_j}, f_j)$ satisfy $(g_1, 1_V)(g_2, 1_V) = (g_1 g_2, 1_V)$ and $(1_U, f_1)(1_U, f_2) = (1_U, f_1 f_2)$. Now for each pair f and g there is only an isomorphism $\sigma_{fg} : (1_U, f)(g, 1_V) \Rightarrow (g, 1_V)(1_U, f)$. That is, the diagram

$$\begin{array}{ccccc}
 U & \longrightarrow & V & \longrightarrow & W \\
 \downarrow 1 & & \Downarrow \alpha & \downarrow 1 & \Downarrow 1 & \downarrow 1 \\
 U & \longrightarrow & V & \longrightarrow & W \\
 \downarrow 1 & & \Downarrow 1 & \downarrow 1 & \Downarrow \beta & \downarrow 1 \\
 U & \longrightarrow & V & \longrightarrow & W
 \end{array} \tag{325}$$

may be different, via an isomorphism, from the diagram

$$\begin{array}{ccccc}
 U & \longrightarrow & V & \longrightarrow & W \\
 \downarrow 1 & & \Downarrow 1 & \downarrow 1 & \Downarrow \beta & \downarrow 1 \\
 U & \longrightarrow & V & \longrightarrow & W \\
 \downarrow 1 & & \Downarrow \alpha & \downarrow 1 & \Downarrow 1 & \downarrow 1 \\
 U & \longrightarrow & V & \longrightarrow & W
 \end{array} \tag{326}$$

When the crucial four 2-arrows sit on the faces of a tetrahedron, σ_{fg} is the resulting internal 3-arrow. When the Mac Lane pentagon is broken on the six faces of a parity cube, one can fill the cube with a cyclically invariant 3-arrow. In general, the composition of a p -arrow and a q -arrow results in a $(p + q - 1)$ -arrow.

B Braid Groups

To Maxwell, electromagnetism was a theory of circular vortices in the aether [133]. Later in the 19th century, Lord Kelvin proposed knotted vortices as atoms for space. Knots had already been studied by great mathematicians like Gauss, who first defined a linking number invariant. The first true knot invariant is due to Alexander, in the late 19th century. Little progress was made on finding invariants that were good at distinguishing knots until 1983, and the appearance of the Jones polynomial [85]. This invariant displayed quantum mechanical structure, and was followed shortly thereafter by a two variable analogue, the Homflypt polynomial [88].

The link invariants are defined in chapter 5. Here we introduce the basic knot groups. The braid group B_n on n string pieces has $n - 1$ generators τ_i , for $i = 1, 2, \dots, n - 1$. Each generator represents a crossing that goes over from the top left, and the inverse τ_i^{-1} is the braid that goes under instead. A braid $b \in B_n$ is a word in these generators. Since B_1 has only one string, which cannot knot itself, B_1 is the trivial group 1. With only one over (+1) and one under (-1) crossing, B_2 is isomorphic to the integers \mathbb{Z} . For B_3 , we have

$$\begin{array}{ccc} \tau_1 & & \tau_2 \\ \begin{array}{c} \diagup \quad \diagdown \\ \diagdown \quad \diagup \end{array} & | & | \begin{array}{c} \diagdown \quad \diagup \\ \diagup \quad \diagdown \end{array} \end{array} \quad (327)$$

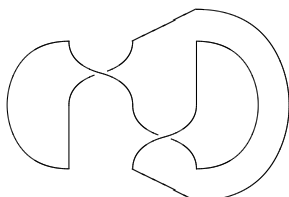
The group multiplication is given by adjoining a braid to the bottom of another braid, so that $\tau_1\tau_2 \neq \tau_2\tau_1$. For all n , the group relations are

$$\begin{aligned} \tau_i\tau_{i+1}\tau_i &= \tau_{i+1}\tau_i\tau_{i+1} & \text{for } i = 1, 2, \dots, n - 2 \\ \tau_i\tau_j &= \tau_j\tau_i & \text{for } |i - j| \geq 2 \end{aligned} \quad (328)$$

The group B_n embeds in any B_m for $m \geq n$ with the selection of n strands within B_m . We then talk of B_∞ , which all includes all possible braid diagrams. A braid $b \in B_n$ has an underlying permutation in S_n , given by the connection of endpoints at the top of the diagram to points at the bottom, so that $\sigma \in S_n$ forgets the crossing information. For S_n one adds the symmetry relation

$$(\sigma_i)^2 = 1 \quad (329)$$

for all i . A braid diagram is a projection onto the plane of a diagram in three dimensions. A *link* is formed by tracing the braid diagram, by joining each top point to the same point at the bottom of the diagram, as in the B_3 example



$$(330)$$

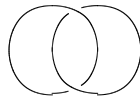
which is unknotted in three dimensional space. The trace can form links with any number of loops. By convention, a *knot* is a one loop link. Markov [219] showed that a traced braid is equivalent to a link, in the sense that two distinct braid representations of the same link in three dimensions are simply related to each other by conjugation.

A link is deformed into an equivalent link by *ambient isotopy* in dimension 3. If we are not allowed to flip knot pieces around in the third dimension, braids are only equivalent up to *planar isotopy*. The Reidemeister moves [220]

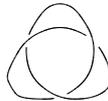
$$\begin{array}{ccc}
 \begin{array}{c} \text{---} \\ | \\ \text{---} \end{array} \text{---} \bigcirc \text{---} & = & \begin{array}{c} | \\ | \end{array} \\
 R1 & & \\
 \begin{array}{c} \text{---} \\ | \\ \text{---} \end{array} \text{---} \bigcirc \text{---} & = & \begin{array}{c} \text{---} \\ | \\ \text{---} \end{array} \text{---} \bigcirc \text{---} \\
 R2 & & \\
 \begin{array}{c} \text{---} \\ | \\ \text{---} \end{array} \text{---} \bigcirc \text{---} & = & \begin{array}{c} \text{---} \\ | \\ \text{---} \end{array} \text{---} \bigcirc \text{---} \\
 R3 & &
 \end{array} \tag{331}$$

define the equivalence relation between different braid diagrams.

Example B.1 The Hopf link

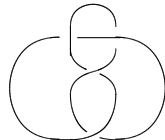


Example B.2 The trefoil knot



is *chiral*, being distinct from its mirror image.

Example B.3 The unique four crossing knot is the achiral figure eight knot.



This is the first true B_3 knot, since the trefoil is represented by τ_1^3 in B_2 . It has the braid word $\tau_1\tau_2^{-1}\tau_1\tau_2^{-1}$.

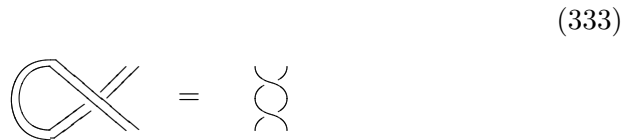
The unknot, trefoil and figure eight knots are all *prime* with respect to the connected sum [221]. This operation $K_1 \sharp K_2$ cuts a small piece from the two knots K_1 and K_2 , and rejoins the knots at these points.



That is, it flips two vertical arcs to two horizontal arcs. This is a fundamental binary operation on planar string diagrams. The collection of all knots along with connected sum form a monoid, with unit the unknot. There is no canonical listing of prime knots by ordinals from the monoid \mathbb{N} , but braids are ordered in a complex way [180].

Let j be the number of positive crossings in $b \in B_n$ and k the number of negative crossings. The *writhe* w of a link is the integer $w = j - k$. For the trefoil, $w = +3$, whereas the mirror trefoil with reversed crossings has $w = -3$.

Braid strands may be replaced by ribbon segments, allowing ribbon twists. A ribbon diagram with only full twists still has an underlying link picture [135], obtained by shrinking all ribbons to strands. As in appendix A, in a ribbon category a writhe component on the underlying link is turned into a full ribbon twist



Observe that a braid crossing, as represented on the plane, consists of three string pieces: one over string and two under strings. The crossing can be used to represent a product $a \circ b = c$ of the two under string segments. Algebras of such link arcs are known as *racks* or *quandles* [222]. The Reidemeister moves define their rules. Finally, there is a category \mathbf{Br} of all B_n braid groups, with objects $n \in \mathbb{N}$ and arrow sets B_n for $n \rightarrow n$.

C Elementary Algebra

An algebra is usually a vector space over a field equipped with a binary, associative product $m(a, b)$ on the vectors. The field provides additive and multiplicative inverses. In constructive number theory, we are more interested in diagram algebras. An element of the algebra is a formal sum of basis diagrams, and the coefficients belong to a restricted set, not necessarily forming a field.

Products are defined using composition of diagrams, and more than one product may exist. For example, braid diagrams are composed vertically as braids, and also horizontally by concatenation into a larger braid group. If this is done with no coefficients, we imagine a coefficient field with one element. Given any diagram representation for the permutation group S_d on d objects, a group algebra of formal combinations of $\sigma \in S_d$ is a diagram algebra. Such algebras are often also *bialgebras* or *Hopf algebras*, which are defined below.

In order to be useful, diagrams should have an interpretation in category theory. A one dimensional category consists of directed edges, or 1-arrows, but we often start with undirected edge diagrams that encode parts of the categorical structure. With rooted trees, for instance, there is an obvious choice of direction: downwards from the branches to the root.

A *monoid* is a set with a binary composition $a \circ b$, which is to say a 1-category with only one object, the source and target of all 1-arrows. Arrow composition is literally the gluing of arrows

$$\rightarrow \rightarrow \rightarrow \dots \quad (334)$$

in a diagram segment of the category, so that the composed path itself defines an arrow in the category. To begin with, binary operations are associative. This says that the two paths in

$$\begin{array}{ccc} a, b, c & \xrightarrow{m \times 1_c} & a \circ b, c \\ 1_a \times m \downarrow & & \downarrow \\ a, b \circ c & \longrightarrow & a \circ b \circ c \end{array} \quad (335)$$

commute, where m is the binary composition map $\mathcal{C} \times \mathcal{C} \rightarrow \mathcal{C}$ on the category \mathcal{C} . Weakened associativity comes from higher dimensional arrows, starting with a 2-arrow filling this square. We should always think of $\psi_{abc} : ((a \circ b) \circ c) \Rightarrow (a \circ (b \circ c))$ as being at least two dimensional. Usually, bracketed objects such as $((a \circ b) \circ c)$ are represented by tree diagrams, and ψ_{abc} is a transformation of trees. As the number of product structures grows, so does the categorical dimension.

C.1 Bialgebras and Hopf Algebras

Multiplication takes two objects a and b and returns $m(a, b)$ at the root of the tree.

$$\begin{array}{c}
 a \quad b \\
 \diagdown \quad \diagup \\
 \quad \quad \quad \\
 m(a, b)
 \end{array} \tag{336}$$

Dually, comultiplication sends one object to two.

$$\begin{array}{c}
 a \\
 \diagup \quad \diagdown \\
 \Delta(a) = x \otimes y
 \end{array} \tag{337}$$

One usually speaks of the whole algebra as an object in a category, and unpackages the structure from there. An ordinary algebra object A in a category \mathbf{C} comes with a multiplication map $m : A \otimes A \rightarrow A$, such that associativity

$$\begin{array}{ccc}
 A \otimes A \otimes A & \xrightarrow{m \otimes 1_A} & A \otimes A \\
 \downarrow 1_A \otimes m & & \downarrow m \\
 A \otimes A & \xrightarrow{m} & A
 \end{array} \tag{338}$$

holds. Often there is also an object I in \mathbf{C} , such that there exists a unit arrow $\eta : I \rightarrow A$ with the property that $\eta \cdot m : I \otimes A \rightarrow A$ is essentially 1_A , and similarly for $m \cdot \eta$. Comultiplication obeys coassociativity

$$\begin{array}{ccc}
 A \otimes A \otimes A & \xleftarrow{\Delta \otimes 1_A} & A \otimes A \\
 \uparrow 1_A \times \Delta & & \uparrow \Delta \\
 A \otimes A & \xleftarrow{\Delta} & A
 \end{array} \tag{339}$$

and comes with a counit $\epsilon : A \rightarrow I$. In a category of vector spaces, the object I is the base field. A *bialgebra* object A has both a multiplication m and comultiplication Δ , such that

$$\begin{array}{ccc}
 A \otimes A & \xrightarrow{m} & A \\
 \downarrow \Delta \times \Delta & & \downarrow \Delta \\
 A \otimes A \otimes A & \xrightarrow{m \times m} & A \otimes A
 \end{array} \tag{340}$$

Example C.1 A *Frobenius algebra* is a bialgebra object A with (m, Δ) and natural transformations $\eta : I \rightarrow A$ and $\epsilon : A \rightarrow I$, such that (m, η) forms a commutative monoid and (Δ, ϵ) forms a cocommutative monoid, and

$$(1 \otimes m)(\Delta \otimes 1) = \Delta m$$

A Hopf algebra H is a bialgebra, along with an arrow $S : H \rightarrow H$ called the *antipode* [223]. The antipode satisfies

$$\begin{array}{ccc}
 & H \otimes H & \xrightarrow{S \otimes 1_H} & H \otimes H & \\
 \Delta \nearrow & & & & \searrow m \\
 H & & & & H \\
 \epsilon \searrow & & & & \nearrow \eta \\
 & I & & &
 \end{array} \tag{341}$$

Example C.2 Given a field \mathbb{F} , the *group algebra* $\mathbb{F}C_3$ over the three element group $C_3 = \{(0), (1), (2)\}$ is the set of all formal linear combinations $v = a_0(0) + a_1(1) + a_2(2)$. Here C_3 is represented using mod 3 arithmetic. The field operations extend to products and scalar multiples for elements v and w . On $\mathbb{F}C_3$ there is a coproduct $\Delta(g) = g \otimes g$ and counit given by the constant 1 on C_3 . The antipode is defined by $S(g) = g^{-1}$ when g is in C_3 , and it extends by linearity. Following the diagram above, $(S \otimes 1)$ gets $g \cdot g^{-1}$, which multiplies to (0) in C_3 . Any group defines such a Hopf algebra.

Example C.3 [224] The renormalisation algebra is closely related to the Hopf algebra of rooted trees. A basis object is a rooted tree. The algebra H is a vector space over all such trees, using coefficients in \mathbb{Q} . The product is generated by the disjoint union of two trees, producing a *forest*. The empty tree e gives the unit, sending $\lambda \in \mathbb{Q}$ to λ , and the counit maps every non empty tree to 0, and e to 1. The comultiplication uses tree cuts, that split a tree into two pieces by removing one edge. An admissible cut set for a tree T is such that any path from a leaf down strikes at most one cut. For example,

$$\Delta(\text{tree}) = \text{tree} \otimes 1 + 1 \otimes \text{tree} + 2 \bullet \otimes \text{tree} + \bullet \bullet \otimes \bullet$$

where lone tree nodes are included. The single left and right cuts give the factor of 2. In general, Δ satisfies $\Delta(e) = e \otimes e$ and

$$\Delta(T) = T \otimes e + (I \otimes R_+) \Delta(R_-(T))$$

where R_+ is the operation of grafting two trees by attaching them to two extra base edges, and R_- is the inverse operation that removes the two root edges. The antipode for the same example is

$$S(\text{tree}) = \text{tree} + 2 \bullet \text{tree} - \bullet \bullet$$

The minus signs pick up the even number of cuts. Each cut, including the empty cut, can be represented by a box around the smaller piece so that the diagrams correspond to nested boxes. This generalises nested boxes around single path trees, which are the same as sequences of bracketings. In renormalisation, subdivergences are subgraphs of Feynman graphs, defined by the partition boxes.

C.2 Shuffles and Lattice Paths

The Hopf algebra $\mathbb{Z}S_d$ for the permutation group S_d is of particular interest to us. A permutation σ in S_d , which acts on the sequence $(123 \cdots d)$, is a *shuffle* [71] if

1. $\sigma^{-1}(1) < \sigma^{-1}(2) < \cdots < \sigma^{-1}(m)$
2. $\sigma^{-1}(m+1) < \sigma^{-1}(m+2) < \cdots < \sigma^{-1}(m+n)$

for $m+n = d$. That is, the sequence σ^{-1} breaks up into two strictly ordered pieces, one of length m and one of length n . Altogether, there are

$$\binom{m+n}{m}$$

(m, n) shuffles. Note that when $m = n$, this is similar to the Catalan number C_n . For fixed m and n , the sum over all shuffles of type (m, n) in S_d is an element h_{mn} in the Hopf algebra $\mathbb{Z}S_d$. For example, for $m = 2$ and $n = 1$, $h_{21} = (123) + (132) + (312)$.

Let s_{mn} be a permutation in S_d that lets $(s_1 \cdots s_m) \in S_m$ act on the first m objects and $(s_{m+1} \cdots s_d) \in S_n$ act on the rest. Then the group algebra product $h_{mn}s_{mn}$ is thought of as a product of the partial permutations in S_m and S_n . For example, $h_{21} \cdot (213) = (213) + (231) + (321)$. This is a graded product for the infinite direct sum $\oplus \mathbb{Z}S_d$ over all d .

The (m, n) shuffles are in one to one correspondence with paths on a cubical planar lattice [73]. The point $(0, 0)$ is the source and (m, n) the target, defining a block of mn lattice squares. The variables $\sigma^{-1}(k)$ within the shuffle are used to label horizontal steps if $k \leq m$, and vertical steps for $k > m$. Shuffles are often written as words in two letter types, as in $X_1Y_1X_2Y_2$ for $m = n = 2$.

C.3 Matrix Tensor Algebra and Distributivity

In a typical category, the \otimes product is the side by side concatenation of diagrams. In matrices, the tensor product increases the dimension. These two facts agree only if the number of braid strands somehow indicates the algebraic dimension. Since matrices are fundamental constructive arrays, we would like to view \otimes products in terms of the dimension raising properties of matrix products.

For two $n \times n$ matrices J and K , the *Schur product* S is given entry by entry as $S_{ij} \equiv J_{ij} \cdot K_{ij}$. This is a kind of word concatenation, as in the example

$$\begin{pmatrix} X\bar{X} & X\bar{Y} \\ Y\bar{X} & Y\bar{Y} \end{pmatrix} = \begin{pmatrix} X & X \\ Y & Y \end{pmatrix} \circ_S \begin{pmatrix} \bar{X} & \bar{Y} \\ \bar{X} & \bar{Y} \end{pmatrix} \quad (342)$$

for a dual pair of vectors (resulting in a Jordan algebra projection). For a general square matrix, if the entries are projections $(P_{ij})^2 = P_{ij}$, then the

Schur product clearly defines a matrix projection. The Schur product is a submatrix of the tensor product. Recall that the tensor product $A \otimes B$ of two 2×2 matrices A and B , usually with commutative entries, is defined as the 4×4 matrix

$$\begin{pmatrix} A_{11}B_{11} & A_{11}B_{12} & A_{12}B_{11} & A_{12}B_{12} \\ A_{11}B_{21} & A_{11}B_{22} & A_{12}B_{21} & A_{12}B_{22} \\ A_{21}B_{11} & A_{21}B_{12} & A_{22}B_{11} & A_{22}B_{12} \\ A_{21}B_{21} & A_{21}B_{22} & A_{22}B_{21} & A_{22}B_{22} \end{pmatrix}. \quad (343)$$

This generalises to any pair of square matrices.

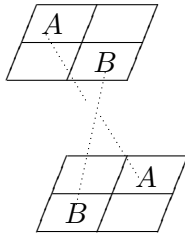
Consider a category with the three composition types \cdot , \otimes and \oplus . Let \cdot give horizontal composition and \otimes vertical. As with matrices, the category also contains objects I_n for $n \in \mathbb{N}$ that act as identities for the \cdot product. Then the object $(A \otimes I_m)(I_n \otimes B)$

$$\begin{array}{|c|c|} \hline A & I_n \\ \hline I_m & B \\ \hline \end{array}$$

usually specifies a unique object $A \otimes B$ by the bicategory interchange law. Similarly for $B \otimes A$. What about \oplus in the third dimension? Using matrix dimensions as a guide, observe that $(A \oplus B) \otimes (B \oplus A)$ should distribute to

$$(A \otimes B) \oplus (B \otimes A) \oplus (A \otimes A) \oplus (B \otimes B),$$

whereas $(A \otimes B) \oplus (B \otimes A)$ would be $(A \oplus B) \otimes (B \oplus A)$ if basic interchange held. That is, basic distributivity is breaking interchange in the third dimension



by creating the AA and BB terms. Distributivity is fundamentally a three dimensional structure. In a higher category, a *distributive law* is a natural transformation $\lambda : \otimes \oplus \rightarrow \oplus \otimes$ between two operation endofunctors, such that $\lambda \cdot (\otimes)_R = (\otimes)_L$ and

$$\begin{array}{ccc} & \oplus \otimes \oplus & \longrightarrow & \otimes \oplus \oplus & \\ & \nearrow & & \searrow & \\ \oplus \oplus \otimes & & & & \otimes \oplus \\ & \searrow & & \nearrow & \\ & \oplus \otimes & \xrightarrow{\lambda} & & \end{array} \quad (344)$$

commutes, along with similar laws for a source $\oplus \otimes \otimes$. Observe that λ resembles a braiding.

Already with \otimes and \oplus we have a string of adjunctions for distributivity [230][187]. If **Mon** is the category of monoids with \otimes and **Ab** is a category of additive groups with \oplus , then there is a category **Ring** that inherits the two operations through the four adjunctions in the square

$$\begin{array}{ccc}
 & \mathbf{Ring}_{\otimes\oplus} & \\
 \nearrow & & \nwarrow \\
 \mathbf{Mon}_{\otimes} & & \mathbf{Ab}_{\oplus} \\
 \nwarrow & & \nearrow \\
 & \mathbf{Set} &
 \end{array}
 \tag{345}$$

and a distributive law gives an arrow inside the square, which is nominally a 3-arrow filling a tetrahedron. As a string diagram, the usual distributive axiom is naturally symmetric, allowing strings to slide past one another through a vertex. A braiding gives a choice between the usual law and a broken distributivity, with the axiom taking the form

$$\tag{346}$$

Note that only a pair of opposite crossings on the left will block the string slide. Each crossing is a braiding $\lambda_{\otimes\oplus}$ on the two functor objects. Since our physical spaces emerge from such particle braid structures, broken distributivity for arithmetic is a fundamental feature of real quantum processes.

The Jacobi rule (147) for Lie algebras is often expressed as a triplet of tree diagrams, each with three leaves. The (s, t, u) Mandelstam variables act on these three particles (234), once the leg (1) is fixed at the root. The three particles are permuted using the 1-circulants in S_3 . A braided version of the Jacobi rule replaces the S_3 permutations by a braid triplet in B_3 . Such a braided Jacobi rule is now a form of broken distributivity, introducing a distinction between left and right handedness.

D The Division Algebras

Dixon's book [1] describes the symmetries of the Standard Model particles using algebras over the four division algebras: the reals \mathbb{R} , complex numbers \mathbb{C} , quaternions \mathbb{H} and octonions \mathbb{O} . Almost all the essential elements of the SM Lagrangian come from transformations involving two dimensional spaces over $\mathbb{C} \otimes \mathbb{H} \otimes \mathbb{O}$, as briefly outlined below.

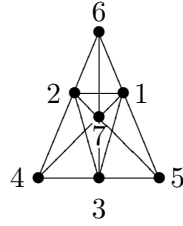
The gauge group $SU(2)$ is associated as usual to the quaternion units q_j , for $j = 1, 2, 3$. A $U(1)$ arises from the appearance of the complex unit i . Finally, the color $SU(3)$ appears as a subgroup of G_2 , the automorphisms of \mathbb{O} . The nonassociative octonions \mathbb{O} [225] are real linear combinations

$$a_0 + a_1 e_1 + a_2 e_2 + a_3 e_3 + a_4 e_4 + a_5 e_5 + a_6 e_6 + a_7 e_7 \quad (347)$$

of 1 and the seven other units e_i . The products $e_i e_j$ satisfy [226]

$$e_i e_j = -\delta_{ij} + \epsilon_{ijk} e_k$$

where the antisymmetric ϵ_{ijk} has norm 1 on the seven lines of a Fano plane



and ϵ_{ijk} is chosen to be positively oriented on the cycles

$$615 \quad 534 \quad 426 \quad 673 \quad 471 \quad 572 \quad 213.$$

The projective Fano plane is the seven lines in the cube \mathbb{F}_2^3 . The line orientation is recovered from an oriented cube with faces of type

$$\begin{array}{c} \rightarrow \\ \downarrow \uparrow \\ \rightarrow \end{array} \quad (348)$$

and the central e_7 placed at the source and target. It uses the labeling

$$\begin{array}{ccccc} & & 2 & \leftarrow & 7 \\ & \swarrow & \uparrow & & \swarrow \\ 6 & \longrightarrow & & \longrightarrow & 1 \\ & \downarrow & & \downarrow & \\ & & 4 & \leftarrow & 3 \\ & \swarrow & & \swarrow & \\ 7 & \longleftarrow & & \longleftarrow & 5 \end{array} \quad (349)$$

By definition, the conjugate of $a \in \mathbb{O}$ is $a_0 - \sum_1^7 a_i e_i$. The *norm* of $a \in \mathbb{O}$ is $N(a) \equiv a\bar{a}$, satisfying $N(ab) = N(a)N(b)$.

The bioctonions $\mathbb{C} \otimes \mathbb{O}$ are the complexification of \mathbb{O} defined using complex coefficients [227], such that the complex unit i commutes with all e_i . It has an octonion conjugate and a complex conjugate $\bar{a}_0 + \sum \bar{a}_i e_i$. The bioctonions contain the split octonion algebra [226]. This may be defined using the 2×2 rational matrices

$$A \equiv \begin{pmatrix} x & a \\ b & y \end{pmatrix} \quad \bar{A} \equiv \begin{pmatrix} y & -a \\ -b & x \end{pmatrix} \quad (350)$$

with x, y in \mathbb{Q} and a, b in a three dimensional space. The matrix product is

$$\begin{pmatrix} x_1 & a_1 \\ b_1 & y_1 \end{pmatrix} \begin{pmatrix} x_2 & a_2 \\ b_2 & y_2 \end{pmatrix} = \begin{pmatrix} x_1 x_2 + a_1 \cdot b_2 & x_1 a_2 + y_2 a_1 - b_1 \times b_2 \\ x_2 b_1 + y_1 b_2 + a_1 \times a_2 & y_1 y_2 + b_1 \cdot a_2 \end{pmatrix}. \quad (351)$$

The 8 basis elements of the split algebra are then given by

$$\begin{aligned} u_0 &= \begin{pmatrix} 0 & 0 \\ 0 & 1 \end{pmatrix} & \bar{u}_0 &= \begin{pmatrix} 1 & 0 \\ 0 & 0 \end{pmatrix} \\ u_i &= \begin{pmatrix} 0 & 0 \\ e_i & 0 \end{pmatrix} & \bar{u}_i &= \begin{pmatrix} 0 & -e_i \\ 0 & 0 \end{pmatrix} \end{aligned} \quad (352)$$

for e_i the three octonion units e_1, e_2 and e_3 . Then $A\bar{A} = \bar{A}A$ equals $(xy - a \cdot b)I_2$. There are two copies of the split octonions in $\mathbb{C} \otimes \mathbb{O}$, with the second one given by iu_j .

Observe that the unit multiplication tables for \mathbb{C}, \mathbb{H} and \mathbb{O} may be defined using addition for the finite fields with 2, 4 and 8 elements. For \mathbb{C} , this table is the 2×2 Fourier matrix F_2 , with the negative entry specifying the rule $i \cdot i = -1$. The 4×4 and 8×8 matrices are also Hadamard [1].

D.0.1 Particles from $\mathbb{R} \otimes \mathbb{C} \otimes \mathbb{H} \otimes \mathbb{O}$

In [1], one defines particle states as follows. To each flat space or spacetime, of type $\mathbb{R}^{0,n}$ or $\mathbb{R}^{1,n}$ respectively, there is associated a Clifford algebra of dimension 2^n or 2^{n+1} generated by the relations

$$\gamma_\alpha \gamma_\beta + \gamma_\beta \gamma_\alpha = 2\eta_{\alpha\beta} I$$

with respect to the metric $\eta_{\alpha\beta}$. We are especially interested in the space $\mathbb{R}^{0,9}$, because its algebra is

$$T_L \equiv \mathbb{R}_L \otimes \mathbb{C}_L \otimes \mathbb{H}_L \otimes \mathbb{O}_L \quad (353)$$

associated to a left adjoint action. The \mathbb{O}_L action is actually associative, but the algebra $T_L(2)$ of 2×2 matrices over T_L is not.

\mathbb{C}_L is the Clifford algebra for $\mathbb{R}^{0,1}$, \mathbb{H}_L the algebra for $\mathbb{R}^{0,2}$ and \mathbb{O}_L the algebra for $\mathbb{R}^{0,6}$. We choose the quaternion basis $q_j = -i\sigma_j$, for Pauli matrices σ_j . Then for $\mathbb{R}^{3,0}$ we obtain the Pauli spinor algebra $\mathbb{C}_L \otimes \mathbb{H}_L$. Its basis is $\{1, iq_j, q_j, i\}$. Let $x = \sum x^j q_j \in \mathbb{H}$, so that that x^j are real. Define

$$\lambda_{\pm} = \frac{1}{2}(1 \pm ix) \quad (354)$$

satisfying $\lambda_+ + \lambda_- = 1$ and $x\lambda_{\pm} = \mp i\lambda_{\pm}$. Any element A of the Pauli algebra decomposes into a pair of spinors $A\lambda_+ + A\lambda_-$.

Now T_L is the tensor product of the Pauli algebra with \mathbb{O}_L . Thus \mathbb{O}_L is responsible for the six extra internal dimensions. For $T = \mathbb{C} \otimes \mathbb{H} \otimes \mathbb{O}$ we first define

$$\rho_{\pm} = \frac{1}{2}(1 \pm ie_7) \quad (355)$$

so that $\rho_+\rho_- = 0$. Then for quaternions x and y , define

$$\begin{aligned} \Delta_0 &\equiv \frac{1}{4}(1 + ix)(1 + ie_7) = \lambda_+\rho_+ \\ \Delta_1 &\equiv \frac{1}{4}(1 - ix)(1 + ie_7) = \lambda_-\rho_+ \\ \Delta_2 &\equiv \frac{1}{4}(1 + iy)(1 - ie_7) = \lambda_+\rho_- \\ \Delta_3 &\equiv \frac{1}{4}(1 - iy)(1 - ie_7) = \lambda_-\rho_- \end{aligned} \quad (356)$$

The Δ_i resolve the identity, $\sum \Delta_i = 1$. Let $X = X^0 + \sum_1^7 X^a ie_a$ be an element of $\mathbb{C} \otimes \mathbb{O}$. The ρ_{\pm} act on the left on \mathbb{O} so that $\rho_+(X^0 - iX^7)$ is a singlet and

$$\rho_+[(X^1 - iX^5)e_1 + (X^2 - iX^3)e_2 + (X^4 - iX^6)e_4]$$

a triplet under $SU(3)$. For the full algebra $\mathbb{C} \otimes \mathbb{O}$, one also obtains the conjugate representations. This is color for the leptons and quarks and their antiparticles. Finally, tensoring with \mathbb{H} one obtains four copies of the representations, giving the $SU(2)$ doublets for the leptons and quarks.

To obtain the correct $U(1)$ symmetries and to understand spontaneous symmetry breaking, we require another set of operators, but everything works in the algebra T . A state Ψ is then an object in T^2 that behaves nicely with respect to the total $U(2) \times U(3)$ symmetry of the actions that define an inner product for T . That is, it is a combination of the Δ_m . The spacetime Clifford algebra for $\mathbb{R}^{1,9}$ is the 2×2 matrices over T_L , isomorphic to $\mathbb{C}(32)$. The (left handed) particles are now given in the table.

$\bar{\nu}$	$\rho_+\Psi\rho_+\lambda_+$	ν	$\rho_-\Psi\rho_-\lambda_-$
e^-	$\rho_+\Psi\rho_+\lambda_-$	e^+	$\rho_-\Psi\rho_-\lambda_+$
u	$\rho_+\Psi\rho_-\lambda_+$	\bar{u}	$\rho_-\Psi\rho_+\lambda_-$
d	$\rho_+\Psi\rho_-\lambda_-$	\bar{d}	$\rho_-\Psi\rho_+\lambda_+$

The sign subscripts clearly label the eight vertices of a parity cube for three qubits.

D.0.2 Jordan Algebras

Although not necessary for the particle description above, in many applications of the octonions in physics one studies the matrix Jordan algebras. A (formally real) Jordan algebra \mathcal{J}_n [225] has a nonassociative product $a \circ b$ such that

$$a \circ (b \circ a^2) = (a \circ b) \circ a^2. \quad (357)$$

We are interested in the 3×3 matrix Jordan algebras over \mathbb{R} , \mathbb{C} , \mathbb{H} , \mathbb{O} and $\mathbb{C}\mathbb{O}$. These are the 3×3 Hermitian matrices with commutative Jordan product $a \circ b \equiv (ab + ba)/2$.

The 2×2 Hermitian matrices over \mathbb{O} also form a Jordan algebra, and it has projections

$$\begin{pmatrix} X\bar{X} & X\bar{Y} \\ Y\bar{X} & Y\bar{Y} \end{pmatrix} \quad (358)$$

for (X, Y) in \mathbb{O}^2 of norm 1. By definition, the projective line $\mathbb{O}\mathbb{P}^1$ is the set of all 2×2 projections P such that the trace of P equals 1. This agrees with the projective lines $\mathbb{F}\mathbb{P}^1$ over the other fields. The 3×3 algebra over \mathbb{O} gives a Moufang plane $\mathbb{O}\mathbb{P}^2$ [228]. The line $\mathbb{O}\mathbb{P}^1$ is basically the sphere $S^8 \simeq \mathbb{O} \cup \infty$, just as $\mathbb{C}\mathbb{P}^1$ is the sphere S^2 . The matrices in $SL_2(\mathbb{O})$ give the spin group $\text{Spin}(9, 1)$, which is the double cover of the Lorentz group in dimension 9. As above, the group $SL_2(\mathbb{O})$ acts on \mathbb{O}^2 as a left handed spinor representation, just as for the twistor $SL_2(\mathbb{C})$.

The 2×2 algebra over \mathbb{O} appears in the 3×3 algebra under the isomorphism [225]

$$\mathcal{J}_3(\mathbb{O}) \simeq \mathcal{J}_2(\mathbb{O}) \oplus \mathbb{O}^2 \oplus \mathbb{R} \simeq \mathbb{R}^3 \oplus V_8 \oplus S_8^+ \oplus S_8^-.$$

Here V_8 , S_8^+ and S_8^- are the three components of *triality* for the octonion number field. S_8^+ and S_8^- are right and left handed spinor representations. Triality is the trilinear map

$$t : V_8 \times S_8^+ \times S_8^- \rightarrow \mathbb{R} \quad (359)$$

associated to the multiplication structure of the division algebra. Trialities with norms are always specified in terms of spinors, since they give representations of $\text{Spin}(n)$. All three components are just \mathbb{R}^8 as vector spaces. An automorphism of the triality is a triplet (f_1, f_2, f_3) of norm preserving maps such that

$$t(f_1(v_1), f_2(v_2), f_3(v_3)) = t(v_1, v_2, v_3)$$

for all v_i . The automorphisms of \mathbb{O} form the Lie group G_2 , and this is contained in the triality automorphism group $\text{Spin}(8)$. The outer automorphisms of $\text{Spin}(8)$ form the permutation group S_3 , which allows any permutation of the spaces V_8 , S_8^+ and S_8^- .

For the full bioctonion algebra $\mathcal{J}_3(\mathbb{C}\mathbb{O})$ we define a trilinear form by [229]

$$T(a, b, c) \equiv (a, b \circ c) = \frac{1}{2}(a, bc) + \frac{1}{2}(a, cb) \quad (360)$$

where (x, y) is the inner product $\text{tr}(x \circ y)$, and the last step uses ordinary matrix product. The complex 3×3 matrices form a subalgebra of $\mathcal{J}_3(\mathbb{C}\mathbb{O})$. There is also a commutative *Freudenthal product*

$$a \times b \equiv a \circ b - \frac{1}{2}\text{tr}(a)b - \frac{1}{2}\text{tr}(b)a + \frac{1}{2}\text{tr}(a)\text{tr}(b)I_3 - \frac{1}{2}(a, b)I_3 \quad (361)$$

and associated cubic form

$$(a, b, c) \equiv (a, b \times c) = (a \times b, c). \quad (362)$$

Then the determinant of $a \in \mathcal{J}$ is given by $\det(a) = (a, a, a)/3$. It is known as the cubic norm of a .

Let D_{ij} denote the minor determinant at position ij in any $n \times n$ complex matrix D . The cofactor matrix C_{ij} has entries $(-1)^{i+j}D_{ij}$ for $i, j = 1, 2, \dots, n$. The adjugate is the transpose $D^* \equiv C_{ij}^T$. There is then a bilinear form on matrices in $\mathcal{J}_3(\mathbb{C})$ given by [182]

$$\beta(A^*, B) = 3(A, A, B). \quad (363)$$

The *Freudenthal triple system* for $\mathcal{J}(\mathbb{F})$ is the larger algebra

$$\mathbb{F} \oplus \mathbb{F} \oplus \mathcal{J} \oplus \mathcal{J}$$

with elements 2×2 matrices A as in (350), such that $x, y \in \mathbb{F}$ and a and b are \mathcal{J} . For \mathcal{J} the 3×3 complex matrices, the Freudenthal triple is a 20 complex dimensional space. The *quartic form* of the system is

$$q(A) \equiv 2(\beta(a, b) - xy)^2 - 8\beta(a^*, b^*) + 8x \det(a) + 8y \det(b). \quad (364)$$

Under a suitable equivalence relation on the Freudenthal triple system for complex matrices [182], any matrix in the algebra may be transformed into elements with $b = 0$, $y = 0$ and $x = 1$, and a diagonal a in the set

$$\begin{pmatrix} 0 & 0 & 0 \\ 0 & 0 & 0 \\ 0 & 0 & 0 \end{pmatrix} \quad \begin{pmatrix} 1 & 0 & 0 \\ 0 & 0 & 0 \\ 0 & 0 & 0 \end{pmatrix} \quad \begin{pmatrix} 1 & 0 & 0 \\ 0 & 1 & 0 \\ 0 & 0 & 0 \end{pmatrix} \quad \begin{pmatrix} 1 & 0 & 0 \\ 0 & 1 & 0 \\ 0 & 0 & k \end{pmatrix}$$

for $k \in \mathbb{C}$. In this case, the quartic form often reduces to $8\det(a)$, which takes values in $\{0, 8k\}$.

As above, $SU(3)$ color appears as a subgroup of G_2 . It makes the split octonions u_0 and \bar{u}_0 into singlets and the u_i and \bar{u}_i a triplet and antitriplet [1][226]. Octonion structure is thus crucial to a definition of quark states.

The automorphisms of $\mathcal{J}_3(\mathbb{O})$ are the Lie group F_4 , which is generated by a pair of traceless Hermitian matrices over \mathbb{O} . This is a $52 = 2 \times 26$ dimensional group. It has an $SU(3) \times SU(3)$ flavor color subgroup, associated to the decomposition

$$26 \mapsto (8, 1) \oplus (3, 3) \oplus (\bar{3}, \bar{3}). \quad (365)$$

The 78 dimensional exceptional group E_6 is associated to the matrix group $sl(3, \mathbb{O})$. There is a 27 dimensional representation of the group E_6 , which has decomposition [226]

$$(\bar{3}, 3, 1) \oplus (3, 1, 3) \oplus (1, \bar{3}, \bar{3}) \quad (366)$$

under $SU(3) \times SU(3) \times SU(3)$. The last factor is the color symmetry and the $(\bar{3}, 3)$ part accounts for the leptons. Since we can associate any such matrices to a 3×3 word matrix for two qutrits, the cyclicity of the E_6 decomposition is the symmetry of the triangle simplex.

The last section suggests a future study of 3×3 matrices over the full $\mathbb{C} \otimes \mathbb{H} \otimes \mathbb{O}$ algebra, where $\mathbb{C} \otimes \mathbb{H}$ is the noncommutative coefficient set. The Hermitian objects then live in a 216 real dimensional space, with a $(1, 3)$ spacetime algebra along the diagonal and the three $(1, 9)$ components off diagonal.

References

- [1] G. M. Dixon, *Division Algebras: Octonions, Quaternions, Complex Numbers and the Algebraic Design of Physics* (Kluwer, 1994)
- [2] M. Marcolli, arXiv:0907.0321
- [3] A. Connes and M. Marcolli, *Noncommutative Geometry, Quantum Fields and Motives* (AMS Colloquium Publ., 2007)
- [4] A. Grothendieck, http://en.wikipedia.org/wiki/Alexander_Grothendieck
- [5] R. Street, J. Pure Appl. Alg. **49**, 283335(1987)
- [6] E. H. Spanier, *Algebraic Topology* (McGrawHill, 1966)
- [7] S. Eilenberg and N. Steenrod, *Foundations of Algebraic Topology* (Princeton, 1952)
- [8] I. Moerdijk and S. Mac Lane, *Sheaves in geometry and logic: a first introduction to topos theory* (Springer, 2000)
- [9] R. Gordon, A. J. Power and R. Street, Mem. Amer. Math. Soc. **117**, 558(1995)
- [10] G. Peano, Math. Annalen, **36**, 157160(1890)
- [11] J. W. Cannon and W. P. Thurston, Geom. Top. **11**, 13151355(2007)
- [12] S. E. Crans, Theory Appl. Cat. **5**, 1269(1999), <http://home.tiscali.nl/secrans/papers/tpgc.html>
- [13] E. Witten, Commun. Math. Phys. **121**, 351399(1989)
- [14] A. Hughston and M. Hurd, Proc. Roy. Soc. London **A378**, 141154(1981)
- [15] B. Greene, *The fabric of the cosmos: space, time and the texture of reality* (Random House, 2004)
- [16] H. Reichenbach, *The direction of time* (U. California Press, 1956)
- [17] M. Planck, Annalen der Physik **4**, 553-558(1901)
- [18] L. Borsten, M. J. Duff and P. Levay, arXiv:1206.3166v1
- [19] L. Borsten, D. Dahanayake, M. J. Duff, H. Ebrahim and W. Rubens, Phys. Rev. A **80**, 032326 (2009)
- [20] P. Levay, arXiv:quantph/0403060v1
- [21] F. Cachazo, L. Mason and D. Skinner, arXiv:1207.4712v1
- [22] T. Adamo and L. Mason, arXiv:1207.3602v1
- [23] A. Hodges, arXiv:1204.1930v1
- [24] J. Fuchs, I. Runkel and C. Schweigert, Contemp. Math. **431**, 203224 (2007), arXiv:math/0511590
- [25] I. Runkel, J. Fuchs and C. Schweigert, arXiv:math/0602079
- [26] V. F. R. Jones, <http://math.berkeley.edu/~vfr/msri.pdf>

- [27] M. A. Nielsen, and I. L. Chuang, *Quantum Computation and Quantum Information* (Cambridge, 2000)
- [28] R. W. Ghrist, *Topology* **36**, 423448 (1997)
- [29] <http://cornellmath.wordpress.com/2007/07/30/sumdivergentseriesii/>,
- [30] T. Apostol, *Introduction to analytic number theory* (SpringerVerlag, 1976)
- [31] D. E. Knuth, *Surreal numbers* (AddisonWesley, 1974)
- [32] L. C. Biedenharn and M. A. Lohe, *Quantum group symmetry and q-tensor algebras* (World Scientific, 1995)
- [33] J. Du, *Lectures on quantum groups*, UNSW, 1994
- [34] J. Fuchs, *Affine Lie Algebras and Quantum Groups* (Cambridge, 1992)
- [35] R. Bott, and L. W. Tu, *Differential Forms in Algebraic Topology* (SpringerVerlag, 1982)
- [36] F. Hirzebruch, *Topological Methods in Algebraic Geometry* (Springer, 1978)
- [37] C. McLarty, *Elementary categories, elementary toposes* (Oxford, 1992)
- [38] P. Johnstone, *Stone spaces* (Cambridge, 1982)
- [39] C. Piron, *Foundations of Quantum Physics* (W.A. Benjamin, 1976)
- [40] R. Penrose and W. Rindler, *Spinors and spacetime: spinor and twistor methods in spacetime geometry* (Cambridge, 1988)
- [41] R. S. Ward, and R. O. Wells, *Twistor Geometry and Field Theory* (SpringerVerlag, 1990)
- [42] J. Schwinger, *Proc. Nat. Acad. Sci. U.S.A.* **46**, 570 (1960)
- [43] W. K. Wootters and B. D. Fields, *Annal. Phys.* **191**, 363381 (1989)
- [44] J. Lawrence, *Phys. Rev. A* **84**, 022338 (2011)
- [45] M. Combescure, arXiv:0710.5642
- [46] M. Combescure, *J. Math. Phys.* **50**, 032104 (2009)
- [47] A. Knutson and T. Tao, *J. Amer. Math. Soc.* **12**, 10551090 (1999), www.ams.org/notices/200102/feaknutson.pdf
- [48] M. Batanin, *Adv. Math.* **136**, 39103 (1998)
- [49] A. Joyal and R. Street, *Adv. Math.* **102**, 2078 (1993)
- [50] M. Batanin, *Adv. Math.* **211**, 684725 (2007)
- [51] M. Batanin, www.maths.mq.edu.au/street/BatanAustMSMq.pdf
- [52] M. Batanin, arXiv:math.CT/0301221
- [53] A. Joyal and R. Street, *Adv. Math.* **88**, 55113 (1991)
- [54] B. Coecke, arXiv:quantph/0510032v1
- [55] B. Coecke, S. Perdix and E. O. Paquette, arXiv:0808.1029v1
- [56] B. Coecke and D. Pavlovic, arXiv:quantph/0608035

- [57] R. Jozsa, arXiv:quantph/0508124v2
- [58] L. Loomis, *An introduction to abstract harmonic analysis* (D. van Nostrand, 1953)
- [59] N. Koblitz, *Padic numbers, padic analysis and zeta functions* (D. van Nostrand, 1996)
- [60] J. Neukirch, *Algebraic number theory* (SpringerVerlag, 1999)
- [61] D. V. Chistyakov, *Theor. Math. Phys.* **109**, 14951507(1996)
- [62] A. Postnikov, arXiv:math/0507163v1
- [63] D. Tamari, *Bull. Soc. Math. France* **82**, 5396(1954)
- [64] J. D. Stasheff, *Trans. Amer. Math. Soc.* **108**, 275292(1963)
- [65] N. Gurski, <http://users.math.yale.edu/mg622/tricats.pdf>
- [66] S. Mac Lane, *Categories for the working mathematician* (SpringerVerlag, 1998)
- [67] D. BarNatan, in *Proceedings of the Georgia international topology conference* (International Press, 1997), www.math.toronto.edu/drorbn/papers/nat/nat.pdf
- [68] J. Loday, <http://wwwirma.ustrasbg.fr/loday/PAPERS/Dichotomy.pdf>
- [69] L. Solomon, *J. Alg.* **41**, 255268(1976)
- [70] M. D. Atkinson, *Bull. London Math. Soc.* **24**, 545551(1992)
- [71] J. L. Loday and M. Ronco, *Adv. Math.* **139**, 293309(1998)
- [72] Online database of integer sequences, <http://oeis.org>
- [73] I. M. Gelfand, M. M. Kapranov, and A. V. Zelevinsky, *Discriminants, Resultants and Multidimensional Determinants* (Birkhauser, 1994)
- [74] S. L. Devadoss, arXiv:math/0102166v1
- [75] W. Zhao, *J. Pure Appl. Alg.* **186**, 311327(2004)
- [76] L. Foissy, arXiv:1007.1547v3
- [77] R. P. Stanley, *Enumerative Combinatorics* (Cambridge, 1999)
- [78] J. Pitman and R. Stanley, *Disc. Comput. Geom.* **27**, 603634(2002)
- [79] J. L. Loday, arXiv:math/0510380v1
- [80] H. Gangl, A. B. Goncharov and A. Levin, arXiv:math/0508066v1
- [81] J. Birman, *Can. J. Math.* **28**, 264290(1976)
- [82] C. Kassel and V. Turaev, *emphBraid groups* (Springer, 2008)
- [83] V. Turaev, *Sem. Bourbaki* **878**, 389409(1999)
- [84] V. F. R. Jones, *Ann. Math.* **126**, 335388(1987)
- [85] V. F. R. Jones, *Bull. Amer. Math. Soc.* **12**, 103111(1985)

- [86] Knot Atlas, http://katlas.math.toronto.edu/wiki/Main_Page
- [87] L. Kauffman, *Topology* **26**, 395407(1987)
- [88] P. Freyd, D. Yetter, J. Hoste, W. B. R. Lickorish, K. Millett and A. Oceanu, *Bull. Amer. Math. Soc.* **12**, 239246(1985);
<http://mathworld.wolfram.com/HOMFLYPolynomial.html>
- [89] I. Moffatt, arXiv:math/0605466v2
- [90] D. Kreimer, *Adv. Theor. Math. Phys.* **2**, 303(1998), arXiv:qalg/9707029
- [91] S. Bloch, H. Esnault and D. Kreimer, arXiv:math/0510011v1
- [92] D. J. Broadhurst and D. Kreimer, *Phys. Lett. B* **393**, 403412(1997)
- [93] S. O. BilsonThompson, arXiv:hep-ph/0503213v2
- [94] R. Penrose, *Rep. Math. Phys.* **12**, 6576(1977)
- [95] J. C. Baez and J. Huerta, arXiv:1003.3436v2
- [96] N. ArkaniHamed, F. Cachazo, C. Cheung and J. Kaplan, arXiv:0907.5418
- [97] N. ArkaniHamed, J. L. Bourjaily, F. Cachazo, S. CaronHuot, and J. Trnka, arXiv:1008.2958
- [98] N. ArkaniHamed, J. L. Bourjaily, F. Cachazo, and J. Trnka, arXiv:1012.6032v1
- [99] L. Mason and D. Skinner, *JHEP* **12**, 018(2010), arXiv:1009.2225
- [100] S. Mandelstam, *Phys. Rev.* **112**, 1344(1958)
- [101] F. Cachazo, P. Svrcek and E. Witten, *JHEP* **0409**, 6(2004)
arXiv:hep-th/0403047v2
- [102] S. J. Parke and T. R. Taylor, *Phys. Rev. Lett.* **56**, 24592460(1986)
- [103] Z. Bern, G. Chalmers, L. Dixon and D. A. Kosower, *Phys. Rev. Lett.* **72**, 2134(1994) arXiv:hep-th/9312333
- [104] R. Britto, F. Cachazo and B. Feng, *Nucl. Phys. B* **715**, 499522(2005)
arXiv:hep-th/0412308
- [105] R. Britto, F. Cachazo, B. Feng and E. Witten, *Phys. Rev. Lett.* **94**, 181602(2005) arXiv:hep-th/0501052
- [106] A. Hodges, <http://www.twistordiagrams.org.uk>
- [107] N. ArkaniHamed, <http://strings2012.mpp.mpg.de/>
- [108] A. Postnikov, <http://math.mit.edu/~apost/courses/18.318>
- [109] D. Speyer and L. K. Williams, arXiv:math/0312297v1
- [110] Z. Bern, J. J. M. Carrasco and H. Johansson, *Phys. Rev. Lett.* **105**, 061602(2010) arXiv:1004.0476
- [111] Z. Bern and T. Dennen, arXiv:1103.0312v1
- [112] N. ArkaniHamed, <http://pirsa.org/11080047>
- [113] E. Witten, *Commun. Math. Phys.* **252**, 189(2004) arXiv:hep-th/0312171

- [114] M. Spradlin and A. Volovich, Phys. Rev. D **80**, 085022(2009)
arXiv:0909.0229v1
- [115] M. Spradlin and A. Volovich, arXiv:1105.2024v2
- [116] A. B. Goncharov, M. Spradlin, C. Vergu and A. Volovich, Phys. Rev. Lett. **105**, 151605(2010) arXiv:1006.5703v2
- [117] A. Goncharov, Adv. Math. **114**, 197318(1995)
- [118] M. Hoffman, <http://www.usna.edu/Users/math/meh/mult.html>
- [119] J. M. Borwein and W. Zudilin, <http://carma.newcastle.edu.au/MZVs>
- [120] F. C. S. Brown, C. R. Acad. Sci. Paris Ser. I **342**, 949954(2006)
arXiv:math/0606419v1
- [121] M. D. Sheppeard, Ph.D. thesis, Canterbury (2007),
<http://hdl.handle.net/10092/1436>
- [122] L. Lewin, *Polylogarithms and Associated Functions* (North Holland, 1981)
- [123] C. Duhr, H. Gangl and J. R. Rhodes, arXiv:1110.0458v1
- [124] S. Crans, J. Pure Appl. Alg. **101**, 3557(1995)
- [125] A. B. Goncharov, arXiv:math/0202154v2
- [126] M. Mulase, <https://www.math.ucdavis.edu/~mulase/publication.html>
- [127] T. Kohno, Topology **31**, 203230(1992)
- [128] P. Higgs, Phys. Rev. **145**, 11561163(1966)
- [129] ATLAS Collaboration,
<https://twiki.cern.ch/twiki/bin/view/AtlasPublic/HiggsPublicResults>
- [130] CMS Collaboration,
<https://twiki.cern.ch/twiki/bin/view/CMSPublic/PhysicsResultsHIG>
- [131] M. D. Sheppeard, <http://vixra.org/abs/1004.0083>
- [132] A. Dharwadker and V. Khachatryan, arXiv:0912.5189v1
- [133] J. C. Maxwell, Phil. Trans. Roy. Soc. London **155**, 459512 (1865)
- [134] L. Wolfenstein, Nucl. Phys. B **186**, 147152 (1981)
- [135] M. C. Shum, J. Pure Appl. Alg. **93**, 57110 (1994)
- [136] W. Ledermann, *Introduction to group characters* (Cambridge U.P.,1987)
- [137] Y. Koide, Lett. Nuovo Cimento **34**, 201 (1982)
- [138] Y. Koide, Phys Lett. B **120**, 161165 (1983)
- [139] C. A. Brannen (2008), <http://www.brannenworks.com/koidehadrons.pdf>
- [140] A. Rivero, arXiv:1111.7232
- [141] M. D. Sheppeard, <http://vixra.org/abs/1008.0015>
- [142] C. Itzykson and J. B. Zuber, *Quantum Field Theory* (McGrawHill, 1985)
- [143] M. D. Sheppeard and G. Dungworth, <http://vixra.org/abs/1102.0010>

- [144] E. Witten, arXiv:0706.3359v1
- [145] A. Dharwadker, http://www.dharwadker.org/standard_model
- [146] <http://mathworld.wolfram.com/SteinerSystem.html>
- [147] http://en.wikipedia.org/wiki/Binary_Golay_code
- [148] V. F. R. Jones, personal communication, Adelaide, 1995
- [149] C. A. Brannen, <http://brannenworks.com/E8/HopfWeakQNs.pdf>
- [150] M. D. Sheppeard, <http://keamonad.blogspot.com>
- [151] B. Pontecorvo, Sov. Phys. JETP **26**, 984(1968)
- [152] S. Eidelman et al, Phys. Lett. B **592**, 1(2004)
- [153] Z. Maki, M. Nakagawa and S. Sakata, Prog. Theor. Phys. **28**, 870 (1962)
- [154] M. Kobayashi and T. Maskawa, Prog. Theor. Phys. **49**, 652657 (1973)
- [155] C. Jarlskog, Phys. Rev. Lett. **55**, 1039(1985)
- [156] Particle Data Group,
<http://pdg.lbl.gov/2012/reviews/rpp2012revvudvus.pdf>
- [157] P. F. Harrison and D. H. Perkins, Phys. Lett. B **530**, 167 (2002),
arXiv:hep-ph/0202074
- [158] P. F. Harrison and W. G. Scott, Phys. Lett. B **547**, 219 (2002),
arXiv:hep-ph/0210197
- [159] T2K Collaboration, <http://t2kexperiment.org/forphysicists/>
- [160] MINOS Collaboration,
<http://www.numi.fnal.gov/PublicInfo/forscientists.html>
- [161] Daya Bay Collaboration, arXiv:1203.1669v2
- [162] Particle Data Group,
<http://pdg.lbl.gov/2012/reviews/rpp2012revneutrinomixing.pdf>
- [163] P. Gibbs, <http://vixra.org/abs/0907.0002>
- [164] S. Lisi, <http://math.stackexchange.com/q/29819>
- [165] J. Beringer et al, Phys. Rev. D **86**, 010001 (2012)
- [166] PhysicsForums, <http://www.physicsforums.com/showthread.php?t=551549>
- [167] D. Look, <http://home.comcast.net/~davelook/site/>
- [168] M. D. Sheppeard, <http://pseudomonad.blogspot.co.nz/2010/07>
- [169] R. Foot, Int. J. Mod. Phys. D **13**, 21612192(2004), arxiv:quant-ph/0402130
- [170] G. Dungworth, <http://www.galaxyzooforum.org/index.php?topic=277933.0>
- [171] H. Fritzsch and D. Holtzmannspotter Phys. Lett. B **338**, 290294(1994)
- [172] S. Friedl and N. Jackson, arXiv:1102.3742v1
- [173] N. Temperley and E. Lieb, Proc. Roy. Soc. A **322**, 251(1971)

- [174] M. Khovanov, *Duke Math. J.* **101**, 359426(2000), arXiv:math/9908171v2
- [175] D. Bar Natan, arXiv:math.GT/0410495
- [176] M. H. Freedman, M. Larsen and Z. Wang, *Commun. Math. Phys.* **9**, 605622(2000)
- [177] R. Penrose, in *Combinatorial Mathematics and its Applications* (Academic Press, 1971)
- [178] M. Mulase, <http://www.math.ucdavis.edu/~mulase/texfiles/2001moduli.pdf>
- [179] S. Devadoss, *Contemp. Math.* **239**, 91114(1999)
- [180] P. Dehornoy, I. Dynnikov, D. Rolfsen and B. Wiest, *Ordering Braids* (Amer. Math. Soc.,2008)
- [181] D. Richter, <http://homepages.wmich.edu/~drichter/mathieu.htm>
- [182] P. Levay and P. Vrana, *Phys. Rev. A* **78**, 022329(2008), arXiv:0806.4076v1
- [183] V. Coffman, J. Kundu and W. K. Wootters, *Phys. Rev. A* **61**, 052306(2000), arXiv:quantph/9907047v2
- [184] O. Holtz and B. Sturmfels, *J. Alg.* **316**, 634648(2007),
- [185] F. Verstraete, J. Dehaene and B. De Moor, *Phys. Rev. A* **68**, 012103(2003)
- [186] B. Coecke and A. Kissinger, arXiv:1002.2540
- [187] M. Barr and C. Wells, *Toposes, triples and theories* (SpringerVerlag, 1985)
- [188] S. Abramsky and B. Coecke, Proceedings of the 19th IEEE conference on Logic in Computer Science (LiCS'04) (2004), <http://arxiv.org/abs/quantph/0402130>
- [189] F. Hoyle and J. V. Narlikar, *Proc. Roy. Soc. A* **273**, 111 (1963)
- [190] L. B. Okun, arXiv:hep-ph/0606202v2; H. M. Hodges, *Phys. Rev. D* **47**, 456459 (1993)
- [191] R. Foot, arXiv:1305.4316; R. Foot, *Phys. Rev. D* **78**, 043529 (2008), arXiv:0804.4518
- [192] L. Riefro, <http://riofriospacetime.blogspot.com/2006/09/recentgmtc3paper.html>
- [193] R. Penrose, *Cycles of time* (Bodley Head, 2010)
- [194] M. Milgrom, *Astrophys. J.* **270**, 365370 (1983)
- [195] B. Famaey and S. McGaugh, arXiv:1112.3960, <http://www.livingreviews.org/lrr201210>
- [196] H. Goldstein, *Classical Mechanics* (AddisonWesley, 1970)
- [197] R. B. Tully and J. R. Fisher, *Astron. Astrophys.* **54**, 661673(1977)
- [198] B. J. Carr and S. W. Hawking, *Month. Not. Roy. Astro. Soc.* **168**, 399(1974)
- [199] H. Nastase, arXiv:0712.0689v2
- [200] E. A. Lord, *Tensors, relativity and cosmology* (Tata McGraw Hill, 1976)

- [201] P. C. W. Davies, *Int. J. Theor. Phys.* **28**, 10511066(1989)
- [202] S. W. Hawking, *Comm. Math. Phys.* **43**, 199220(1975); J. D. Bekenstein, *Phys. Rev. D* **7**, 23332346(1973)
- [203] The Planck Mission, http://www.nasa.gov/mission_pages/planck/index.html
- [204] F. Zwicky, *Helv. Phys. Acta* **6**, 110127(1933)
- [205] V. C. Rubin and W. K. Ford, *Astrophys. J.* **159**, 379(1970)
- [206] DM Portal, <http://lpsc.in2p3.fr/mayet/dm.php>
- [207] S. Perlmutter et al, *Astrophys. J.* **517**, 565586(1999)
- [208] A. G. Riess et al, *Astronom. J.* **116**, 10091038(1998)
- [209] D. Sijacki, V. Springel and M. G. Haehnelt, arXiv:0905.1689v2
- [210] XENON Collaboration, <http://xenon.astro.columbia.edu/>
- [211] CDMS Collaboration, <http://cdms.physics.ucsb.edu/>
- [212] DAMA Collaboration, <http://people.roma2.infn.it/dama/web/home.html>
- [213] S. Alexander, <http://pirsa.org/12050017>
- [214] G. 'tHooft, arXiv:grqc/9310026v2
- [215] G. 'tHooft, *Nucl. Phys. B* **256**, 727745(1985)
- [216] L. Susskind, L. Thorlacius and J. Uglum, *Phys. Rev. D* **48**, 37433761(1993), arXiv:hep-th/9306069v2
- [217] T. Leinster, *Higher operads, higher categories*, arXiv:math/0305049
- [218] J. W. Gray, *Formal category theory: adjointness for 2categories* (Springer, 1974)
- [219] W. B. R. Lickorish, *An introduction to knot theory* (Springer, 1997)
- [220] K. Reidemeister, *Abh. Math. Sem. Univ. Hamburg* **1**, 2432(1926)
- [221] D. Rolfsen, *Knots and links* (Publish or Perish, 1976)
- [222] R. Fenn and C. Rourke, *J. Knot Th. Ramif.* **1**, 343406(1992)
- [223] E. Abe, *Hopf algebras* (Cambridge, 1980)
- [224] D. Kreimer, *Knots and Feynman Diagrams* (Cambridge, 2000)
- [225] J. Baez, <http://math.ucr.edu/home/baez/octonions>
- [226] S. Catto, arXiv:hep-th/0302079v1
- [227] M. Rios, arXiv:1005.3514
- [228] R. Moufang, *Math. Ann.* **110**, 416430(1935)
- [229] K. McCrimmon, in *A Taste of Jordan Algebras* (Springer, 2003)
- [230] J. Beck, *Lect. Notes Math.* **80**, 119140(1969) doi:10.1007/BFb0083084